Heavy metal removal from dilute solutions using cysteine-rich protein-coated air bubbles

Amir Mohammad Nazari

Department of Mining and Materials Engineering
McGill University
Montreal, Canada

November, 2014

A thesis submitted to McGill University

in partial fulfillment of the requirements of the degree of

Doctor of Philosophy

To my beloved ones: parents and sister

Abstract

This study probed biosorption behavior of a unitary (copper ions) and ternary systems (copper-nickel-cobalt and copper-nickel-calcium ions) at the laboratory scale using a novel material known as air-filled emulsion (AFE). AFE, a stable colloidal suspension, is composed of microscopic bubbles (<10 μm) enclosed by a thin film of cysteine-rich protein generated by ultrasonic action. Fine bubbles are dispersed through the aqueous solution introducing, a high surface area between protein and metal ions. The method using AFE as an extractant is combination of air-assisted solvent extraction (AASX) and biosorption techniques.

It was observed that manipulation of experimental conditions such as solution pH, temperature, biosorbent and copper concentration had a significant impact on metal ion uptake; both for unitary and ternary systems. In the case of the system containing only copper ions, increasing solution pH to 5 led to a greater copper uptake for both egg white protein emulsion (EWPEM) (15%) and bovine serum albumin emulsion (BSAEM) (53%). At lower pH, metal removal diminished and no copper removal was obtained at pH 2 due to the high concentration of hydrogen ions. For the ternary system encompassing copper, nickel and cobalt ions, pH increases resulted in higher metal removal; although bovine serum albumin (BSA)-coated bubbles illustrated higher affinity for copper ions than for nickel and cobalt ions. Increasing the temperature up to 65 ºC increased copper uptake to approximately 98%; however nickel and cobalt removal did not exhibit a significant change. BSAEM also demonstrated very different adsorption behaviors for copper, nickel and cobalt at various biomass and metal ion concentrations. Increasing BSAEM dosage from 10 g/L caused a decrease in copper, nickel and cobalt adsorption percentage, and approximately 2% copper uptake was obtained at a BSAEM concentration above 17.5 g/L. This is due to the agglomeration of air bubbles at higher BSAEM concentration, and consequently lower likelyhood of interactions between active sites and metal ions.

The data obtained from X-ray photoelectron spectroscopy (XPS) and Fourier transform infrared spectroscopy (FTIR) clearly showed that the thiol, amino and carboxylic groups of bovine serum albumin (BSA) and egg white protein (EWP)-coated bubbles were responsible for metal adsorption.

Separation of the copper-loaded microcells from the aqueous solution was also investigated. Flotation, a technique commonly used to float hydrophobic minerals, was employed to remove the microbubbles by means of attachment to the surface of larger air bubbles. In absence of cationic surfactant, approximately 0.5% copper recovery was obtained at pH ranging from 5 to 8 due to lack of hydrophobic groups on the surface of copper-loaded BSA. A cationic flocculant was used to form the large flocs of copper-loaded bubbles, and consequently increase the buoyancy of bubbles. A combination of collector and flocculant at a concentration of 3×10^{-4} M and 0.025 g/L, respectively, led to an increase in copper recovery to nearly 35% at pH 7.

The presence of calcium ions noticeably hindered copper ion adsorption which reduced by 70% as calcium ions compete with metal ions to occupy active binding sites.

Résumé

Ce projet de recherche jette un regard sur les possibilités de biosorption en laboratoire de systèmes unitaire (ions de cuivre) et tertiaires (ions de cuivre-nickel-cobalt et cuivre-nickel-calcium) en utilisant un nouveau type d'émulsions d'air (EA). Les EA sont des suspensions colloïdes stables générées par une action ultrasonique. Elles sont composées de bulles microscopiques (<10 μm) entourées d'une mince couche de protéines riches en cystéine. Les petites bulles sont dispersées dans la solution aqueuse introduisant ainsi une grande surface active entre les protéines et les ions métalliques. La technique utilisant les EA comme agent d'extraction est une combinaison de l'extraction par solvant assistée d'air (ESAA) et de la biosorption.

Pour les systèmes unitaire et tertiaires, il a été observé que la variation des conditions expérimentales tels que le pH de la solution, la température, la concentration de biosorbant et de cuivre ont des impacts significatifs sur la capture des ions métalliques. Pour le système contenant seulement des ions de cuivre, l'augmentation du pH de la solution jusqu'à 5 a amélioré la capture du cuivre dans le cas de l'émulsion de protéine de blanc d'œuf (EPBO) (15%) et dans le cas de l'émulsion de sérum-albumine bovin (ESAB) (53%). À un pH moindre, la récupération a été plus faible et aucune récupération n'a été obtenue à un pH de 2 à cause de la forte concentration d'ions d'hydrogène. Dans le cas du système tertiaire contenant des ions de cuivre, nickel et cobalt, l'augmentation du pH a amélioré la récupération des métaux et les bulles couvertes de sérum-albumine bovin ont montrées plus d'affinité avec les ions de cuivre que ceux de nickel et de cobalt. L'augmentation de la température jusqu'à 65 ºC a favorisé la récupération du cuivre jusqu'à environ 98%; par contre, la récupération du nickel et du cobalt n'a pas été affectée significativement. L'ESAB a aussi montré des mécanismes d'adsorption différents pour le cuivre, le nickel et le cobalt à différentes biomasses et concentrations ioniques des métaux. L'augmentation du dosage d'ESAB à plus de 10 g/L a causé un baisse d'adsorption du cuivre, du nickel et du cobalt avec environ 2% de récupération de cuivre obtenue à une concentration de 17.5 g/L d'ESAB. La présence d'agglomérations de bulle d'air lorsque la concentration d'ESAB est plus élevée cause cet effet car ces agglomérations diminuent le potentiel d'interaction entre les sites actifs et les ions métalliques.

Les données obtenues par spectroscopie de photoélectrons X (SPX) et spectroscopie infrarouge avec transformation de Fourrier (SITF) ont clairement montrées que les groupes thiol, amino et carboxyle des minces couches de sérum-albumine bovin (SAB) et de protéines de blanc d'œufs (PBO) recouvrant les bulles sont responsable de l'adsorption des métaux.

La séparation des microcellules chargées de cuivre de la solution aqueuse a aussi été testée. La flottation, une technique généralement utilisée pour récupérer les minéraux hydrophobiques à été utilisée pour retirer les microbulles par l'attachement de celles-ci à la surface de plus grosses bulles d'air. En absence d'un agent de surface cationique, environ 0.5% du cuivre a été récupéré à un pH entre 5 et 8 considérant l'absence de groupes hydrophobes à la surface du SAB chargé de cuivre. Un floculant cationique a été utilisé pour former des flocs de bulles chargées de cuivres et donc augmenter la flottabilité de celles-ci. Une combinaison de collecteur et de floculant avec des concentrations respectives de 3×10^{-4} M et 0.025 g/L a permis d'augmenter la récupération du cuivre à presque 35% à un pH de 7.

Finalement, la présence d'ions de calcium a sensiblement inhibé l'adsorption d'ions de cuivre. Celle-ci a été réduite de 70 % comme les ions de calcium entrent en compétition avec les ions métalliques pour occuper les sites de liaison actifs.

Contribution of authors

This thesis is manuscript-based. All the manuscripts are co-authored with Prof. Kristian E. Waters and Dr. Philip W. Cox (University of Birmingham) in their capacity as research supervisors. The manuscripts are presented as Chapters 3, 4, 5 and 6 of the thesis. The candidate designed and conducted the experiments. The candidate wrote every chapter and considered the comments from the supervisors in generating the final version.

Acknowledgements

Firstly, I would like to express my deepest gratitude to my supervisor, Professor Kristian Waters, for his guidance, suggestions, constant support during my studies at McGill University.

My gratitude is also extended to my co-supervisor Dr. Philip Cox for his invaluable guidance and support throughout this work.

I would like to express my deep gratitude to my parents and sister for their unconditional support, patience, and encouragement.

I want to thank Dr. Cesar Gomez and Dr. Mitra Mirnezami for their valuable insights and suggestions on the work.

Also, I would like to express my appreciation to Ray Langlois for his assistance in the experimental setup.

I want to thank my friends at McGill University, who helped me in several ways. They include Dr. Amir Sheikhi, Salman Safari, Hesam Mahjoubi, Dr. Azin Zangooi, Dr. Barnabe Ngabe, Dr. Jarrett Quinn, Dr. Hope Tan, Aysan Molaei, Shiva Mohammadi Jam, Darryel Boucher, Frank Rosenblum and Adam Jordens.

A special and warm thank goes to Mrs. Barbara Hanley, graduate studies coordinator in the Department of Mining & Materials Engineering at McGill University for all the help.

I also thank both Mr. Andrew Golsztajn and Mr. Ranjan Roy who helped me a lot for the sample preparation, as well as measuring the concentration of samples by ICP.

I would like to acknowledge the financial support of Vale Base Metals, McGill University for McGill Engineering Doctoral Award (MEDA), and the Natural Sciences and Engineering Research Council of Canada (NSERC) for funding through the Collaborative Research and Development Grant Program (CRDPJ-428685 – 11).

Table of contents

List of tables

List of Figures

Nomenclature and abbreviations

AFE	Air-filled emulsion
AMD	Acid mine drainage
AASX	Air-assisted solvent extraction
SX	Solvent extraction
BSA	Bovine serum albumin
EWP	Egg white protein
HSA	Human serum albumin
HF	Hydrophobin
A/W/O	Air in water-oil
DST	Dynamic surface tension
MST	mesoequilibrium surface tension
SLM	Supported liquid membrane
ELM	Emulsion liquid membrane
C_{EM}	Concentration of emulsion
C_{AFE}	Concentration of air-filled emulsion
$C_{Cu,Ni,Co}$	Concentration of copper, nickel and cobalt
C_{Ca}	Concentration of calcium
C_{Cu}	Concentration of copper
C_{Ni}	Concentration of nickel
XPS	X-ray photoelectron spectroscopy

FTIR	Fourier transform infrared spectroscopy
ICP	Inductively couple plasma spectroscopy
BSAEM	Bovine serum albumin emulsion
EWPEM	Egg white protein emulsion
HTAB	Hexadecyltrimethyl ammonium bromide
DA	Dodecylamine
HA	Hexadecylamine
b_j	The quantity of active sites (i) per gram of biosorbent (mol/g)
X	BSAEM concentration (g/L)
K_j	Equilibrium constant of the functional group (i)
N	The number of functional groups on the surface of microcells
K_w	Equilibrium constant of water at 25 °C (1.023×10^{-14})
iep	Isoelectric point
T_d	Denaturation temperature

Chapter 1. Introduction

1.1. Introduction

Industrial pollution directly or indirectly released into the environment can consist of high levels of heavy metals. Heavy metals are typically the metals with a specific gravity greater than 5 g/cm^3 which are grouped into three classes: toxic metals (Cr, Pb, Zn, Cu, Ni, Cd, As, Co, Sn, etc.); precious metals (Pd, Pt, Ag, Au, Ru, etc.); and radionuclides (U, Th, Ra, Am, etc) (Volesky, 1990; Bishop, 2002). Acid mine drainage (AMD) is a significant source of heavy metals, resulting from industrial activities particularly mining operations. AMD is generated once the sulfidic minerals such as pyrite and pyrrhotite are exposed to the water and oxygen producing acidity and high concentration of metals and sulfate in the water (Younger *et al.*, 2002). This leads to serious environmental contaminants and is a threat to biolife due to the toxicity of heavy metals even at low concentrations (0.001-0.01 g/L); their long-term existence in nature, and accumulation in food chain (Volesky, 1990; Volesky, 2001; Bishop, 2002; Volesky, 2007). Environment Canada reported that 74.9% of total consumed water (497.2 million cubic meters) by mining industries in 2009 was withdrawn by the metal mines, and 77.2% of intake water was sourced from surface freshwater (rivers, lakes). They also claimed that 72.8%, 10.8% and 9% of wastewaters were discharged to the surface freshwater, tailing ponds and ground water respectively, and 59.9% of effluents were not treated prior to discharge. The costs estimated for the treatment of effluents was 42.6% of the total costs (The costs related to water use in the mining industries in 2009 was $165.7 million dollars) while treatment in intake water before it was used represented another 11.3% of total costs (Statistics Canada, 2012). Hence, in order to eliminate heavy metals from waste streams as well as to recover the plentiful resource of valuable heavy metals, several physico-chemical treatment methods such as reverse osmosis, chemical precipitation and filtration, electrochemical treatment, oxidation/reduction, evaporation, adsorption and ion-exchange have been employed. (Dean *et al.*, 1972; Reed, 1998; Kentish and Stevens, 2001; Reddad *et al.*, 2002). However, each process has limitations, such as high-energy requirements (reverse osmosis); capital cost

(electrochemical extraction); and high cost of sorbing agents (sorption and ion-exchange) (Xu and Liu, 2008; Wang *et al.*, 2009; Benaïssa and Elouchdi, 2011; Masood and Malik, 2011).

Solvent extraction (SX) is a key technique in hydrometallurgical operations to recover metal species such as uranium, copper, zinc, nickel and cobalt from concentrated solution (Fisher and Notebaart, 1983; Lo *et al.*, 1983; Thorsen, 1983), where the concentration of metal ions is relatively high (≥ 0.5 g/L) (Flett *et al.*, 1973; Ritcey and Ashbrook, 1979; Preston and Luklinska, 1980; Kentish and Stevens, 2001; Sahu *et al.*, 2004). Uranium extraction for the Manhattan project during World War II was the first major commercial application for solvent extraction (Tarkan, 2006). Solvent loss, high capital outlay, high solvent consumption (solvent/aqueous ratio (~1)) and phase disengagement difficulties are obstacles once the SX is applied to treat waste solutions containing low amount of metal ions (<0.5 g/L) (Tarkan and Finch, 2005; Li *et al.*, 2008). Therefore several methods were built on the basis of increasing surface area between organic solvent and dilute solution to reduce the required amount of extractant for metal uptake. For example, Finch and co-workers proposed a novel technique known as air-assisted solvent extraction (AASX) to remove copper ions using LIX-coated air bubbles (Chen *et al.*, 2003; Tarkan and Finch, 2005). Some parameters, such as required time for formation of solvent-coated bubbles make this method impractical to treat large volumes of dilute heavy-metal bearing effluents, the ambition to fix the impediments associated with the AASX resulted in using air-filled emulsion (AFE) as a material to treat dilute streams such as AMD.

According to the author's knowledge, air-filled human serum albumin (HSA) was first generated by Feinstein and co-workers as contrast agents in echosonography (Keller *et al.*, 1986; Feinstein *et al.*, 1988). Suslick and Grinstaff (1990) used a sonication technique to form microcells containing bovine serum albumin (BSA) as a shell and n-dodecane, n-decane, n-hexane, cyclohexane and toluene as a core (Suslick and Grinstaff, 1990; Grinstaff and Suslick, 1991). They also proposed the mechanism being responsible for microcapsule formation which was based on two processes: (i) Ultrasonic emulsification, resulting in the distribution of microspheres through the solution as well as the formation of protein clusters at the A/W interface; (ii) Cavitation, which accounts for the stabilization of microcells *via* disulfide crosslinking of proteins around the microcells. Protein-coated bubbles have shown their functionality in drug delivery, micro-encapsulation of dyes and flavors, magnetic resonance

imaging (MRI) (Avivi and Gedanken, 2005; Grinberg *et al.*, 2007; Cavalieri *et al.*, 2008; Han *et al.*, 2008; Grinberg *et al.*, 2009; Cavalieri *et al.*, 2010; Han *et al.*, 2010; Cavalieri *et al.*, 2011; Shchukina and Shchukin, 2011; Zhou *et al.*, 2011; Kwan and Borden, 2012). The general concept for using air-filled emulsion to remove heavy metal ions was selected from the work conducted by Tchuenbou-Magaia *et al.* (2009 & 2011) who investigated the reduction of fat content of food, since the taste of food remained constant with the so-termed AFE (Tchuenbou-Magaia *et al.*, 2009; Tchuenbou-Magaia *et al.*, 2011). They generated microcells encapsulated by a thin film of hydrophobin (HF), egg white protein (EWP) and BSA-coated bubbles by means of sonication method to generate an air-filled tri-phasic emulsion (A/W/O). The colloidal system illustrated quite a high stability, with no coalescence and disproportionation after two months. Due to both high cost and lack of availability of HF, it is not currently feasible to utilize it in mass production. So that the other alternatives such as BSA, EWP and soy proteins have been considered (Tchuenbou-Magaia *et al.*, 2011).

AFE is prone to uptake heavy metal ions in the light of various binding sites present in cysteine-rich proteins (White *et al.*, 1956; Shindo and Brown, 1965; Mandal *et al.*, 1997; Rigo *et al.*, 2004; Dokken *et al.*, 2009; Ghosh *et al.*, 2012; Rubino and Franz, 2012). AFE containing micrometer-scale air bubbles (<10 μm) introduces long retention time in contact with metal ions due to both their high stability obtained from disulfide bond (S-S) and their fine size. This leads to higher probability of interaction between functional groups of protein-coated bubbles and metal ions. Furthermore, wastes acquired from the food and dairy industries are an abundant resource to prepare cysteine-rich protein, rendering AFE a potentially cost-efficient and ecofriendly material (Myrnes and Johansen, 1994; Batista, 1999; Ostojić *et al.*, 2005).

1.2. Thesis objectives

The goal of this thesis is to introduce an innovative material to the waste water treatment field based on increasing the effective surface area between organic and metal ions to eliminate heavy metals from dilute streams.

Specific objectives are addressed as follows:

(i) Probing the capability of EWP- and BSA-AFE to remove copper ions, and the effect of operating conditions such as solution pH, metal ion concentration, AFE dosage and temperature

(ii) Investigating the competitive sorption of copper, nickel and cobalt ions in a ternary system, and the influence of experimental conditions

Objectives 3 and 4 explore the potential of AFE to treat waste contaminants on large scale:

(iii) Separating metal ion-loaded AFE from the aqueous solution using flotation

(iv) Examining the viability of AFE in removing metal ions from synthetic process water in presence of calcium ions under different conditions

1.3. Thesis structure

The thesis is written as a "manuscript-based thesis". It is arranged in seven chapters, Chapter 3, 4, 5 and 6 being either published or submitted for publication. Metal sorption capability of EWP- and BSA-air-filled emulsions is probed using a unary system containing copper ions under different experimental conditions (Chapter 3). This is extended to the multiple metal ion system and competitive biosorption of copper, nickel and cobalt is assessed with BSA-coated air cells (Chapter 4). Afterwards, in order to recover metal ions from the solution, separation of the metal-loaded AFE (pregnant solution) which is based on the engineering aspects of this work is carried out (Chapter 5). Finally, to examine the capacity of AFE for treating waste water, BSA-AFE is used to remove nickel and copper from a synthetic process water, made to mimic a tailings pond from Vale's operations in Sudbury (Ontario, Canada) (Chapter 6).

The thesis includes a general introduction (Chapter 1), a literature review (Chapter 2), and conclusions covering all findings (Chapter 7). The structure of the thesis may be summarized as follows:

Chapter 1:

The introduction, objectives and structure of the thesis are presented.

Chapter 2:

A review of mechanism of AMD generation, treatment methods including conventional techniques and SX, techniques originated based on increasing surface area, cysteine-rich protein structure, adsorption kinetics of protein and finally the mechanism behind the formation of AFE is given.

Chapter 3:

The chapter explores the capacity of EWP- and BSA-coated bubbles to adsorb copper ions through a unary system in different experimental conditions. In addition, active binding sites being capable of metal ion removal are determined by means of FTIR and XPS. This chapter was published in Separation and Purification Technology as:

Nazari, A.M., Cox, P.W. and Waters, K.E., 2014. Copper-ion removal from dilute solutions using ultrasonically synthesised BSA and EWP-coated air bubbles, Separation and Purification Technology, 132, 218-225.

Chapter 4:

The chapter studies selectively biosorption of copper, nickel and cobalt using BSA-coated air cells in the various experimental conditions, and functionalities involved in metal ion uptake are determined using FTIR and XPS. This chapter has been accepted for publication in the Journal of Water Process Engineering as:

Nazari, A.M., Cox, P.W. and Waters, K.E., 2014. Biosorption of copper, nickel and cobalt ions from dilute solutions using BSA-coated air bubbles, Journal of Water Process Engineering, 3, 10-17.

Chapter 5:

The chapter investigates the separation of metal ion-loaded AFE by flotation technique. Moreover, the role of various types of surfactant and cationic flocculant is illustrated in separation process. This chapter was presented at the conference "Biohydrometallurgy 2014" (Falmouth, UK) and subsequently accepted for publication in Minerals Engineering as:

Nazari, A.M., Cox, P.W. and Waters, K.E., 2014. Biosorptive flotation of copper ions from dilute solution using BSA-coated bubbles, Minerals Engineering.

DOI: 10.1016/j.mineng.2014.07.023

Chapter 6:

The chapter probes the capability of BSA-AFE for removing metal ions present in process water containing calcium ions. This chapter was submitted to ACS Sustainable Chemistry & Engineering as:

Nazari, A.M., Cox, P.W. and Waters, K.E., 2014. Copper and nickel ion removal from synthetic process water using BSA air-filled emulsion, ACS Sustainable Chemistry & Engineering.

Chapter 7:

Overall conclusions, contribution to the original knowledge and suggestions for future work are detailed.

Appendix A:

The stability of EWP-coated microcells is discussed using light microscopy image and particle size distribution curve at various ultrasonic power and air flow rate, and also it is shown that cavitation process has a significant role in stabilization of microbubbles.

Appendix B:

Physico-chemical properties of cysteine-rich proteins are listed.

Appendix C:

Speciation diagrams of copper, nickel and cobalt are shown.

Appendix D:

Derivation procedures of the proton-binding model are shown.

References

Avivi, S. and Gedanken, A., 2005. The preparation of avidin microspheres using the sonochemical method and the interaction of the microspheres with biotin. Ultrasonics Sonochemistry 12(5), 405-409.

Batista, I., 1999. Recovery of proteins from fish waste products by alkaline extraction. European Food Research and Technology 210(2), 84-89.

Benaïssa, H. and Elouchdi, M.A., 2011. Biosorption of copper ions from synthetic aqueous solutions by drying bed activated sludge. Journal of Hazardous Materials 194, 69-78.

Bishop, P.L. (2002) Pollution prevention: fundamentals and practice, Tsinghua University Press, Beijing, China.

Cavalieri, F., Ashokkumar, M., Grieser, F. and Caruso, F., 2008. Ultrasonic synthesis of stable, functional lysozyme microbubbles. Langmuir 24(18), 10078-10083.

Cavalieri, F., Zhou, M. and Ashokkumar, M., 2010. The design of multifunctional microbubbles for ultrasound image-guided cancer therapy. Current Topics in Medicinal Chemistry 10(12), 1198-1210.

Cavalieri, F., Zhou, M., Caruso, F. and Ashokkumar, M., 2011. One-pot ultrasonic synthesis of multifunctional microbubbles and microcapsules using synthetic thiolated macromolecules. Chemical Communications 47(14), 4096-4098.

Chen, F., Finch, J.A., Distin, P.A. and Gomez, C.O., 2003. Air assisted solvent extraction. Canadian Metallurgical Quarterly 42(3), 277-280.

Dean, J.G., Bosqui, F.L. and Lanouette, K.H., 1972. Removing heavy metals from wastewater. Environmental Science & Technology 6(6), 518-522.

Dokken, K.M., Parsons, J.G., McClure, J. and Gardea-Torresdey, J.L., 2009. Synthesis and structural analysis of copper cysteine complexes. Inorganica Chimica Acta 362(2), 395-401.

Feinstein, S.B., 1988. Ultrasonic imaging agent and method of preparation. Patent No. 4, 774, 958.

Feinstein, S.B., Lang, R.M., Dick, C., Neumann, A., Al-Sadir, J., Chua, K.G., Carroll, J., Feldman, T. and Borow, K.M., 1988. Contrast echocardiography during coronary arteriography in humans: perfusion and anatomic studies. Journal of the American College of Cardiology 11(1), 59-65.

Fisher, J. and Notebaart, C., 1983. Commercial processes for copper. Handbook of Solvent Extraction, p.649, John Wiley & Sons, New York (USA).

Flett, D.S., Okuhara, D.N. and R., S.D., 1973. Solvent extraction of copper by hydroxyl oximes. Journal of Inorganic and Nuclear Chemistry 35(7), 2471-2487.

Ghosh, S., Pandey, N.K., Bhattacharya, S., Roy, A. and Dasgupta, S., 2012. Fibrillation of hen egg white lysozyme triggers reduction of copper(II). International Journal of Biological Macromolecules 51(1), 1-6.

Grinberg, O., Hayun, M., Sredni, B. and Gedanken, A., 2007. Characterization and activity of sonochemically-prepared BSA microspheres containing Taxol-An anticancer drug. Ultrasonics Sonochemistry 14(5), 661-666.

Grinberg, O., Gedanken, A., Patra, C., Patra, S., Mukherjee, P. and Mukhopadhyay, D., 2009. Sonochemically prepared BSA microspheres containing Gemcitabine, and their potential application in renal cancer therapeutics. Acta Biomaterialia 5(8), 3031-3037.

Grinstaff, M.W. and Suslick, K.S., 1991. Air-filled proteinaceous microbubbles: synthesis of an echo-contrast agent. Proceedings of the National Academy of Sciences 88(17), 7708-7710.

Han, Y., Radziuk, D., Shchukin, D. and Moehwald, H., 2008. Stability and size dependence of protein microspheres prepared by ultrasonication. Journal of Materials Chemistry 18(42), 5162-5166.

Han, Y., Shchukin, D., Yang, J., Simon, C., Fuchs, H. and Möhwald, H., 2010. Biocompatible protein nanocontainers for controlled drugs release. ACS Nano 4(5), 2838-2844.

Keller, M.W., Feinstein, S.B., Briller, R.A. and Powsner, S.M., 1986. Automated production and analysis of echo contrast agents. Journal of Ultrasound in Medicine 5(9), 493-498.

Kentish, S.E. and Stevens, G.W., 2001. Innovations in separations technology for the recycling and re-use of liquid waste streams. Chemical Engineering Journal 84(2), 149-159.

Kwan, J.J. and Borden, M.A., 2012. Lipid monolayer collapse and microbubble stability. Advances in Colloid and Interface Science 183-184, 82-99.

Li, C.-W., Chen, Y.-M. and Hsiao, S.-T., 2008. Compressed air-assisted solvent extraction (CASX) for metal removal. Chemosphere 71(1), 51-58.

Lo, T.C., Baird, M. and Hanson, C., 1983. Commercial processes for uranium from ore. Handbook of Solvent Extraction, 763-782, Wiley-Interscience, New York (USA).

Mandal, S., Das, G., Singh, R., Shukla, R. and Bharadwaj, P.K., 1997. Synthesis and studies of Cu(II)-thiolato complexes: bioinorganic perspectives. Coordination Chemistry Reviews 160, 191-235.

Masood, F. and Malik, A., 2011. Biosorption of metal ions from aqueous solution and tannery effluent by Bacillus sp. FM1. Journal of Environmental Science and Health. Part A, Toxic/Hazardous Substances & Environmental Engineering 46(14), 1667-1674.

Myrnes, B. and Johansen, A., 1994. Recovery of lysozyme from scallop waste. Preparative Biochemistry & Biotechnology 24(1), 69-80.

Ostojić, S., Pavlović, M., Živić, M., Filipović, Z., Gorjanović, S., Hranisavljević, S. and Dojčinović, M., 2005. Processing of whey from dairy industry waste. Environmental Chemistry Letters 3(1), 29-32.

Preston, J.S. and Luklinska, Z.B., 1980. Solvent extraction of copper(II) with ortho-hydroxyoximes—I kinetics and mechanism of extraction. Journal of Inorganic and Nuclear Chemistry 42(3), 431-439.

Reddad, Z., Gerente, C., Andres, Y. and Le Cloirec, P., 2002. Adsorption of several metal ions onto a low-cost biosorbent: kinetic and equilibrium studies. Environmental Science & Technology 36(9), 2067-2073.

Reed, B.E., 1998. Waste water treatment: Heavy metals. Environmental Analysis and Remediation 8, 5220-5225.

Rigo, A., Corazza, A., di Paolo, M.L., Rossetto, M., Ugolini, R. and Scarpa, M., 2004. Interaction of copper with cysteine: stability of cuprous complexes and catalytic role of cupric ions in anaerobic thiol oxidation. Journal of Inorganic Biochemistry 98(9), 1495-1501.

Ritcey, G.M. and Ashbrook, A.W. (1979) Solvent extraction: principles and application to process metallurgy, Elsevier, Amsterdam (NL)

Rubino, J.T. and Franz, K.J., 2012. Coordination chemistry of copper proteins: How nature handles a toxic cargo for essential function. Journal of Inorganic Biochemistry 107(1), 129-143.

Sahu, S.K., Agrawal, A., Pandey, B.D. and Kumar, V., 2004. Recovery of copper, nickel and cobalt from the leach liquor of a sulphide concentrate by solvent extraction. Minerals Engineering 17(7), 949-951.

Shchukina, E.M. and Shchukin, D.G., 2011. LbL coated microcapsules for delivering lipid-based drugs. Advanced Drug Delivery Reviews 63(9), 837-846.

Shindo, H. and Brown, T.L., 1965. Infrared spectra of complexes of L-Cysteine and related compounds with zinc, cadmium, mercury and lead. Journal of the American Chemical Society 87(9), 1904-1908.

Statistics Canada (2012) Industrial water use-2009, Ministry of Industry, Ottawa, Canada.

Suslick, K.S. and Grinstaff, M.W., 1990. Protein microencapsulation of nonaqeous liquids. Journal of the American Chemical Society 112(1), 7807-7809.

Tarkan, H.M. and Finch, J.A., 2005. Air-assisted solvent extraction: towards a novel extraction process. Minerals Engineering 18(1), 83-88.

Tarkan, H.M., 2006. Air-assisted solvent extraction. Ph.D. thesis, McGill University (CA).

Tchuenbou-Magaia, F.L., Norton, I.T. and Cox, P.W., 2009. Hydrophobins stabilised air-filled emulsions for the food industry. Food Hydrocolloids 23(7), 1877-1885.

Tchuenbou-Magaia, F.L., Norton, I.T. and Cox, P.W., 2011. Suspensions of air cells with cysteine-rich protein coats : Air-filled emulsions. Journal of Cellular Plastics 47(3), 217-232.

Thorsen, G., 1983. Commercial processes for cadmium and zinc. Handbook of Solvent Extraction, 709-716, Wiley-Interscience, New York (USA).

Volesky, B. (1990) Biosorption of heavy metals, CRC press, Florida (USA).

Volesky, B., 2001. Detoxification of metal-bearing effluents: biosorption for the next century. Hydrometallurgy 59(2), 203-216.

Volesky, B., 2007. Biosorption and me. Water Research 41(18), 4017-4029.

Wang, X.S., Li, Z.Z. and Sun, C., 2009. A comparative study of removal of Cu(II) from aqueous solutions by locally low-cost materials: marine macroalgae and agricultural by-products. Desalination 235(1), 146-159.

White, J.M., Manning, R.A. and Li, N.C., 1956. Metal interaction with sulfur-containing amino acids. Nickel and copper complexes. Journal of the American Chemical Society 78(11), 2367-2370.

Xu, H. and Liu, Y., 2008. Mechanisms of Cd^{2+}, Cu^{2+} and Ni^{2+} biosorption by aerobic granules. Separation and Purification Technology 58(3), 400-411.

Younger, P.L., Banwart, S.A. and Hedin, R.S. (2002) Mine water hydrology, Springer (NL).

Zhou, M., Cavalieri, F. and Ashokkumar, M., 2011. Tailoring the properties of ultrasonically synthesised microbubbles. Soft Matter 7(2), 623-630.

Chapter 2. Literature review

2.1. Acid mine drainage

Large quantities of dilute heavy metal effluents obtained from industrial activities are released into the environment. Acid mine drainage (AMD) is an example of metal-rich contaminants which is a by-product of mining, metal extraction and processing industries. AMD has serious adverse effects on the environment and living organisms, since it typically contains an elevated concentration of metals (manganese, iron and heavy metals) and metalloids (arsenic) (Ritcey and Ashbrook, 1979), shown in Table 2.1. Generally, AMD formation is a combined chemical and/or microbiological process. The most common mechanism of generation of acidic sulfur-rich wastewater is through the oxidation of pyrite and pyrrhotite. Oxidation of pyrite consists of a series of chemical reactions, detailed in Equation 2.1-2.4 (Brown *et al.*, 2002; Younger *et al.*, 2002; Ritcey, 2005). Firstly, ferrous ions are produced by either dissociation or oxidation of pyrite (Equation 2.1). Afterwards, the ferrous ions are oxidized to ferric ions (Equation 2.2). This reaction is slow and rate-determining step. In accordance with Equation 2.3, ferric ions are subjected to hydrolysis to form ferric hydroxide $Fe(OH)_3$ in the solution, resulting in a lowering of the pH in presence of H^+. Additional oxidation of pyrite is associated with the ferric ions generating more ferrous ions and acidity. In terms of microbiological process, thiobacillus ferrroxidans is the most significant bacterium, obtaining energy for growth from the oxidation of ferrous to ferric ions leading to an increase in the rate of acid generation (Evangelou, 1995; Brown *et al.*, 2002). The role of other sulfide minerals in formation of acid mine drainage is less pronounced than that of the iron sulfides, and as such are considered to be leached by the acid.

$$FeS_{2\,(s)} + 7/2\ O_2 + H_2O \rightarrow Fe^{2+} + 2\ SO_4^{2-} + 2\ H^+ \quad (2.1)$$

$$Fe^{2+} + 1/4\ O_2 + H^+ \rightarrow Fe^{3+} + 1/2\ H_2O \quad (2.2)$$

$$Fe^{3+} + 3\ H_2O \rightarrow Fe(OH)_{3\,(s)} + 3\ H^+ \quad (2.3)$$

$$FeS_{2\,(s)} + 14\ Fe^{3+} + 8\ H_2O \rightarrow 15\ Fe^{2+} + 2\ SO_4^{2-} + 16\ H^+ \quad (2.4)$$

Table 2.1: Chemical composition of some metal-bearing contaminants (mg/L) (Brown *et al.*, 2002; Younger *et al.*, 2002; Ritcey, 2005)

Constitute	A	B	C	D	E
pH	2.6	3.6	3-5.5	2.7	3.5
Al	18	15	50	0.03	30
As	0.02	-----	-----	0.02	9
Cd	0.03	0.1	-----	0.07	1
Cu	1.6	6	-----	14	1.5
Fe	50	50	50-300	144	300
Pb	0.01	0.1	-----	0.1	-----
Mn	32	20	20-300	7	12
Ni	-----	0.1	-----	0.07	-----
Zn	10	25	-----	28	120
Sulfate	2100	-----	20-2000	1000	-----

A: Big Five Tunnel, Colorado, USA (abandoned precious metal mine); B: Pennsylvania Mine, Colorado, USA (abandoned gold/silver mine); C: Typical coal mine drainage; D: Parys Mountain, Anglesey, UK (abandoned copper mine); E: Wheal Jane, Cornwall, UK (abandoned tin mine).

2.2. Treatment methods

Treatment methods for AMD are categorized as being either passive or active treatment methods. Passive treatment includes chemical and biological systems which is desirable to treat metal-bearing-effluent from abandoned mines (operating and maintenance costs are minimal). Chemical passive treatment involves both naturalizing acidity and precipitating metal ions by allowing waste streams to flow through a bed of limestone, not by the active addition of alkaline materials. Biological passive treatment is carried out by using algae, microbial mats and sulfate-reducing bacteria to harness mine waters. For example, wetlands have recently received growing attention for AMD treatment, which were initially used in the USA (Brown *et al.*, 2002; Younger *et al.*, 2002; Ritcey, 2005).

Details of active treatment methods are given in Table 2.2. The conventional active process for treating mine water is through raising solution pH using limestone, sodium hydroxide or other alkaline materials and also flocculants to both neutralize the acidity of the solution and to allow the settling of the metal in the form of hydroxide species.

This part deals with a brief introduction on the conventional removal methods such as solvent extraction and also the techniques proposed on the basis of increasing surface area between extractant and metal ions for treating dilute metal-bearing streams.

Table 2.2: Details of active treatment methods (Reed, 1998)

Process	Chemical/energy input	Metal reclamation	Major advantages	Major disadvantages
Chemical precipitation	Precipitant, flocculent, acid base, mixing and fluid handling	Metal sludge	Well established, low effluent concentration	High chemical dosages, several unit operations
Electric recovery	Electrical power	Solid metal scrap	Well-established, direct recovery of solid metal, no chemical consumption	Energy intensive, high capital costs, reduced efficiency at dilute concentrations
Ion-exchange	Regenerated solutions, fluid handling	Concentrated soluble metal stream	Highly selective, effectiveness <100 mg/L	Chemical regeneration requirements, adsorbent expense, prone to fouling in mixed waste
Disposal adsorbents	Replacement adsorbent, fluid handling	Metal immobilizes on solid adsorbent	Simple metal remove process, low adsorbent cost, effective <100 mg/L	Selectivity, recurring cost of new adsorbent, disposal cost of spent adsorbent
Liquid-liquid solvent extraction	Organic solvent/water contact, loading and stripping in mixer and settlers or columns	Concentrated soluble metal stream	Selective, continuous concentrated metal solution recycle	Capital costs, solvent loss to air/water, solvent disposal

2.2.1. Solvent extraction

The term liquid-liquid or solvent extraction (SX) is attributed to the separation of a solute from an organic phase by mass transfer between two immiscible phases, one of which is an aqueous phase containing metal ions, and the other being an organic solvent. In other words, the solvent selectively uptakes specific molecules or ions from aqueous solution, although unwanted species remain. The loaded-organic extractant is thereafter mixed with the stripping aqueous phase in order to transfer metal ions back into the solution. SX is a commonly used technique for large scale operations such as extraction metallurgy and waste water treatment where the concentration of metal ions is high (≥ 0.5 g/L). As shown in Figure 2.1, SX is employed to extract copper from bio-leached solution. In the case of dilute waste streams with a low concentration of metal ions (<0.5 g/L), SX is restricted by the long extraction times and a high

solvent/aqueous ratio (~1) which results in high organic losses through entrainment in the aqueous phase.

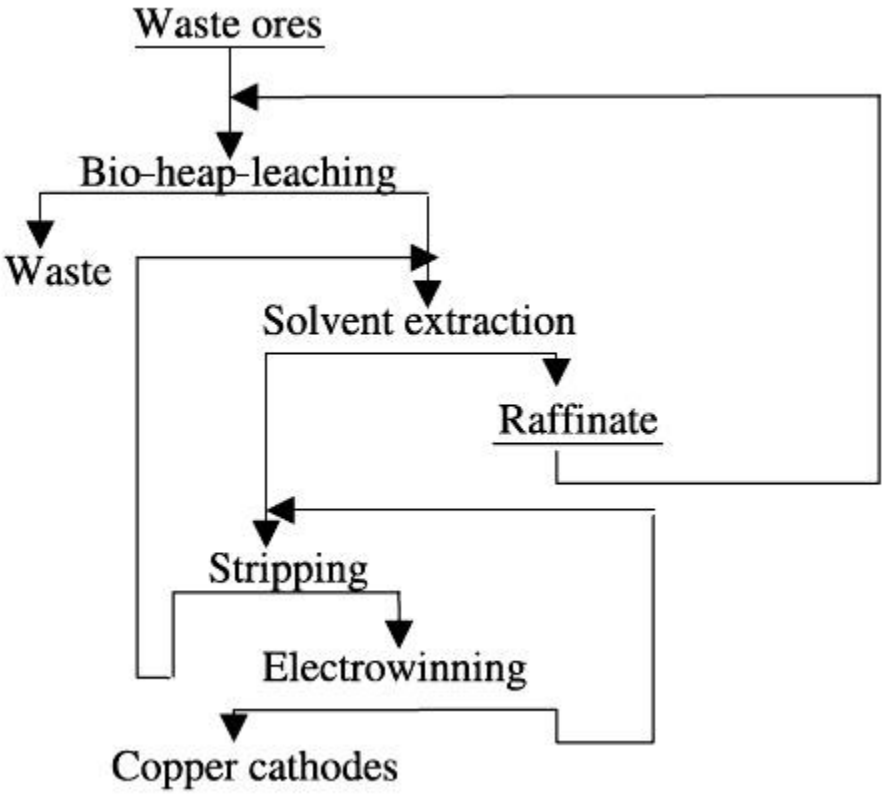

Figure 2.1: Bioleaching-SX-electrowining flowsheet in Dexing Copper Mine (Songrong *et al.*, 2002)

2.2.2. Proposed treatment methods: increasing surface area between extractant and metal ions

In order to overcome the challenges associated with the conventional methods including SX for treating dilute metal-bearing contaminants, several methods based on increasing the interfacial surface area between solvent and aqueous solution have been proposed, such as emulsion liquid membrane (ELM), (Li, 1968; Ho and Li, 1996; Valenzuela *et al.*, 2005; Sengupta *et al.*, 2006) and supported liquid membrane (SLM) (Largman and Sifniades, 1978; Parthasarathy and Buffle, 1994; Kocherginsky *et al.*, 2007). Although they introduce a huge surface area to volume ratio, operational difficulties restrict their function such as liquid membrane instability and fouling. Colloidal gas aphrons (CGA) have been introduced as a promising method to treat waste water streams (Ciriello *et al.*, 1982; Cabezon *et al.*, 1994).

CGAs are gas bubbles in the size range of 10-100 μm, encapsulated by a soapy shell (Sebba, 1987; Save *et al.*, 1994; Hashim and Gupta, 1998; Hashim *et al.*, 2012). They provide a colloidal system which is highly stable, and exhibit little coalescence owing to the presence of similar electrical charge on their surface. A novel technique known as air-assisted solvent extraction (AASX) has also been proposed to treat dilute solutions on the basis of solvent coated bubbles (Figure 2.2) (Chen *et al.*, 2003; Tarkan and Finch, 2005). This is carried out by directing an air stream through a solvent container (C) to generate the foam (A). The foam was passed through a capillary and solvent coated bubbles form at the orifice (B). Afterwards, solvent-coated bubbles disengage at the solution surface to generate a layer of copper-loaded solvent (D). AASX has received growing attention in recent years due to a high specific surface area of organic phase as well as high aqueous/organic ratio and excellent phase separation resulted from buoyancy (Tarkan and Finch, 2005). According to Finch and co-workers, only 30 % of copper removal (3.54×10^{-4} mol) was obtained from 150 ml aqueous solution of 500 mg/L copper using 1 mL of solvent. The rate of solvent coated air cell formation was restricted by the rate of air flow. Consequently, the required time to incorporate 1 mL of solvent as a thin layer was approximately 122 min (with an average bubble diameter of 0.44 cm and average thickness of 3 μm) (Li *et al.*, 2008). Increasing the air flow rate forces the solvent out, rendering the formation of solvent-coated bubbles impossible. The contact time (rising time of solvent coated air bubbles through aqueous phase) was 0.57 s which is inversely proportional to the rising velocity of the bubbles (22.5 cm/s). Therefore, in the case of very dilute solutions, relatively low contact time between solvent-coated bubbles and metal ions, coupled with rapid disengagement of the bubbles and the limit of air flow directly influence the efficiency of this method. One way to boost the removal of metal ions from a dilute solution is through the generation of small bubbles to generate a highly stable colloidal system with well-dispersed air cells leading to increase both specific surface area and contact time.

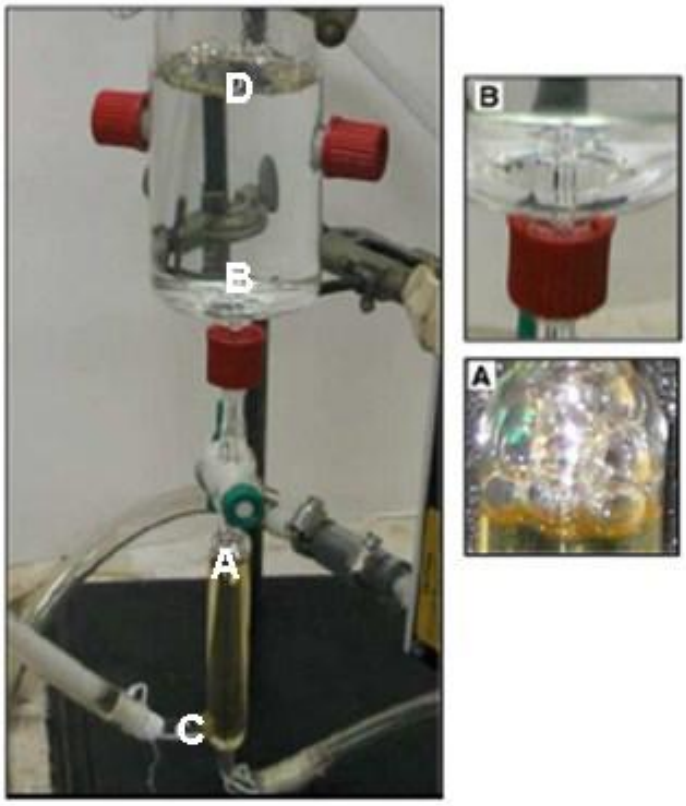

Figure 2.2: Schematic view of test setup for generation of solvent-coated bubbles, an air stream is passed through the solvent container (C), the foam is generated (A), the foam is passed through the capillary, and solvent-coated bubble is generated at the orifice (B), solvent-coated bubbles disengage at the solution surface (D). (Tarkan and Finch, 2005)

2.2.3. Biosorption

Adsorption is the physical adherence and chemical bonding between molecules and ions (adsorbate) onto the surface of another molecule (adsorbent). It is considered a promising technique to remove metal pollutants from wastewaters by means of various sorbents such as activated carbon, polymer fibers and resins (Jia *et al.*, 2002; Sánchez-Polo and Rivera-Utrilla, 2002; Deng *et al.*, 2003; Deng and Ting, 2005). Many efforts have been undertaken to introduce alternative adsorbents to reduce the cost of adsorption system, as conventional adsorbents (activated carbon) are expensive. Biosorbent, a biomass of living or non-living organisms consisting of algae, bacteria, fungi, yeasts, and also products derived from these organisms are extensively employed in the processing of industrial waste waters (Sadowski, 2001; Deng *et al.*, 2003; Volesky, 2007; Wang *et al.*, 2009; Masood and Malik, 2011). The byproducts obtained

from food, beverage and agricultural industries as well as different types of sludge and wastes from biotechnological and pharmaceutical productions are an abundant source of biosorbent (Reddad *et al.*, 2002; Deng and Ting, 2005; Xu and Liu, 2008). Therefore, biosorption is considered as an ecofriendly and low-cost technique. Biosorption is a physico-chemical technique to remove metal contaminants through different mechanisms such as physical adsorption, ion exchange, surface complexation and precipitation illustrated in Figure 2.3.

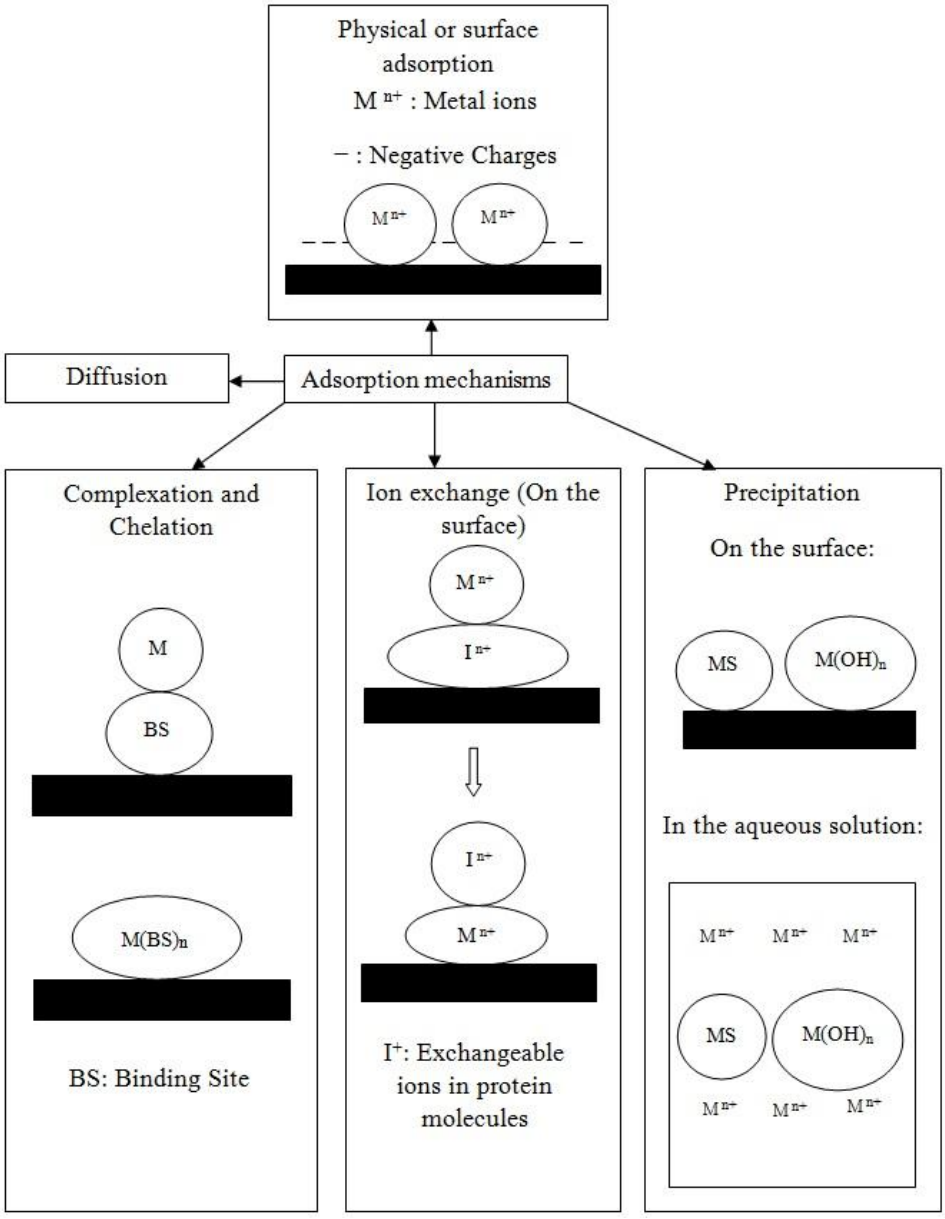

Figure 2.3: Various mechanisms involved in metal ion sorption.

2.2.4. Air-filled emulsion

Formation of microbubbles enclosed by a bimolecular thin film has received increasing attention over recent years owing to their high stability and functionality in drug delivery, micro-encapsulation of dyes and flavors, magnetic resonance imaging (MRI) and low fat food system (Avivi and Gedanken, 2005; Shchukin *et al.*, 2005; Grinberg *et al.*, 2007; Cavalieri *et al.*, 2008; Gedanken, 2008; Han *et al.*, 2008; Grinberg *et al.*, 2009; Cavalieri *et al.*, 2010; Han *et al.*, 2010; Vassileva and Koseva, 2010; Cavalieri *et al.*, 2011; Nakatsuka *et al.*, 2011; Shchukina and Shchukin, 2011; Zhou *et al.*, 2011; Kwan and Borden, 2012). Most studies have focused on cysteine-rich protein coatings such as egg white protein (EWP), bovine serum albumin (BSA), human serum albumin (HSA) and hydrophobin (Avivi *et al.*, 2003; Cavalieri *et al.*, 2008; Gedanken, 2008; Tchuenbou-Magaia *et al.*, 2009; Vassileva and Koseva, 2010; Tchuenbou-Magaia *et al.*, 2011). Stability of the proteinaceous microcapsules arises from the formation of covalent disulfide bonds creating a cage-like structure around a gas core. Cysteine-rich proteins are also capable of sorbing metal ions from wastewater streams due to the presence of functional groups on the surface (White *et al.*, 1956; Shindo and Brown, 1965; Mandal *et al.*, 1997; Rigo *et al.*, 2004; Dokken *et al.*, 2009; Ghosh *et al.*, 2012; Rubino and Franz, 2012). This colloidal system is similar to the AASX technique in terms of both extent of specific surface area of organic phase and phase separation resulted from presence of fine coated bubbles. AFE and AASX are distinguishable by the size of bubble, mechanism of bubble formation as well as the nature of coating material. Such a system containing fine protein-stabilised air cells (<10μm) dispersed through the aqueous medium is termed an air-in-water emulsion, or an air-filled emulsion (AFE). The aim of this study is to use these protein-coated air cells to remove metal ions from aqueous systems based on the combination of AASX and biosorption methods. AFE leads to an increase in both the specific surface area and contact time of biomass with metal ions, making this technique potentially suitable to treat dilute metal solutions.

2.3. Cysteine-rich proteins

Proteins are macromolecules comprising of one or more polypeptides folded into a globular or fibrous form (Haynes and Norde, 1994). There are many different types and serve

various biological roles. A polypeptide is made up of linear chain amino acids linked together by the peptide or amide bonds (HN-C=O). There are 20 types of amino acids found in proteins, where their structures differ in the nature of the side chain.

Cysteine is a type of amino acid, consisting of a thiol group at the side chain of peptide. As illustrated in Figure 2.4, cysteine residues in two different peptide chains can link together by means of a covalent disulfide bond under mild oxidizing condition, and are easily cleaved back to the thiols under mild reducing conditions.

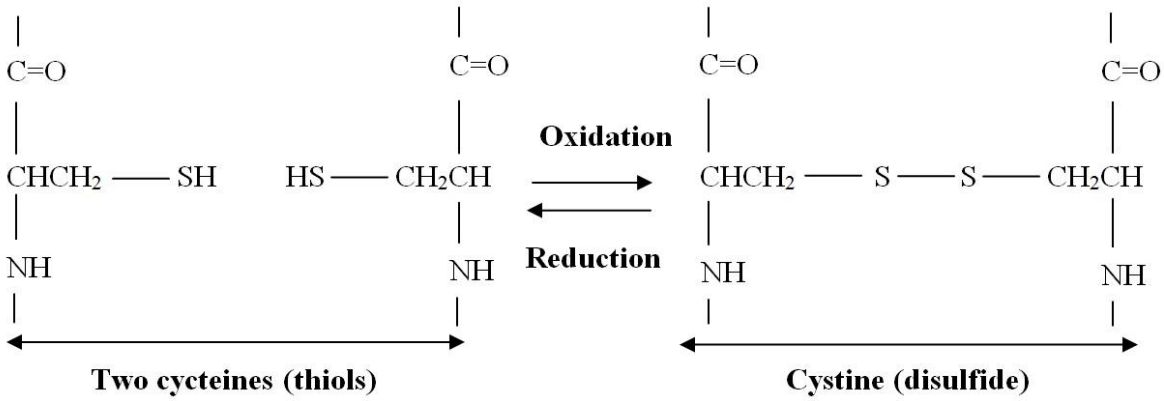

Figure 2.4: Structures of cysteine and cystine

Chicken egg white protein (EWP) is a cysteine-rich protein made up of different types of proteins folded into a compact and tight conformation, due to both intramolecular covalent disulfide bridges and hydrogen bonds. It is used as a major ingredient in many food industries such as bakery products, meringues, meat products and cookies due to its nutritional quality. Many studies have recently been conducted on EWP, investigating functional properties such as gelling, foaming, emulsification and binding adhesion (Mine, 1995; Van der Plancken *et al.*, 2006; Arzeni *et al.*, 2012). The major constituents of EWP and their physiochemical properties are detailed in Table 2.3. Ovalbumin is the only EWP to contain free sulfhydryl (SH) groups folded within the core of protein due to tertiary structure of globular protein that become exposed upon heating (Mine, 1996; Van der Plancken *et al.*, 2007). The denaturation temperature of ovalbumin is close to 84 °C.

Table 2.3: Physico-chemical properties of the major constituents of EWP (Mine, 1995)

Protein	Albumin (%, dry-mass basis)	Iep	Molecular weight (kDa)	T_d (°C)
Ovalbumin	54	4.5	44.5	84
Ovotransferrin	12	6.1	77.7	61
Ovomucoid	11	4.1	28	77
Ovomucin	3.5	4.5-5	$5.5\text{-}8.3\times10^3$	--
Lysozyme	3.4	10.7	14.3	75
G2 globulin	4	5.5	49	92.5
G3 globulin	4	5.8	49	--
Avidin	0.05	10	68.3	--

T_d: Denaturation temperature, iep: Isoelectric point

2.4. Adsorption kinetics of proteins at A/W interface

The kinetics of protein adsorption at the air/water (A/W) interface is a significant factor in controlling both the formation and stabilization of air-filled emulsions. The adsorption kinetics of the proteins demonstrate the time needed to construct stabilised air bubbles, final bubble size and the optimisation of the energy input applied in emulsification.

Many studies have been conducted to investigate the protein adsorption at a fluid interface by means of measuring the interfacial tension between two phases (Ghosh and Bull, 1963; MacRitchie and Alexander, 1963; Benjamins and De Feijter, 1975; Benjamins *et al.*, 1975; Graham and Phillips, 1979; Tripp *et al.*, 1995; Beverung *et al.*, 1999). Time-dependent surface tension (dynamic surface tension (DST)) gives an indication of the adsorption behavior of proteins at the A/W interface (Benjamins *et al.*, 1975; Tripp *et al.*, 1995). At dilute protein concentrations, the adsorption process at the A/W interface displays four distinct regimes depicted in Figure 2.5. The first is induction, or diffusion-limited, regime where the protein molecules diffuse from the bulk solution to the interface. The A/W interface possesses interfacial tension approximately that of the pure solvent. The second regime is identified by a sharp decline in surface tension due to protein molecule adsorption at the A/W interface. At high protein concentrations, this will be the first kinetic regime observed. The third DST kinetic regime is the mesoequilibrium surface tension (MST) regime, indicated by a slow rate of decrease in surface tension due to molecular reorientation and conformational changes in the adsorbed protein molecules. The fourth is steady state regime reached when protein molecules have achieved both the equilibrium surface concentration and conformation.

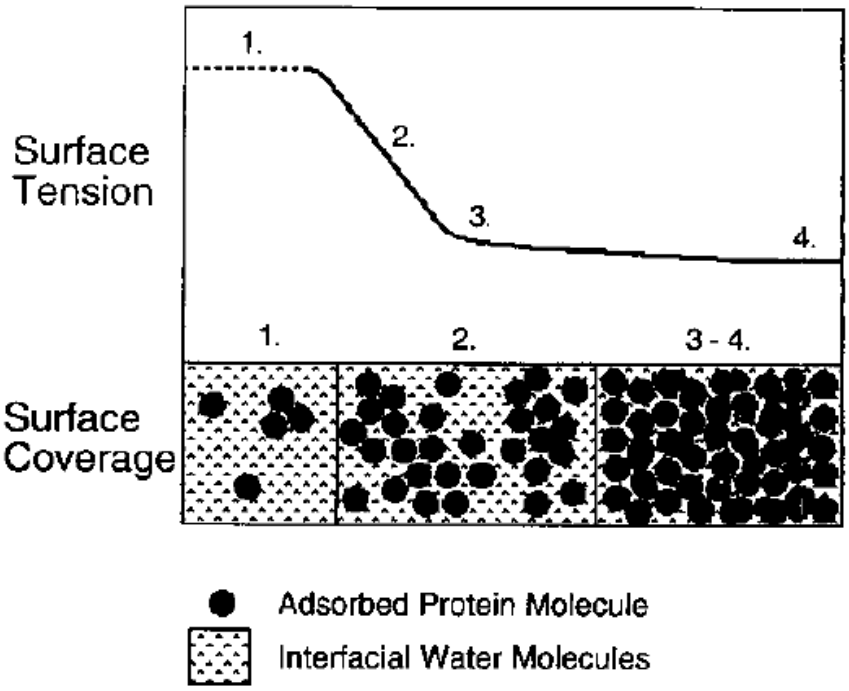

Figure 2.5: Schematic of dynamic interfacial tension during protein molecules adsorption at the A/W interface, illustrating the four kinetics regimes.1-Induction regime (<50% surface coverage) that generally observed for dilute solution and slowly adsorbing surfactants. 2-Sharp decrease in dynamic surface tension (50%<surface coverage<100%). 3-mesoequilibrium surface tension, slow decline in tension attributed to conformational changes and molecular rearrangement. 4- equilibrium surface tension (Tripp *et al.,* 1995).

Globular proteins are categorized in two groups in terms of flexibility and conformational stability during adsorption at interface (Tripp *et al.*, 1995). Rigid or hard globular proteins exhibit a high degree of conformational stability and a low degree of flexibility due to intra and interchain molecular interactions such as disulfide and hydrogen bonds. Moreover, they demonstrate a high resistance against thermal, chemical and shear-induced denaturation. Soft globular proteins are flexible and can rearrange their tertiary structure to expedite adsorption at the interfaces. Foamability is a measure of how easily protein molecules are unfolded and present at the A/W interface. Thus a soft globular protein with a high unfolding ability presents a high foamability compared to the hard globular protein (Foegeding *et al.*, 2006).

Protein hydrophobicity plays a significant role in protein adsorption at the A/W interface, which is based on the number and distribution of nonpolar amino acid groups that remain

exposed at the molecular surface of a globular protein molecule (Kato and Nakai, 1980; Kato *et al.*, 1981). For example, a globular protein with a high portion of nonpolar surface regions indicates a high surface hydrophobicity resulting in a large decrease in surface tension, and a subsequent high affinity for the A/W interface and consequently high emulsifying activity. The surface hydrophobicity is frequently improved as partial denaturation occurs due to the exposure of the nonpolar amino groups (in the light of rupture of noncovalent and hydrogen bonds) buried in the interior tertiary structure of globular protein (Dickinson, 1986). It could be concluded that the foamability of globular proteins is attributed to their conformational stability and surface hydrophobicity.

2.5. Emulsions

Colloidal suspensions are fundamentally composed of two components where one phase (dispersed) is distributed in the second phase (continuous phase). It is possible for a suspension to have more than one type of dispersed phase (*e.g.* ice cream); or multi-components of dispersed or continuous phases such as an aqueous medium containing electrolyte, surfactant, polymers and other molecular species. As illustrated in Table 2.4, the dispersed phase could be in the form of particles, droplets or bubbles ranging from 1 nm-10 µm. An emulsion is a stable colloidal system where the continuous and dispersed components are the same phase, such as two liquids. Liquid emulsions are often classified either as water-in-oil emulsion or as oil-in water depending upon the presence of an emulsifier and the volume fraction of oil to water. Microbubbles dispersed in an aqueous medium can also often be considered to be a gas emulsion, if the stability of the system ensures that the two phases do not separate.

Table 2.4: Main types of colloidal systems (Cosgrove, 2005)

Continuous Phase → / Dispersed Phase ↓	Gas	Liquid	Solid
Gas (Bubbles)	----------	Foam (beer)	Solid foam (polystyrene cup)
Liquid (Droplets)	Liquid aerosol (Mist)	Liquid emulsion (Mayonnaise)	Solid emulsion (Butter)
Solid (Particles)	Solid aerosol (smoke)	Sol (ink)	Solid sol (stained glass)

2.6. Emulsion generation

Suspensions are naturally unstable due to the contact between dispersed phase (*e.g.* microbubbles) and aqueous medium being unfavorable in terms of thermodynamics (Behrend and Schubert, 2001; Schubert and Ax, 2003). Therefore, an energy input that is greater than the Laplace pressure acting across the A/W interfaces is required for generation of the dispersed state. This is provided *via* various means, including rotor-stator devices, an ultrasonic probe, a high-pressure homogeniser and a porous membrane (Figure 2.6). In addition, the energy is directly proportional to the interfacial tension. The energy required to form a droplet/bubble increases as the interfacial tension elevates, and the nature of forces which are capable of droplet or bubble formation is based on the type of apparatus used. Abismail *et al.*, (1999) reported that ultrasound emulsification is more efficient compared to mechanical agitation in terms of droplet size and reduced surfactant amount as well as energy consumption (Abismaïl *et al.*, 1999). Since then, many studies have been conducted on ultrasound emulsification as a function of acoustic power and frequency, as well as exposure time (Cavalieri *et al.*, 2008; Han *et al.*, 2008; Zhou *et al.*, 2011).

An ultrasonic probe is positioned at the liquid interface to produce ultrasound waves transmitted through the entire liquid. The positive and negative pressures are exerted on a liquid by acoustic waves known as the rarefaction and compression cycles respectively (Ashokkumar *et al.*, 2009). Liquid molecules absorb the ultrasound energy leading to fluctuations about their mean position. At sufficiently high ultrasonic intensity, the rarefaction cycle will pull molecules apart and break down the intermolecular bonds to create voids or cavities (bubbles) inside the liquid medium.

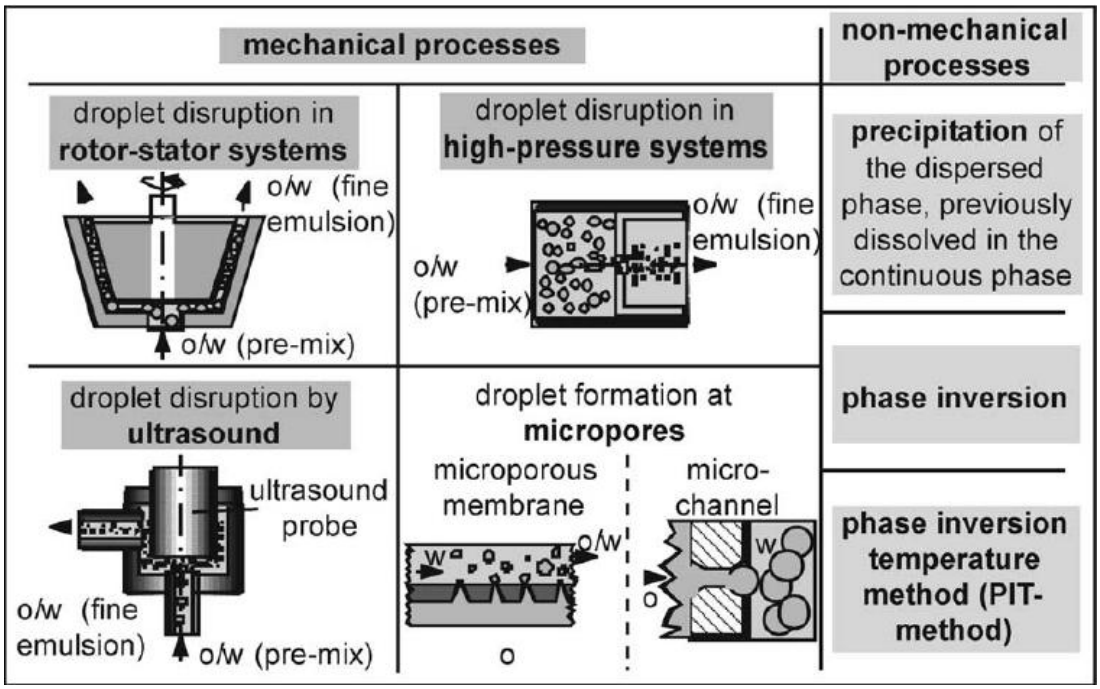

Figure 2.6: Common apparatuses for emulsification (Behrend and Schubert, 2001).

The bubble volume increases and decreases during the rarefaction and compression cycles until they become unstable at a certain size and violently collapse generating extremely high temperatures (5,000 K) and pressures (2,000 atm) inside the bubble shown in Figure 2.7. This phenomenon is known as acoustic cavitation. The intense local heating and high pressure obtained by bubble cavitation is responsible for the radical formation by decomposition of solvent molecules (Gedanken, 2008; Bang and Suslick, 2010). These mechanical and chemical effects of cavitation are exploited in the generation of AFEs.

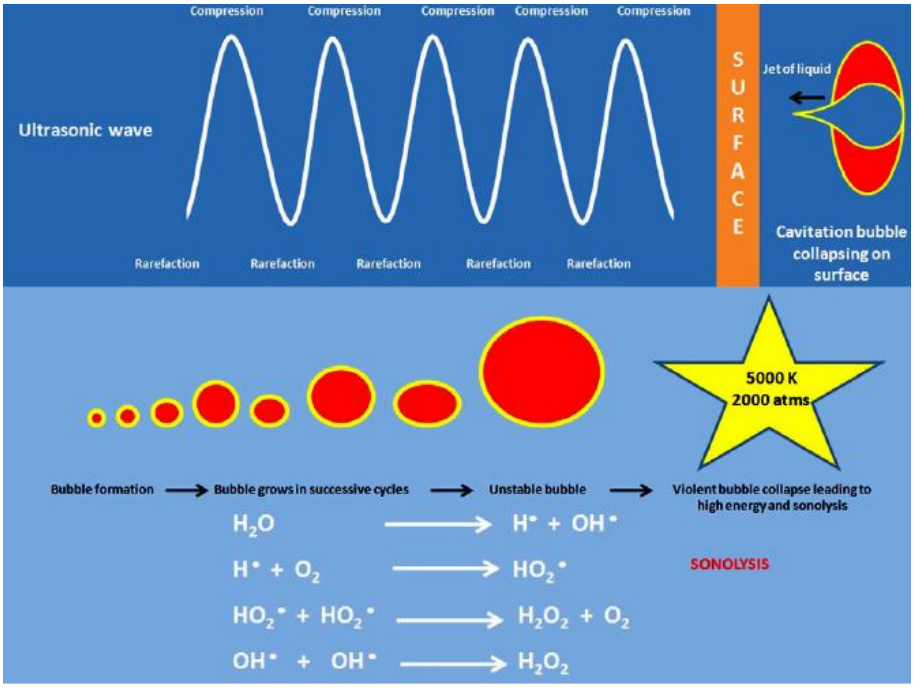

Figure 2.7: Cavitation bubble formation at various stages during alternating compression and rarefaction cycles of the ultrasonic wave and asymmetric bubble collapse on a surface leading to (i) high energy with temperature up to 5000 K and pressure up to 2000 atm and (ii) the sonolysis of water caused by the high energy where $OH^\cdot$ are hydroxyl radicals, $HO_2^\cdot$ are perhydroxyl radicals and H_2O_2 is hydrogen peroxide (Pollet, 2010).

2.7. Ultrasonically-stabilised protein-air emulsions

Lately, ultrasound has been widely used to form proteinaceous microcapsules with a gas or non-aqueous liquid core coated by protein molecules (Cavalieri *et al.*, 2008; Han *et al.*, 2008; Cavalieri *et al.*, 2011). Keller *et al.* (1988) used sonication to produce albumin coated bubbles with a short storage life and low stability. A high-intensity ultrasound probe was utilised by Suslick and Grinstaff (1990) to synthesize microcapsules under air or O_2. Protein microspheres consisted of bovine serum albumin (BSA) as a wall material that surrounded n-dodecane, n-decane, n-hexane, cyclohexane and toluene. Cavalieri *et al.* (2008) synthesized stable egg white lysozyme microbubbles by high intensity sonication. Prior to sonication, DL-dithiothreitol (DTT) was used in order to disrupt the disulfide bonds and form thiol groups.

Tchuenbou-Magaia *et al.* (2009) constructed hydrophobin-coated air cells using sonication. The air-filled emulsions were employed to reduce the fat content in food. They then produced highly stable air cells with cysteine-rich proteins including bovine serum albumin (BSA) and egg

white protein (EWP) using a sonochemical method (Tchuenbou-Magaia *et al.*, 2011). These air cells were as stable as those produced with hydrophobin (HFBII), however protein pre-treatment, protein concentration, pH (protein's iep) and temperature must be controlled. Zhou *et al.* (2010) constructed air-filled lysozyme microbubbles by emulsification followed by the cross-linking of protein molecules under high-intensity ultrasound (Zhou *et al.*, 2011). They investigated the effects of sonication time and acoustic power on the size, size distribution, morphology and the stability of the lysozyme microbubbles. An increase in the ultrasonic power and time resulted in the formation of larger microbubbles with a broader size distribution.

Suslick and Grinstaff (1990) first proposed the mechanism behind protein stabilised microsphere formation. The mechanism is based on the combination of two steps. The first is ultrasonic emulsification including both microscopic dispersion of air cells in the aqueous solution and formation of protein clusters at the A/W interface, caused by hydrophobic interactions resulting from chemical or thermal denaturation (Suslick and Grinstaff, 1990; Grinstaff and Suslick, 1991; Zhou *et al.*, 2011). The second step is cavitation, responsible for stabilisation of microbubbles by means of formation of radicals, and disulfide crosslinking of protein molecules (Suslick and Grinstaff, 1990; Grinstaff and Suslick, 1991; Cavalieri *et al.*, 2011). In other words, water molecules decompose to $OH^{\cdot}$ and $H^{\cdot}$ radicals which form H_2, H_2O_2 and in the presence of O_2, superoxide ($HO_2^{\cdot}$) (Del Duca *et al.*, 1958; Lippitt *et al.*, 1972; Dibbern *et al.*, 2006; Gedanken, 2008; Bang and Suslick, 2010). Suslick and coworkers suggested that superoxide (crosslinking agent) is the most probable oxidant radical involved in the crosslinking reaction through disulfide bond formation between protein cysteine residues.(Cavalieri *et al.*, 2008; Gedanken, 2008). Subsequently, the formation of stable microcapsules is dependent on the presence of O_2 (in air) rather than an inert atmosphere such as He, Ar or N_2 (Suslick and Grinstaff, 1990; Suslick *et al.*, 1994).

Avivi and Gedanken (2002) proposed that the formation of stable protein microcapsules could be applicable for proteins that do not contain any sulfur-containing residues (Cysteine) such as poly(glutamic acid) and Streptavidin microspheres (Avivi and Gedanken, 2002). The mechanism of microbubble stabilisation is based on an increase in the hydrophobic residues and strong interaction between them as a result of the protein denaturation (at acidic pH). Suslick *et al.* (2006) also synthesized a new class of protein microcapsules with polyglutamic acid

stabilized by hydrogen bonding, van der Waals, hydrophobic and electrostatic interactions rather than covalent disulfide bonding (Dibbern *et al.*, 2006).

References

Abismaïl, B., Canselier, J.P., Wilhelm, a.M., Delmas, H. and Gourdon, C., 1999. Emulsification by ultrasound: drop size distribution and stability. Ultrasonics Sonochemistry 6(1), 75-83.

Arzeni, C., Pérez, O.E. and Pilosof, A.M.R., 2012. Functionality of egg white proteins as affected by high intensity ultrasound. Food Hydrocolloids 29(2), 308-316.

Ashokkumar, M., Bhaskaracharya, R., Kentish, S., Lee, J., Palmer, M. and Zisu, B., 2009. The ultrasonic processing of dairy products – An overview. Dairy Science & Technology 90(2-3), 147-168.

Avivi, S. and Gedanken, A., 2002. S-S bonds are not required for the sonochemical formation of proteinaceous microspheres: the case of streptavidin. Biochemistry Journal 366, 705-707.

Avivi, S., Nitzan, Y., Dror, R. and Gedanken, A., 2003. An easy sonochemical route for the encapsulation of tetracycline in bovine serum albumin microspheres. Journal of the American Chemical Society 125(51), 15712-15713.

Avivi, S. and Gedanken, A., 2005. The preparation of avidin microspheres using the sonochemical method and the interaction of the microspheres with biotin. Ultrasonics Sonochemistry 12(5), 405-409.

Bang, J.H. and Suslick, K.S., 2010. Applications of ultrasound to the synthesis of nanostructured materials. Advanced Materials 22(10), 1039-1059.

Behrend, O. and Schubert, H., 2001. Influence of hydrostatic pressure and gas content on continuous ultrasound emulsification. Ultrasonics Sonochemistry 8(3), 271-276.

Benjamins, J., De Feijter, J.A., Evans, M.T.A., Graham, D.E. and Phillips, M.C., 1975. Dynamic and static properties of proteins adsorbed at the air water interface. Faraday Discussions of the Chemical Society 59, 218-229.

Beverung, C.J., Radke, C.J. and Blanch, H.W., 1999. Protein adsorption at the oil/water interface: characterization of adsorption kinetics by dynamic interfacial tension measurements. Biophysical Chemistry 81(1), 59-80.

Brown, M., Barley, B. and Wood, H. (2002) Minewater treatment: technology, application and policy, IWA Publishing, London (UK).

Cabezon, L.M., Caballero, M. and Perez-Bustamante, J.A., 1994. Coflotation separation for the determination of heavy metals in water using colloidal gas aphrons systems. Separation Science and Technology 29(11), 1491-1500.

Cavalieri, F., Ashokkumar, M., Grieser, F. and Caruso, F., 2008. Ultrasonic synthesis of stable, functional lysozyme microbubbles. Langmuir 24(18), 10078-10083.

Cavalieri, F., Zhou, M. and Ashokkumar, M., 2010. The design of multifunctional microbubbles for ultrasound image-guided cancer therapy. Current Topics in Medicinal Chemistry 10(12), 1198-1210.

Cavalieri, F., Zhou, M., Caruso, F. and Ashokkumar, M., 2011. One-pot ultrasonic synthesis of multifunctional microbubbles and microcapsules using synthetic thiolated macromolecules. Chemical Communications 47(14), 4096-4098.

Chen, F., Finch, J.A., Distin, P.A. and Gomez, C.O., 2003. Air assisted solvent extraction. Canadian Metallurgical Quarterly 42(3), 277-280.

Ciriello, S., Barnett, S.M. and Deluise, F.J., 1982. Separation science and technology removal of heavy metals from aqueous solutions using microgas dispersions. Separation Science and Technology 17(4), 521-534.

Del Duca, M., Yeager, E., Davies, M.O. and Hovarka, F., 1958. Isotropic technique in the study of the sonochemical formation of hydrogen peroxide. The journal of Acoustical Society of America 30 (4), 301-307.

Deng, S., Bai, R. and Chen, J.P., 2003. Behaviors and mechanisms of copper adsorption on hydrolyzed polyacrylonitrile fibers. Journal of Colloid and Interface Science 260(2), 265-272.

Deng, S. and Ting, Y.-P., 2005. Characterization of PEI-modified biomass and biosorption of Cu, Pb and Ni. Water Research 39(10), 2167-2177.

Dibbern, E.M., Toublan, F.J.-J. and Suslick, K.S., 2006. Formation and characterization of polyglutamate core-shell microspheres. Journal of the American Chemical Society 128(20), 6540-6541.

Dickinson, E., 1986. Mixed proteinaceous emulsifiers: review of competitive protein adsorption and the relationship to food colloid stabilization. Food Hydrocolloids 1(1), 3-23.

Dokken, K.M., Parsons, J.G., McClure, J. and Gardea-Torresdey, J.L., 2009. Synthesis and structural analysis of copper cysteine complexes. Inorganica Chimica Acta 362(2), 395-401.

Evangelou, V.P., 1995. Pyrite oxidation and its control, CRC Press, Boca Raton, USA.

Foegeding, E.A., Luck, P.J. and Davis, J.P., 2006. Factors determining the physical properties of protein foams. Food Hydrocolloids 20(2), 284-292.

Gedanken, A., 2008. Preparation and properties of proteinaceous microspheres made sonochemically. Chemistry - A European Journal 14(13), 3840-3853.

Ghosh, S. and Bull, H.B., 1963. Adsorbed films of bovine serum albumin: tensions at air-water surfaces and paraffin-water interfaces. Biochimica et Biophysica Acta 66, 150-157.

Ghosh, S., Pandey, N.K., Bhattacharya, S., Roy, A. and Dasgupta, S., 2012. Fibrillation of hen egg white lysozyme triggers reduction of copper(II). International Journal of Biological Macromolecules 51(1), 1-6.

Graham, D.E. and Phillips, M.C., 1979. Proteins at liquid interfaces I. Kinetics of adsorption and surface denaturation. Journal of Colloid and Interface Science 70 (3), 403-414.

Grinberg, O., Hayun, M., Sredni, B. and Gedanken, A., 2007. Characterization and activity of sonochemically-prepared BSA microspheres containing Taxol-An anticancer drug. Ultrasonics Sonochemistry 14(5), 661-666.

Grinberg, O., Gedanken, A., Patra, C., Patra, S., Mukherjee, P. and Mukhopadhyay, D., 2009. Sonochemically prepared BSA microspheres containing Gemcitabine, and their potential application in renal cancer therapeutics. Acta Biomaterialia 5(8), 3031-3037.

Grinstaff, M.W. and Suslick, K.S., 1991. Air-filled proteinaceous microbubbles: synthesis of an echo-contrast agent. Proceedings of the National Academy of Sciences 88(17), 7708-7710.

Han, Y., Radziuk, D., Shchukin, D. and Moehwald, H., 2008. Stability and size dependence of protein microspheres prepared by ultrasonication. Journal of Materials Chemistry 18(42), 5162-5166.

Han, Y., Shchukin, D., Yang, J., Simon, C., Fuchs, H. and Möhwald, H., 2010. Biocompatible protein nanocontainers for controlled drugs release. ACS Nano 4(5), 2838-2844.

Hashim, M.A. and Gupta, B.S., 1998. The application of colloidal gas aphrons in the recovery of fine cellulose fibres from paper mill wastewater. Bioresource Technology 64(3), 199-204.

Hashim, M.A., Mukhopadhyay, S., Gupta, B.S. and Sahu, J.N., 2012. Application of colloidal gas aphrons for pollution remediation. Journal of Chemical Technology and Biotechnology 87(3), 305-324.

Haynes, C.A. and Norde, W., 1994. Globular proteins at solid/liquid interfaces. Colloids and Surfaces B: Biointerfaces 2(6), 517-566.

Ho, W.S.W. and Li, N.N., 1996. Recent advances in emulsion liquid membranes, Chemical separations with liquid membranes. ACS Symposium Series, 642, 208-221.

Jia, Y.F., Xiao, B. and Thomas, K.M., 2002. Adsorption of metal ions on nitrogen surface functional groups in activated carbons. Langmuir 18(2), 470-478.

Kato, A. and Nakai, S., 1980. Hydrophobicity determined by a fluorescence probe method and its correlation with surface properties of proteins. Biochimica et Biophysica Acta-Protein Structure 624(1), 13-20.

Kato, A., Tsutsui, N., Matsudomi, N., Kobayashi, K. and Nakai, S., 1981. Effects of partial denaturation on surface properties of ovalbumin and lysozyme. Agricultural and Biological Chemistry 45(12), 2755-2760.

Keller, M.W., Glasheen, W., Teja, K., Gear, A. and Kaul, S., 1988. Myocardial contrast echocardiography without hyperemic response ot hemodynamic effect or reactive hyperemia: a major advantage in the imaging of regional myocardial perfusion. Journal of the American College of Cardiology 12(4), 1039-1047.

Kocherginsky, N.M., Yang, Q. and Seelam, L., 2007. Recent advances in supported liquid membrane technology. Separation and Purification Technology 53(2), 171-177.

Kwan, J.J. and Borden, M.A., 2012. Lipid monolayer collapse and microbubble stability. Advances in Colloid and Interface Science 183-184, 82-99.

Largman, T. and Sifniades, S., 1978. Recovery of copper from aqueous solutions by means of supported liquid membranes. Hydrometallurgy 3(2), 153-162.

Li, C-W, Chen, Y-M and Hsiao, S-T, 2008. Compressed air-assisted solvent extraction (CASX) for metal removal. Chemosphere 71(1), 51-58.

Li, N.N., 1968. Separating hydrocarbons with liquid membranes. U.S. patent No. 3, 410, 794.

Lippitt, B., McCord, J.M. and Fridovich, I., 1972. The sonochemical reduction of cytochrome c and its inhibition by superoxide dismutase. Journal of Biological Chemistry 247(14), 4688-4690.

MacRitchie, F. and Alexander, A.E., 1963. Kinetics of adsorption of proteins at interface part III. the role of electrical barriers in adsorption. Journal of Colloid Science 18(5), 464-469.

Mandal, S., Das, G., Singh, R., Shukla, R. and Bharadwaj, P.K., 1997. Synthesis and studies of Cu(II)-thiolato complexes: bioinorganic perspectives. Coordination Chemistry Reviews 160, 191-235.

Masood, F. and Malik, A., 2011. Biosorption of metal ions from aqueous solution and tannery effluent by Bacillus sp. FM1. Journal of Environmental Science and Health. Part A, Toxic/Hazardous Substances & Environmental Engineering 46(14), 1667-1674.

Mine, Y., 1995. Recent advances in the understanding of egg white protein functionality. Trends in Food Science & Technology 6(7), 225-232.

Mine, Y., 1996. Effect of pH during the dry heating on the gelling properties of egg white proteins. Food Research International 29(2), 155-161.

Nakatsuka, M.A., Hsu, M.J., Esener, S.C., Cha, J.N. and Goodwin, A.P., 2011. DNA-coated microbubbles with biochemically tunable ultrasound contrast activity. Advanced Materials 23(42), 4908-4912.

Parthasarathy, N. and Buffle, J., 1994. Capabilities of supported liquid membranes for metal speciation in natural waters: application to copper speciation. Analytica Chimica Acta 284(3), 649-659.

Reddad, Z., Gerente, C., Andres, Y. and Le Cloirec, P., 2002. Adsorption of several metal ions onto a low-cost biosorbent: kinetic and equilibrium studies. Environmental Science & Technology 36(9), 2067-2073.

Reed, B.E., 1998. Waste water treatment: Heavy metals. Environmental Analysis and Remediation 8, 5220-5225.

Rigo, A., Corazza, A., di Paolo, M.L., Rossetto, M., Ugolini, R. and Scarpa, M., 2004. Interaction of copper with cysteine: stability of cuprous complexes and catalytic role of cupric ions in anaerobic thiol oxidation. Journal of Inorganic Biochemistry 98(9), 1495-1501.

Ritcey, G.M. and Ashbrook, A.W. (1979) Solvent extraction: principles and application to process metallurgy, Elsevier, Amsterdam (NL)

Ritcey, G.M., 2005. Tailings management in gold plants. Hydrometallurgy 78(1), 3-20.

Rubino, J.T. and Franz, K.J., 2012. Coordination chemistry of copper proteins: How nature handles a toxic cargo for essential function. Journal of Inorganic Biochemistry 107(1), 129-143.

Sadowski, Z., 2001. Effect of bisorption of Pb, Cu and Cd on the zeta potential and flocculation of Nacardia SP. Minerals Engineering 14(5), 547-552.

Sánchez-Polo, M. and Rivera-Utrilla, J., 2002. Adsorbent-adsorbate interactions in the adsorption of Cd(II) and Hg(II) on ozonized activated carbons. Environmental Science and Technology 36(17), 3850-3854.

Save, S.V., Pangarkar, V.G. and Kumar, S.V., 1994. Liquid-liquid extraction using aphrons. Separations Technology 4(2), 104-111.

Schubert, H. and Ax, K., 2003. Product engineering of dispersed systems. Trends in Food Science & Technology 14(1), 9-16.

Sebba, F., 1987. Foams and biliquid foams-aphrons. Wiley, New York (USA).

Sengupta, B., Sengupta, R. and Subrahmanyam, N., 2006. Copper extraction into emulsion liquid membranes using LIX 984N-C®. Hydrometallurgy 81(1), 67-73.

Shchukin, D.G., Köhler, K., Möhwald, H. and Sukhorukov, G.B., 2005. Gas-filled polyelectrolyte capsules. Angewandte Chemie International Edition 44(21), 3310-3314.

Shchukina, E.M. and Shchukin, D.G., 2011. LbL coated microcapsules for delivering lipid-based drugs. Advanced Drug Delivery Reviews 63(9), 837-846.

Shindo, H. and Brown, T.L., 1965. Infrared spectra of complexes of L-Cysteine and related compounds with zinc, cadmium, mercury and lead. Journal of the American Chemical Society 87(9), 1904-1908.

Songrong, Y., Jiyuan, X., Guanzhou, Q. and Yuehua, H., 2002. Research and application of bioleaching and biooxidation technologies in China. Minerals Engineering 15(5), 361-363.

Suslick, K.S. and Grinstaff, M.W., 1990. Protein microencapsulation of nonaqeous liquids. Journal of the American Chemical Society 112(1), 7807-7809.

Suslick, K.S., Grinstaff, M.W., Kolbeck, K.J. and Wong, M., 1994. Characterization of sonochemically prepared proteinaceous microspheres. Ultrasonics Sonochemistry 1(1), 65-68.

Tarkan, H.M. and Finch, J.A., 2005. Air-assisted solvent extraction: towards a novel extraction process. Minerals Engineering 18(1), 83-88.

Tchuenbou-Magaia, F.L., Norton, I.T. and Cox, P.W., 2009. Hydrophobins stabilised air-filled emulsions for the food industry. Food Hydrocolloids 23(7), 1877-1885.

Tchuenbou-Magaia, F.L., Norton, I.T. and Cox, P.W., 2011. Suspensions of air cells with cysteine-rich protein coats : Air-filled emulsions. Journal of Cellular Plastics 47(3), 217-232.

Tripp, B.C., Magda, J.J. and Andrade, J.D., 1995. Adsorption of globular proteins at the air/water interface as measured *via* dynamic surface tension: concentration dependence, mass transfer consideration, and adsorption kinetics. Journal of Colloid and Interface Science 173(1), 16-27.

Valenzuela, F., Fonseca, C., Basualto, C., Correa, O., Tapia, C. and Sapag, J., 2005. Removal of copper ions from a waste mine water by a liquid emulsion membrane method. Minerals Engineering 18(1), 33-40.

Van der Plancken, I., Van Loey, A. and Hendrickx, M.E., 2006. Effect of heat-treatment on the physico-chemical properties of egg white proteins: A kinetic study. Journal of Food Engineering 75(3), 316-326.

Van der Plancken, I., Van Loey, A. and Hendrickx, M.E., 2007. Foaming properties of egg white proteins affected by heat or high pressure treatment. Journal of Food Engineering 78(4), 1410-1426.

Vassileva, E.D. and Koseva, N.S. (2010) Sonochemically born proteinaceous micro- and nanocapsules, Elsevier, Advances in Protein Chemistry and Structural Biology 80, Oxford (UK).

Volesky, B., 2007. Biosorption and me. Water Research 41(18), 4017-4029.

Wang, X.S., Li, Z.Z. and Sun, C., 2009. A comparative study of removal of Cu(II) from aqueous solutions by locally low-cost materials: marine macroalgae and agricultural by-products. Desalination 235(1), 146-159.

White, J.M., Manning, R.A. and Li, N.C., 1956. Metal interaction with sulfur-containing amino acids. Nickel and copper complexes. Journal of the American Chemical Society 78(11), 2367-2370.

Xu, H. and Liu, Y., 2008. Mechanisms of Cd^{2+}, Cu^{2+} and Ni^{2+} biosorption by aerobic granules. Separation and Purification Technology 58(3), 400-411.

Younger, P.L., Banwart, S.A. and Hedin, R.S. (2002) Mine water hydrology, Springer, Amsterdam (NL).

Zhou, M., Cavalieri, F. and Ashokkumar, M., 2011. Tailoring the properties of ultrasonically synthesised microbubbles. Soft Matter 7(2), 623-630.

Chapter 3. Copper ion removal from dilute solutions using ultrasonically synthesised BSA- and EWP-coated air bubbles

3.1. Introduction

Large volumes of dilute heavy metal contaminants are produced in the industrialized world including mining, metallurgical operations, steel making, petroleum, chemical manufacturing, coal and nuclear power generation (Reddad *et al.*, 2002; Deng and Ting, 2005; Masood and Malik, 2011). Heavy metals in waste have an adverse effect on the local environment due to their toxicity and accumulation in the food chain (Chen *et al.*, 2002; Sheng *et al.*, 2004; Chen and Yang, 2006; Volesky, 2007). Therefore, a series of physico-chemical treatment methods such as reverse osmosis, chemical precipitation and filtration, electrochemical treatment, oxidation/reduction, evaporation and ion-exchange have been explored for heavy metal removal (Dean *et al.*, 1972; Kentish and Stevens, 2001; Reddad *et al.*, 2002). Each process has drawbacks, including high energy consumption, high operational cost, high capital cost and low selectivity (Xu and Liu, 2008; Wang *et al.*, 2009; Benaïssa and Elouchdi, 2011; Masood and Malik, 2011).

Solvent extraction (SX) is a frequently used technique in hydrometallurgical processing where the concentration of metal is relatively high (≥ 0.5 g/L) (Flett *et al.*, 1973; Ritcey and Ashbrook, 1979; Preston and Luklinska, 1980; Kentish and Stevens, 2001; Sahu *et al.*, 2004). However, long extraction times and a high solvent/aqueous ratio (~1) make this method inefficient for dilute solutions (<0.5 g/L) (Tarkan and Finch, 2005; Li *et al.*, 2008). To overcome these challenges, several methods based on increasing the interfacial surface area between solvent and aqueous solution have been proposed, such as emulsion liquid membrane (ELM) (Valenzuela *et al.*, 2005; Sengupta *et al.*, 2006), supported liquid membrane (SLM) (Largman and Sifniades, 1978; Parthasarathy and Buffle, 1994; Kocherginsky *et al.*, 2007) and colloidal gas aphrons (CGA) (Ciriello *et al.*, 1982; Cabezon *et al.*, 1994). A novel technique known as air-assisted solvent extraction (AASX) has also been proposed to treat dilute solutions on the basis of solvent coated bubbles (Chen *et al.*, 2003; Tarkan and Finch, 2005). AASX exhibits promising properties such as a high specific surface area of the organic phase, high aqueous/organic ratio

and excellent phase separation resulting from buoyancy effects (Tarkan and Finch, 2005). However, relatively low contact time between solvent-coated bubbles and metal ions, coupled with rapid disengagement of the bubbles render this method inefficient for treating large volumes of dilute solutions.

One way to boost metal ion removal from a dilute solution is through the construction of small bubbles to generate a highly stable colloidal system with well-dispersed air cells leading to an increased specific surface area, contact time and subsequently adsorption kinetics. Microbubbles (<10 μm) enclosed by a biomolecular thin film have recently received increasing attention owing to their high stability and functionality in drug delivery, micro-encapsulation of dyes and flavors, magnetic resonance imaging (MRI) and low fat foods (Avivi and Gedanken, 2005; Grinberg *et al.*, 2007; Cavalieri *et al.*, 2008; Han *et al.*, 2008; Grinberg *et al.*, 2009; Cavalieri *et al.*, 2010; Han *et al.*, 2010; Cavalieri *et al.*, 2011; Shchukina and Shchukin, 2011; Zhou *et al.*, 2011; Kwan and Borden, 2012). Most studies have focused on cysteine-rich protein coatings such as egg white protein (EWP), bovine serum albumin (BSA) and human serum albumin (HSA) (Avivi *et al.*, 2003; Cavalieri *et al.*, 2008; Gedanken, 2008; Vassileva and Koseva, 2010; Tchuenbou-Magaia *et al.*, 2011). Cysteine-rich proteins are also capable of sorbing metals ions from wastewater streams due to the functional groups present on the surface (White *et al.*, 1956; Shindo and Brown, 1965; Mandal *et al.*, 1997; Rigo *et al.*, 2004; Dokken *et al.*, 2009; Ghosh *et al.*, 2012; Rubino and Franz, 2012). The colloidal system containing fine protein-stabilised air cells which are dispersed through the aqueous medium is termed an air-filled emulsion (AFE). AFE is generated through sonication technique. The mechanism behind protein stabilised microsphere formation is based on the combination of two steps. The first is ultrasonic emulsification including both microscopic dispersion of air cells in the aqueous solution and formation of protein clusters at the A/W interface, caused by hydrophobic interactions resulting from chemical or thermal denaturation (Suslick and Grinstaff, 1990; Grinstaff and Suslick, 1991; Zhou *et al.*, 2011). The second step is cavitation, responsible for stabilisation of microbubbles by means of formation of radicals, and subsequently disulfide crosslinking of protein molecules (Suslick and Grinstaff, 1990; Grinstaff and Suslick, 1991; Cavalieri *et al.*, 2011).

This chapter proposes the use of AFE to remove copper ions from dilute solutions using EWP and BSA-coated bubbles. The effect of operational conditions such as solution pH, sorbent concentration, copper concentration, and temperature on copper adsorption qualitatively and quantitatively was explored.

3.2. Materials and methods

3.2.1. Materials

Dried chicken EWP (Sigma-Aldrich, Canada) and BSA (fraction V) (Bishop Canada Inc.) were used as supplied. All solutions were made using reverse osmosis purified water (pH of 5.8 at 25 ºC). Anhydrous cupric sulfate ($CuSO_4$) (Fisher Scientific, Canada) was used to produce the aqueous copper solution. Hydrochloric acid (36%), nitric acid (67%) and hydrogen peroxide (50%) (Fisher Scientific, Canada) were used for acid digestion of the proteins. The solution pH was adjusted using 1 M sodium hydroxide and 1 M sulfuric acid (98%). 10^{-3} M KCl (Fisher Scientific, Canada) as a supporting electrolyte was utilised to measure ζ-potential of protein-coated air cells.

3.2.2. Emulsion preparation

Five g of protein was dissolved in 100 g of water, stirred at room temperature for a minimum of 2 hours. Insoluble particles present in EWP were removed by centrifugation (IEC Centra CL2 centrifuge, Thermo Electron Co.) (4,000 rpm, 30 min, 25 ºC), while BSA particles were completely dissolved in water. The pH of the EWP solution was adjusted to 4 to reach the isoelectric point of EWP. The natural pH of BSA (7) was used to generate AFE. 80 mL of protein solution was placed in a jacketed beaker to maintain the temperature of bulk solution at 50±2 ºC and an ultrasonic horn (22 mm in diameter) was positioned at the air-protein solution interface as illustrated in Figure 3.1. The solution was irradiated with a high intensity sonicator (UP 400 S, 24 kHz, Hielscher Inc., U.S.A.) while compressed air was bubbled through the solution at 60 mL/min using a frit. Sonication time and power were 3 min and 90 W respectively. A second centrifugation (1,000 rpm, 30 min, 25 ºC) was performed after 2 hours (to allow the

dissipation of all the large, unstable bubbles and foam) to concentrate bubbles in a top layer and separate protein debris from the EWP and BSA emulsion.

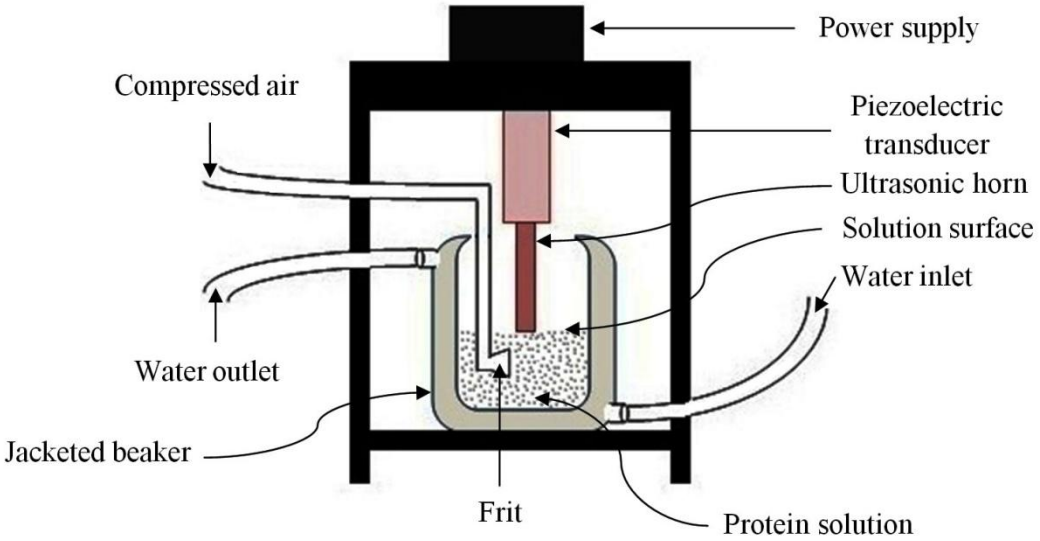

Figure 3.1: Schematic view of test setup for emulsion preparation

3.2.3. Sorption experiments

The stock copper (II) solutions were prepared by dissolving anhydrous cupric sulfate in water, and stirred for approximately 2 hours. A series of batch adsorption experiments were conducted in 50 mL centrifuge tubes to examine the effect of temperature, biomass concentration, copper concentration and pH on copper adsorption. Details of the experimental conditions are given in Table 3.1; where C_{EM} and C_{Cu} represent emulsion (BSAEM and EWPEM) and copper concentration respectively. The required amount of BSAEM or EWPEM was added to the copper solution using electronic pipette (Eppendorf Research Pro., Canada). Afterwards, the centrifuge tubes were hand shaken for 2 min to mix biosorbent and copper solution. In order to investigate the temperature effect on copper uptake, the sample temperature was controlled using a water bath. Then, 15 mL of solution was withdrawn after one day followed by centrifugation (15 min, 4000 rpm) and then filtration (Filter Paper No. P8, Fisher Scientific, Canada) to remove BSAEM and EWPEM and also residual insoluble particles from the solution. When investigating the effect of pH, 1 M sulfuric acid and/or 1 M sodium hydroxide was used.

Table 3.1: Details of batch adsorption experiment

Variable parameter	pH	Temperature	C_{Cu}	C_{EM}
pH	1.5-5	20 °C	0.1 g/L	10 g/L
Temperature	5	20 °C-65 °C	0.1 g/L	10 g/L
C_{Cu}	5	20 °C	0.01-0.1 g/L	10 g/L
C_{EM}	5	20 °C	0.1 g/L	1.5-25 g/L

3.2.4. Inductively coupled plasma emission spectroscopy

Five mL of supernatant after centrifugation and filtration was acid digested in two steps to remove carbon, which causes matrix interference in inductively coupled plasma emission spectroscopy (ICP-ES) (Wasilewska *et al.,* 2002). Details of the volumes of hydrochloric acid, nitric acid and hydrogen peroxide added to the sample are given in Table 3.2. Sample temperature was increased to 95 ºC to increase the reaction kinetics. 1 mL of hydrogen peroxide was added to those samples still containing precipitate after second stage. The residual copper concentration was measured by ICP-ES (Thermo Scientific 6000 series). The adsorption capacity of BSAEM and EWPEM was quantified using the percent of copper removal (R, %), calculated from the following equation:

$$R\% = \frac{(C_0 - C)}{C_0} \times 100 \qquad 3.1$$

Where C_0 and C are the initial and equilibrium copper concentration respectively (g/L). The equilibrium condition is achieved once there is no more change in the copper concentration in the system. The volume of protein added to the solution was taken into account in determining the initial concentration of copper ions.

Table 3.2: Details of acid digestion experiment

Stage	HCl	HNO_3	H_2O_2	Temperature	Time (h)
1st	5 mL	-----	-----	95 °C	2
2nd	-----	2 mL	0.5 mL	95 °C	1

3.2.5. Zeta potential measurements

Zeta-potential measurements were performed on both EWPEM and BSAEM using the microelectrophoretic apparatus ZetaPlus (Brookhaven Instruments Corporation, U.S.A.).

This instrument determines the electrophoretic mobility and converts to ζ-potential using Smoluchowski approximation. 10^{-3} M KCl was used as background electrolyte and to create

BSA and EWP-coated bubbles. Afterwards, 5 ml of AFE was diluted to 30 ml using 10^{-3} M KCl. Reported values are an average of 10 measurements.

3.2.6. X-ray photoelectron spectroscopy

X-ray photoelectron spectroscopy (XPS) of EWPEM and BSAEM, before and after metal ion adsorption was carried out using a monochromatic X-ray photoelectron spectrometer (Thermo Fisher scientific) to determine both the elemental composition and functional groups responsible for metal ion removal. The XPS was equipped with an Al Kα X-ray source (1486.6 eV, 0.834 nm), a microfocused monochromator, and ultrahigh vacuum chamber (10^{-9} Torr). Prior to XPS measurements, BSA and EWP powders and also precipitates of BSAEM and EWPEM obtained after copper adsorption were dried at 60 °C for 72 hours in a vacuum oven (VWR shellabs 1430). Afterwards they were finely ground using a hand mortar and pestle. An electron flood gun was employed during XPS analysis to prevent any surface charge effect. Elemental surveys from 0 to 1350 eV and high resolution were conducted with the pass energy adjusted to 1 and 0.1 eV respectively. Measurements were carried out on the three points for each sample with a spot size of 400 µm. The spectral deconvolution was performed using the software Thermo Avantage (Version 4.60).

3.2.7. Fourier transform infrared

In order to identify the functionalities being capable of interacting with copper ions in BSAEM and EWPEM, Fourier transform infrared spectroscopy (FTIR) technique was used. The spectra were recorded using a Bruker Tensor 27 IR spectrometer within the wavenumber range of 500-4000 cm^{-1}. 1024 scans and 4 cm^{-1} resolutions were applied in collecting spectra. The background obtained from the scan of KBr was automatically subtracted from the sample spectra.

3.3. Results and Discussion

3.3.1. FTIR results

The absorbance spectra of EWP and BSA before and after copper adsorption in the range of wavenumber 500-4000 cm^{-1} were recorded to clarify the nature of the interaction between copper ions and protein-coated bubbles. Intense characteristic bands obtained from functional groups present in the biosorbent are given in Table 3.3. As illustrated in Figure 3.2, the broad and strong absorbance peaks at 3342 and 3326 cm^{-1} for both BSA and EWP are representative of amino groups (NH_2) which is consistent with the peaks at 1174 (BSA) and 1159 (EWP) attributed to C–N stretching vibration. The bands at 2967 and 2875 cm^{-1} (BSA), 2967 and 2876 cm^{-1} (EWP) are due to asymmetric and symmetric vibration of CH_2. Strong bands at 1692 (BSA) and 1695 (EWP) cm^{-1} are attributed to the C=O and C–N (amide I) stretching vibration, although amide (II) bands at 1555 (BSA) and 1568 cm^{-1} (EWP) point to C–N stretching and N–H bending respectively. The IR bands at 1445 and 1399 (BSA) cm^{-1}, 1455 and 1402 (EWP) cm^{-1} are assigned to C–H bending. The absorbance band at 1079 cm^{-1} for EWP is the result of C–O deformation, while BSA absorbance does not show any band for C–O bending. No vibrational band centered around 2550 cm^{-1} (Mandal *et al.*, 2001; Panigrahi *et al.*, 2006) was detected for S–H, as only a few thiol groups are present in the structure of BSA and EWP.

Copper-loaded BSAEM illustrates absorbance bands at 1694, 1559 and 1456 cm^{-1} move to higher bands, while $–NH_2$ stretching, C–H asymmetric stretching of $–CH_2$, C–H bending and C–N deformation bands wave numbers are shifted to lower bands pointing to a major role of carboxylic, amide and amine groups of BSAEM in copper binding.

After copper adsorption by EWPEM, The peaks at 3326, 2967, 2876 and 1695 cm^{-1} are shifted to a higher wave number; however C–N stretching and N–H deformation absorbance band reduces to 1560 cm^{-1}. Furthermore, absorbance bands at 1455, 1402, 1159 and 1079 disappear. These facts indicate that carboxylic, amide and amine groups of EWPEM possibly are involved in copper adsorption.

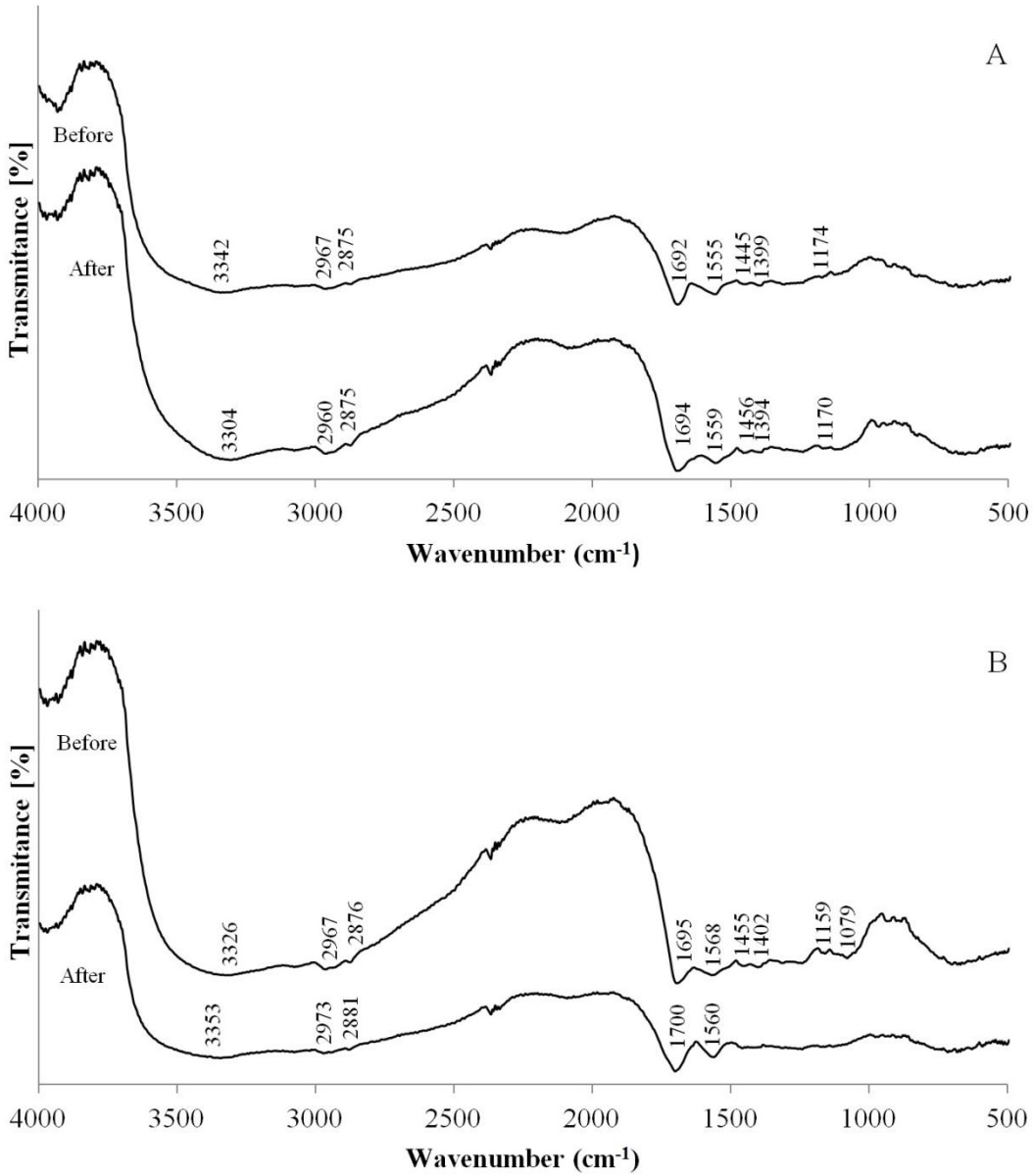

Figure 3.2: FTIR spectra of A) BSA and B) EWP before and after copper adsorption

Table 3.3: Wave numbers for main band in FTIR

Functional group	Wave number (cm^{-1})				
	EWP	EWPEM-Cu	BSA	BSAEM-Cu	Ref.
$–NH_2$ stretching	3326	3353	3342	3304	(Pagnanelli *et al.*, 2000)
C–H asymmetric stretching of $–CH_2$	2967	2973	2967	2960	(Wang *et al.*, 2010)
C–H symmetric stretching of $–CH_2$	2876	2881	2875	2875	(Wang *et al.*, 2010)
C=O and C–N (amide I) stretching	1695	1700	1692	1694	(Deng and Ting, 2005)
C–N stretching and N–H (amide II) bending	1568	1560	1555	1559	(Sun *et al.*, 2011)
C–H bending	1455	-------	1445	1456	(Bueno *et al.*, 2008)
C–H bending	1402	-------	1399	1394	(Bueno *et al.*, 2008)
C–N bending	1159	-------	1174	1170	(Deng and Ting, 2005)
C–O bending	1079	-------	-------	-------	(Villaescusa *et al.*, 2004)

3.3.2. XPS results

XPS has received much attention as technique in studying the nature of chemical bonds between adsorbates and adsorbents (Deng and Ting, 2005; Chen and Yang, 2006; Zheng *et al.*, 2009). In this work, XPS analysis was employed to probe the chemical interaction between functional groups present on the surface of EWP and BSA-coated bubbles and adsorbed copper ions. Figures 3.3A and 3.4A show a wide scan XPS spectrum of BSA and EWP respectively; Figure 3.3B and 3.4B show a survey scanning spectrum of copper-loaded BSAEM and copper-loaded EWPEM. The appearance of the Cu2p peak at a binding energy of 933.3 eV for both BSAEM and EWPEM in the XPS spectra (shown in Figure 3.3B and 3.4B) is attributed to the copper accumulation on the EWP and BSA-coated bubbles.

The S2p spectral region of neat BSA and EWP illustrates a doublet peak at binding energies of 163.5-164.7 and 163.2-164.4 eV which are attributed to S–S bond. No detectable intensity is present for thiol group which is consistent with the results obtained from FTIR. Figure 3.5A and 3.5B illustrate presence of three doublets in the sulfur spectrum. Binding energies of 161.5, 162.8 (copper-loaded BSAEM) and 161.6, 162.6 (copper-loaded EWPEM) indicate that the sulfur atoms are bound to the copper atoms as a thiolate species (Uvdal *et al.*,

1992; Dilimon *et al.*, 2012). The other doublet peaks are representative of disulfide and oxidized sulfur species. Due to the presence of sulfate ions (SO_4^{2-}) in the solution, an additional doublet peak at binding energies of 168, 169.3 (copper-loaded BSAEM) and 167.9, 169.3 (copper-loaded EWPEM), attributed to oxidized sulfur, is observed (Rupp and Weser, 1976).

The Cu2p spectra of copper (Figure 3.6A and 3.6B and Table 3.4) indicate the presence of CuO, Cu_2O, Cu(0), Cu–S in copper-loaded BSAEM and EWPEM which is in agreement with the mechanism of copper adsorption reported by several published literature (Atzei *et al.*, 2000; Rigo *et al.*, 2004; Dokken *et al.*, 2009; Dilimon *et al.*, 2012). Copper (II) is initially reduced to Cu (I) by RSH (a carbon-bonded to a sulfyhydryl) (Equation 3.2) forming an oxidized cystine (RS–SR) and then RSH reacts with Cu (I) to form the copper thiolate species (Equation 3.3). It is also feasible that Cu (0) forms as a result of the reduction of Cu (I) by RSH as shown in Equation 3.4.

$$2CuO + 2RSH \rightarrow Cu_2O + RS–SR + H_2O \quad (3.2)$$

$$Cu_2O + 2RSH \rightarrow 2RSCu + H_2O \quad (3.3)$$

$$Cu_2O + 2RSH \rightarrow 2Cu + RS–SR + H_2O \quad (3.4)$$

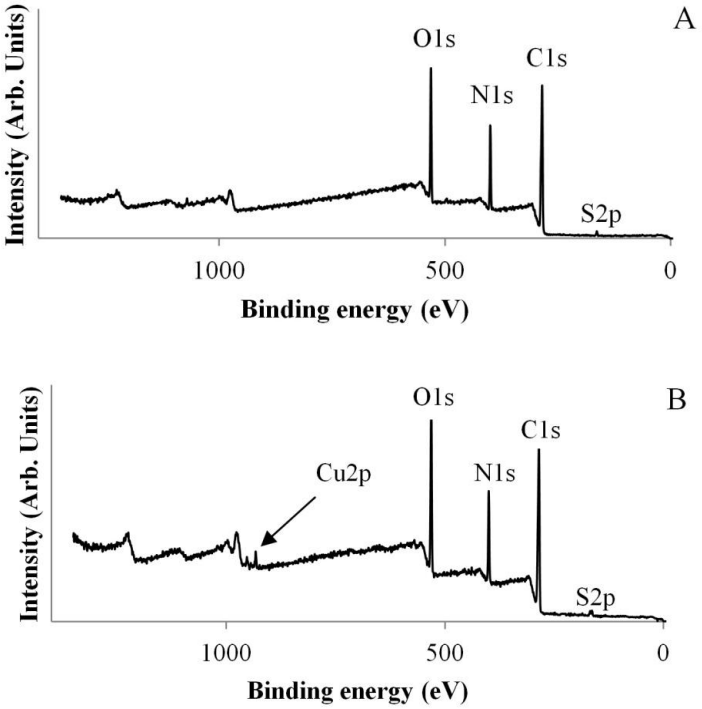

Figure 3.3: XPS survey scanning spectrum of (A) as received BSA and (B) copper-loaded BSAEM

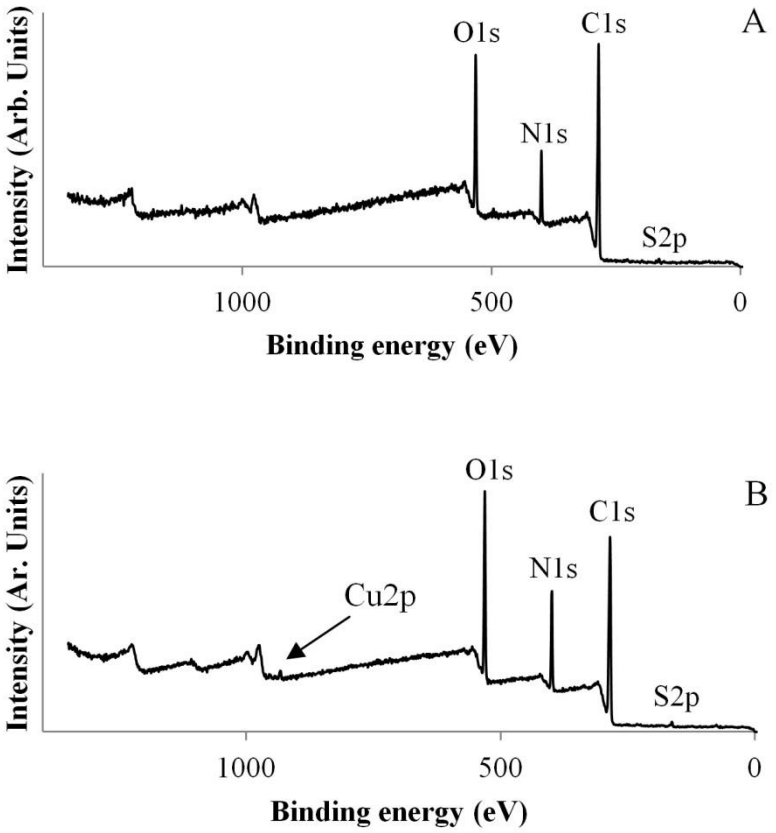

Figure 3.4: XPS survey scanning spectrum of (A) as received EWP and (B) copper-loaded EWPEM

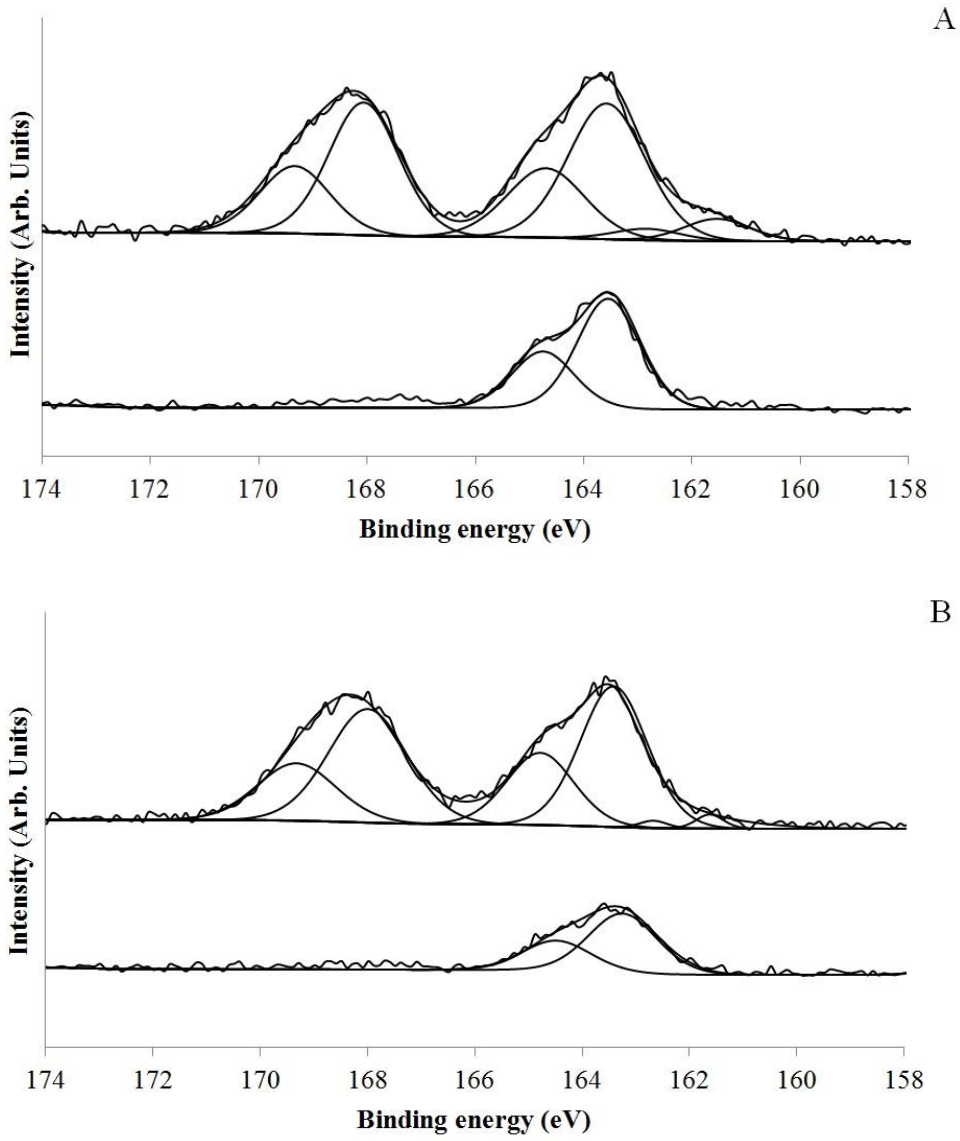

Figure 3.5: S2p spectra of (A) BSAEM and (B) EWPEM before and after copper adsorption

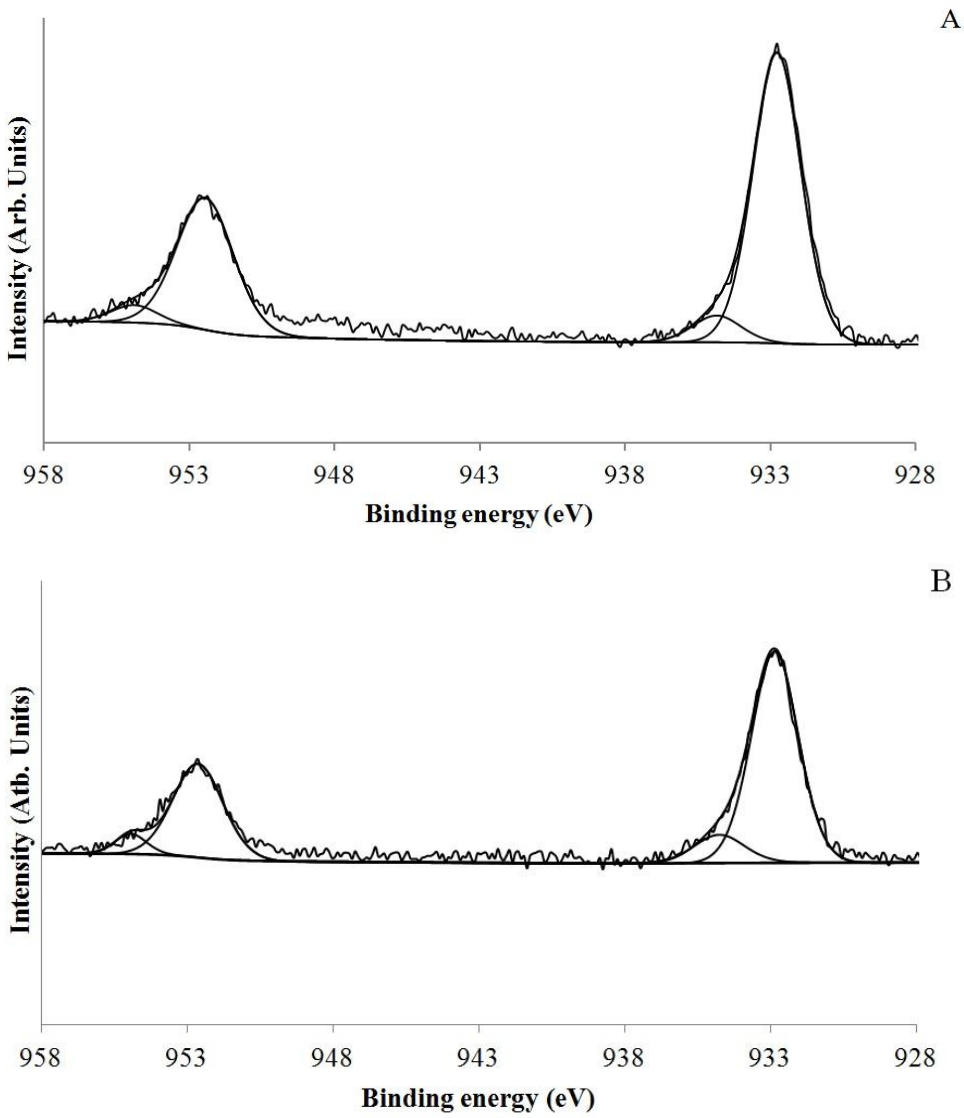

Figure 3.6: Cu2p spectra of (A) copper-loaded BSAEM and B) copper-loaded EWPEM

Table 3.4: Binding energies of sulfur and copper in BSAEM and EWPEM before and after copper adsorption

Valence state	Sample	Component	Binding energy (eV)
S2p3/2	BSA	S–S	163.5
	Cu-loaded BSAEM	Cu–S	161.5
		S–S	163.5
		S–O	168
	EWP	S–S	163.2
	Cu-loaded EWPEM	Cu–S	161.6
		S–S	163.4
		S–O	167.9
S2p1/2	BSA	S–S	164.7
	Cu-loaded BSAEM	Cu–S	162.8
		S–S	164.7
		S–O	169.3
	EWP	S–S	164.4
	Cu-loaded EWPEM	Cu–S	162.6
		S–S	164.7
		S–O	169.3
Cu2p3/2	Cu-loaded BSAEM	Cu (0), Cu_2O, Cu–S	932.4
		CuO	934.6
	Cu-loaded EWPEM	Cu(0), Cu_2O,Cu–S	932.8
		CuO	934.8
Cu2p1/2	Cu-loaded BSAEM	Cu(0), Cu_2O,Cu–S	952.3
		CuO	954.6
	Cu-loaded EWPEM	Cu(0), Cu_2O, Cu–S	952.6
		CuO	934.5

3.3.3. Effect of pH

The impact of pH on the copper adsorption mechanism is taken into account in terms of both the surface functional group of adsorbent, and adsorbate solution chemistry which is based on the copper ion speciation and competition between positively charged ions (Deng and Ting, 2005; Chen and Yang, 2006). Copper exists mostly in the form of Cu^{2+} at pH below 5, however increasing the pH to above 5 results in the hydrolysis of Cu^{2+} ions and subsequently formation of $Cu(OH)^{+}$, $Cu(OH)_2$, $Cu(OH)_3^{-}$ and $Cu(OH)_4^{-2}$ in more alkaline solutions, as shown in Table 3.5 (Doyle and Liu, 2003). In this study, adsorption experiments were performed at a pH below 5 to prevent the occurrence of copper hydrolysis products in the system.

Figure 3.7 details the percentage of copper removal by the EWPEM and BSAEM as a function of the solution pH. No copper removal was obtained at pH 1.5 and 2 due to the high concentration of hydrogen ions. The positively charged hydrogen ions compete with the metal ions for binding on the ligands present on the air cells' surface, and fewer active sites are

available for the formation of copper ion complexes. Furthermore, strong electrical repulsion at lower pH for EWPEM prevents the metal ions from contacting the bubbles' surface.

Table 3.5: Copper speciation at pH >6

Species	Reaction
$Cu(OH)^{+}$	$Cu^{2+} + H_2O \leftrightarrow Cu(OH)^{+} + H^{+}$
	$Cu^{2+} + 2H_2O \leftrightarrow Cu(OH)_2 + 2H^{+}$
$Cu(OH)_3^{-}$	$Cu^{2+} + 3H_2O \leftrightarrow Cu(OH)_3^{-} + 3H^{+}$
$Cu(OH)_4^{-2}$	$Cu^{2+} + 4H_2O \leftrightarrow Cu(OH)_4^{-2} + 4H^{+}$

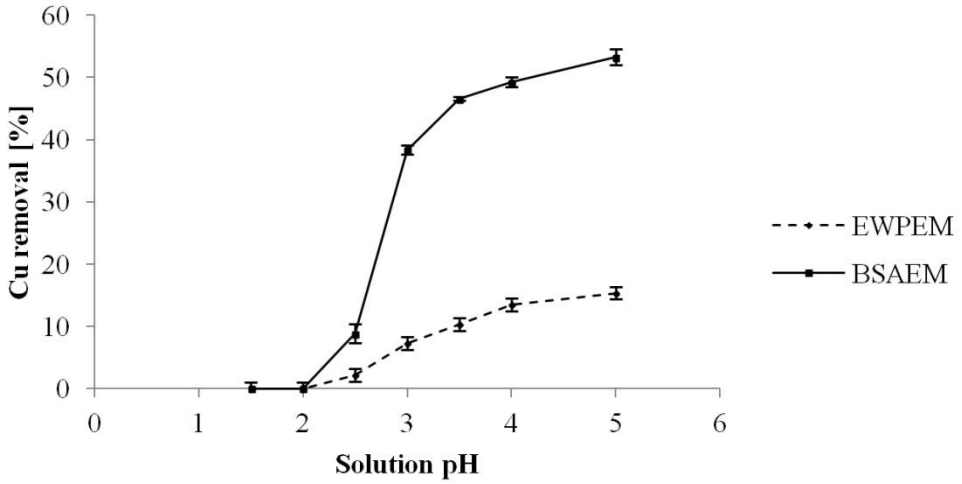

Figure 3.7: Effect of solution pH on copper removal (Copper concentration: 0.1 g/L, biosorbent concentration: 10 g/L, Contact time: one day, temperature: 20 °C). Each error bar illustrates the standard deviation of five measurements.

Figure 3.8 shows the zeta potential of the emulsions and it can be seen that the isoelectric point for both BSAEM and EWPEM is between a pH of 4 and 5. In aqueous acid solution, COO^{-} and $-S^{-}$ act as the basic site and accept a proton to yield -COOH and -SH respectively. It was observed that a higher pH led to greater metal uptake for both EWPEM and BSAEM, and eventually the maximum copper adsorption was obtained at pH 5, as the rise in solution pH not only decreases the hydrogen ion concentration but also increases attractive electrostatic interaction for metal cations with both biosorbents. Figure 3.7 also indicates that EWPEM has a lower extent of copper binding compared to that observed for BSAEM. This might be due to the higher number of active binding sites present at the surface of BSA-protein coated microcells.

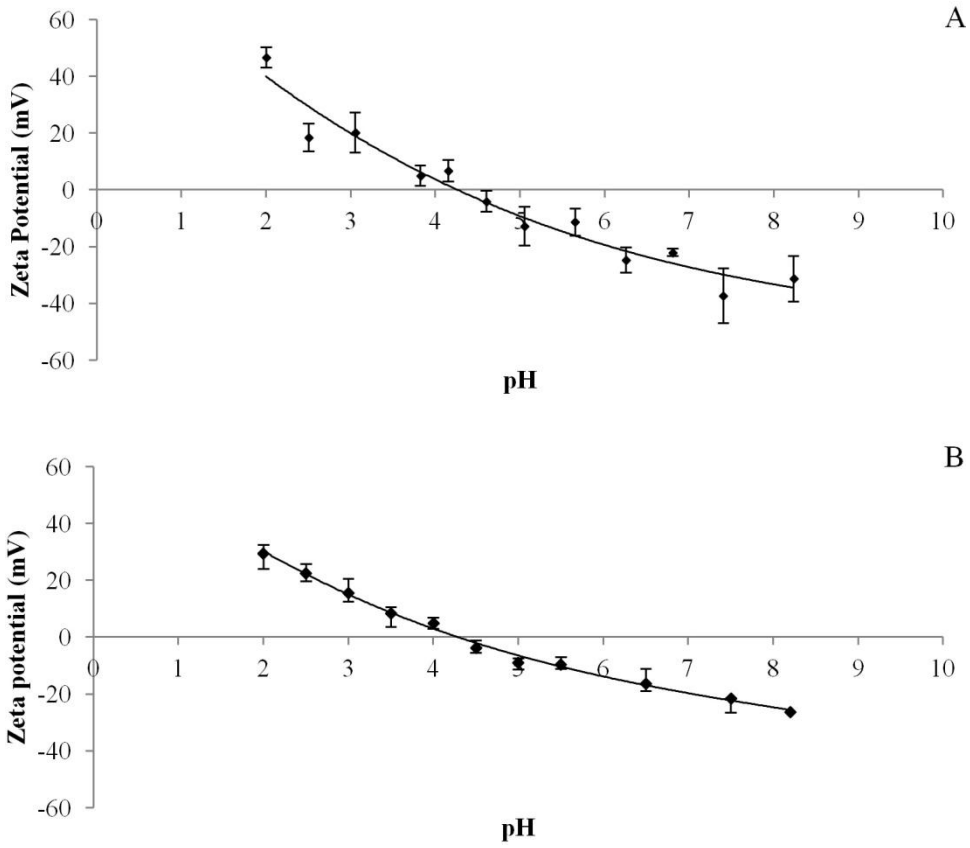

Figure 3.8: pH- Zeta potential diagrams of A) BSAEM and B) EWPEM.

3.3.4. Effect of temperature

Temperature has a noticeable effect on copper removal. As shown in Figure 3.9, as temperature was raised from 20 °C to 65 °C copper uptake improved up to 98% and 72% with BSAEM and EWPEM respectively. The increase of copper uptake with temperature rise might be due to the exposure of more functional groups which are initially buried in the interior of the protein structure (Kato *et al.*, 1981; Dickinson, 1986; Mine, 1996; Van der Plancken *et al.*, 2006). BSA and EWP exhibit a highly compact and tight structure due to the presence of hydrogen bonds and covalent disulfide bridges at room temperature. Increasing the temperature to 65 °C results in the rupture of hydrogen and noncovalent bonds, unfolding the protein structure and subsequently revealing active binding sites. The other reason for higher copper removal is an increase in reaction kinetics, as temperature rise causes ions present in the solution

to move faster resulting in higher probability of interaction between copper ions and functional groups on the surface of protein-coated bubbles.

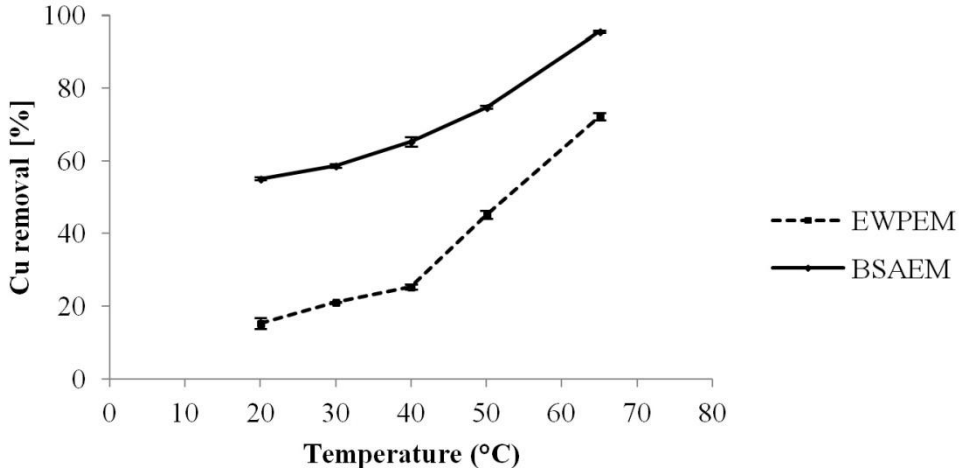

Figure 3.9: Effect of temperature on copper removal (Copper concentration: 0.1 g/L, biosorbent concentration: 10 g/L, Contact time at respective temperature: two hours, solution pH: 5). Each error bar illustrates the standard deviation of five measurements.

3.3.5. Effect of biosorbent concentration

The effect of biosorbent concentration (1.5 - 25 g/L) on copper ion removal from the cupric sulfate solution at pH 5 was investigated for both EWPEM and BSAEM. As shown in Figure 3.10, an increase in the BSAEM concentration resulted in the higher copper removal, until maximum metal uptake was reached at a concentration of 8 g/L. Further biomass addition diminished the copper removal and less than 5% copper uptake was observed above 20 g/L. This could be due to the formation of bubble aggregates at greater biosorbent dosage, thus reducing the effective surface area of bubbles. The number of functionalities for copper adsorption is therefore reduced. Figure 3.10 also details the copper removal percentage at different EWPEM concentrations. Increasing EWPEM concentration to 25 g/L increased copper uptake due to the presence of a greater number of active sites for copper removal at higher biomass dosage. However this amount is not comparable with that of BSAEM, as discussed in Section 3.3.3.

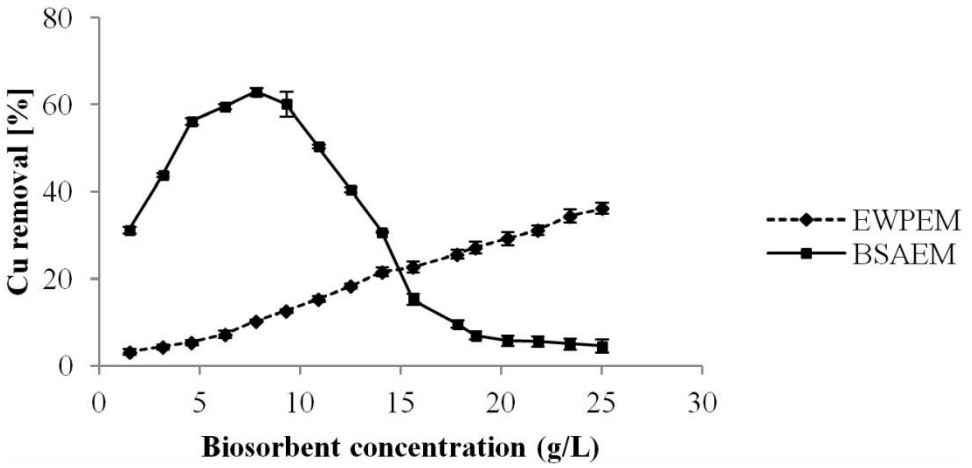

Figure 3.10: Effect of BSAEM and EWPEM dosage on copper removal (Copper concentration: 0.1 g/L, Contact time: one day, solution pH: 5, temperature: 20 °C). Each error bar illustrates the standard deviation of five measurements.

3.3.6. Effect of copper concentration

In order to investigate the effect of metal concentration on copper sorption, several experiments were carried out, the results of which are shown in Figure 3.11 for BSAEM and EWPEM. At 0.1 g/L, maximum copper removal was obtained at a BSAEM concentration of 10 g/L, however no metal uptake was seen at low copper concentrations (0.02 and 0.01 g/L). Reducing biosorbent amount to 1.2 g/L led to an increase in copper removal, up to almost 80% at a copper concentration of 0.01 g/L.

It is evident that the EWPEM is capable of binding many cupric ions at low concentration (<0.1 g/L) for specific biosorbent dosage due to the presence of more functional groups in the solution. It is interesting to note the extent of copper removal for 1.2 g/L of EWPEM is greater than that of 10 g/L. It is likely be an ionic strength effect that decreases in low copper concentration.

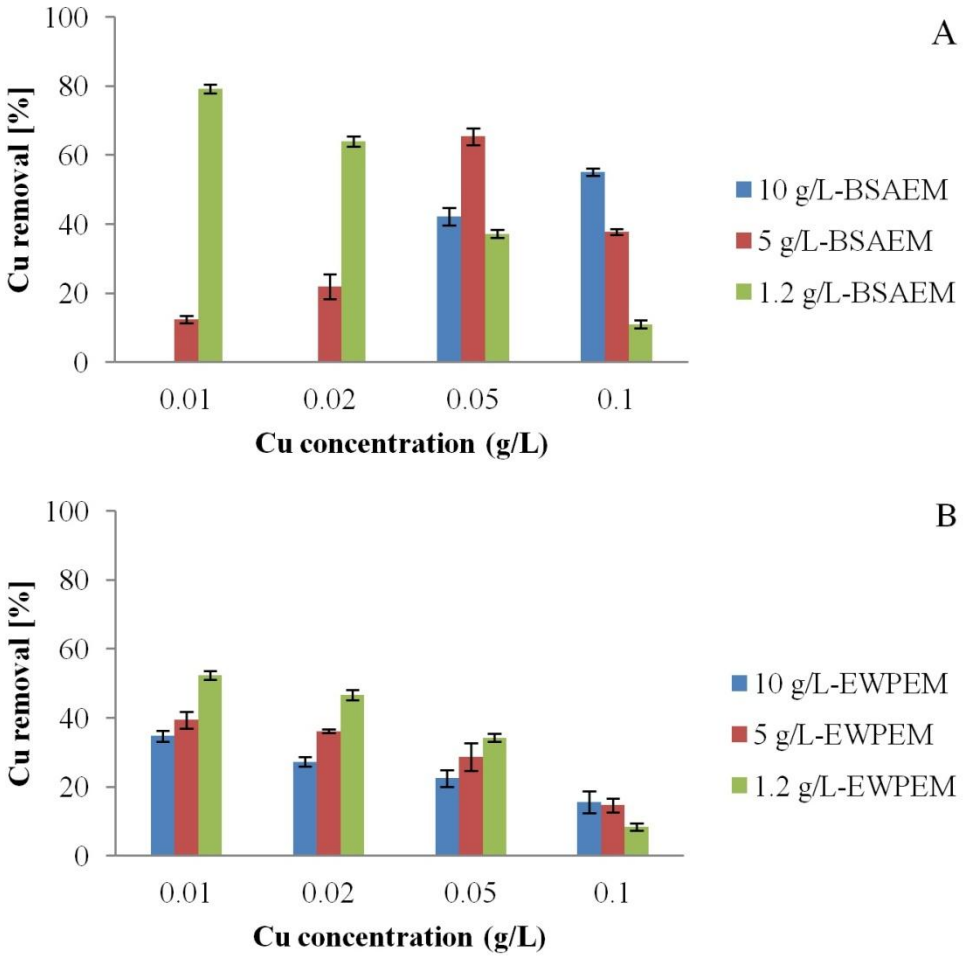

Figure 3.11: Effect of BSAEM and EWPEM dosage on copper removal (Copper concentration: 0.1 g/L, Contact time: one day, solution pH: 5, temperature: 20 °C). Each error bar illustrates the standard deviation of five measurements.

3.4. Conclusions

Micro-sized air cells stabilized by BSA and EWP constructed through an ultrasonic technique were used to remove copper ions from dilute solutions. FTIR and XPS techniques indicate that the thiol, amide, amine and carboxylate group existing on the surface of bubbles are capable of sorbing copper ion. As shown in Figure 3.12, copper adsorption by BSAEM and EWPEM is due to a combination of two mechanisms: physical adsorption and complexation, where copper ions are initially attracted *via* electrostatic interaction; and afterwards chemical bond would be created between copper ions and functional groups. BSAEM has a higher affinity for copper uptake compared to that of EWPEM. It was observed that increasing both solution pH

up to 5 and temperature led to higher copper adsorption. It was also shown that the lower the biosorbent dosage, the more copper was removed at low concentration of copper ions.

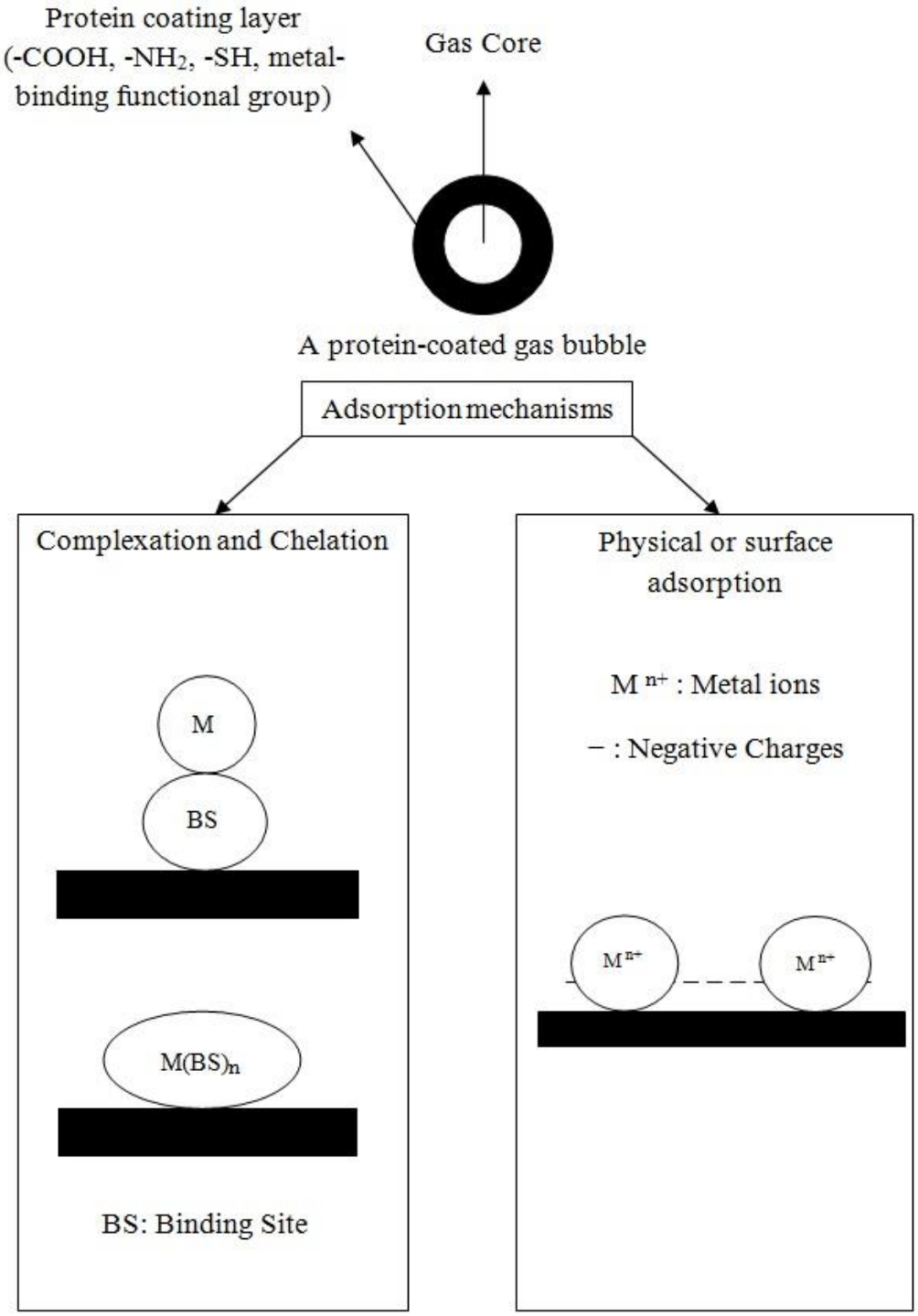

Figure 3.12: Proposed mechanism for copper adsorption by BSAEM and EWPEM

References

Atzei, D., Sadun, C. and Pandolfi, L., 2000. X-ray photoelectron spectra of complexes with 1-(D-3-mercapto-2-methylpropionyl)-1-proline and Ni, Cd and Cu: synthesis and LAXS study of Cu derivative. Spectrochimica Acta. Part A: Molecular and Biomolecular Spectroscopy 56(3), 531-540.

Avivi, S., Nitzan, Y., Dror, R. and Gedanken, A., 2003. An easy sonochemical route for the encapsulation of tetracycline in bovine serum albumin microspheres. Journal of the American Chemical Society 125(51), 15712-15713.

Avivi, S. and Gedanken, A., 2005. The preparation of avidin microspheres using the sonochemical method and the interaction of the microspheres with biotin. Ultrasonics Sonochemistry 12(5), 405-409.

Benaïssa, H. and Elouchdi, M.A., 2011. Biosorption of copper ions from synthetic aqueous solutions by drying bed activated sludge. Journal of Hazardous Materials 194, 69-78.

Bueno, B.Y.M., Torem, M.L., Molina, F. and de Mesquita, L.M.S., 2008. Biosorption of lead (II), chromium (III) and copper (II) by R. opacus: wquilibrium and kinetic studies. Minerals Engineering 21(1), 65-75.

Cabezon, L.M., Caballero, M. and Perez-Bustamante, J.A., 1994. Coflotation separation for the determination of heavy metals in water using colloidal gas aphrons systems. Separation Science and Technology 29(11), 1491-1500.

Cavalieri, F., Ashokkumar, M., Grieser, F. and Caruso, F., 2008. Ultrasonic synthesis of stable, functional lysozyme microbubbles. Langmuir 24(18), 10078-10083.

Cavalieri, F., Zhou, M. and Ashokkumar, M., 2010. The design of multifunctional microbubbles for ultrasound image-guided cancer therapy. Current Topics in Medicinal Chemistry 10(12), 1198-1210.

Cavalieri, F., Zhou, M., Caruso, F. and Ashokkumar, M., 2011. One-pot ultrasonic synthesis of multifunctional microbubbles and microcapsules using synthetic thiolated macromolecules. Chemical Communications 47(14), 4096-4098.

Chen, F., Finch, J.A., Distin, P.A. and Gomez, C.O., 2003. Air assisted solvent extraction. Canadian Metallurgical Quarterly 42(3), 277-280.

Chen, J.P., Hong, L., Wu, S. and Wang, L., 2002. Elucidation of interactions between metal ions and Ca alginate-based ion-exchange resin by spectroscopic analysis and modeling simulation. Langmuir 18(24), 9413-9421.

Chen, J.P. and Yang, L., 2006. Study of a heavy metal biosorption onto raw and chemically modified Sargassum sp. *via* spectroscopic and modeling analysis. Langmuir 22(21), 8906-8914.

Ciriello, S., Barnett, S.M. and Deluise, F.J., 1982. Separation science and technology removal of heavy metals from aqueous solutions using microgas dispersions. Separation Science and Technology 17(4), 521-534.

Dean, J.G., Bosqui, F.L. and Lanouette, K.H., 1972. Removing heavy metals from wastewater. Environmental Science and Technology 6(6), 518-522.

Deng, S. and Ting, Y.-P., 2005. Characterization of PEI-modified biomass and biosorption of Cu, Pb and Ni. Water Research 39(10), 2167-2177.

Dickinson, E., 1986. Mixed proteinaceous emulsifiers: review of competitive protein adsorption and the relationship to food colloid stabilization. Food Hydrocolloids 1(1), 3-23.

Dilimon, V.S., Denayer, J., Delhalle, J. and Mekhalif, Z., 2012. Electrochemical and spectroscopic study of the self-assembling mechanism of normal and chelating alkanethiols on copper. Langmuir 28(17), 6857-6865.

Dokken, K.M., Parsons, J.G., McClure, J. and Gardea-Torresdey, J.L., 2009. Synthesis and structural analysis of copper cysteine complexes. Inorganica Chimica Acta 362(2), 395-401.

Doyle, F.M. and Liu, Z., 2003. The effect of triethylenetetraamine (Trien) on the ion flotation of Cu^{2+} and Ni^{2+}. Journal of Colloid and Interface Science 258(2), 396-403.

Flett, D.S., Okuhara, D.N. and R., S.D., 1973. Solvent extraction of copper by hydroxyl oximes. Journal of Inorganic and Nuclear Chemistry 35(7), 2471-2487.

Gedanken, A., 2008. Preparation and properties of proteinaceous microspheres made sonochemically. Chemistry-A European Journal 14(13), 3840-3853.

Ghosh, S., Pandey, N.K., Bhattacharya, S., Roy, A. and Dasgupta, S., 2012. Fibrillation of hen egg white lysozyme triggers reduction of copper(II). International Journal of Biological Macromolecules 51(1), 1-6.

Grinberg, O., Hayun, M., Sredni, B. and Gedanken, A., 2007. Characterization and activity of sonochemically-prepared BSA microspheres containing Taxol-An anticancer drug. Ultrasonics Sonochemistry 14(5), 661-666.

Grinberg, O., Gedanken, A., Patra, C., Patra, S., Mukherjee, P. and Mukhopadhyay, D., 2009. Sonochemically prepared BSA microspheres containing Gemcitabine, and their potential application in renal cancer therapeutics. Acta Biomaterialia 5(8), 3031-3037.

Grinstaff, M.W. and Suslick, K.S., 1991. Air-filled proteinaceous microbubbles: synthesis of an echo-contrast agent. Proceedings of the National Academy of Sciences 88(17), 7708-7710.

Han, Y., Radziuk, D., Shchukin, D. and Moehwald, H., 2008. Stability and size dependence of protein microspheres prepared by ultrasonication. Journal of Materials Chemistry 18(42), 5162-5166.

Han, Y., Shchukin, D., Yang, J., Simon, C., Fuchs, H. and Möhwald, H., 2010. Biocompatible protein nanocontainers for controlled drugs release. ACS Nano 4(5), 2838-2844.

Kato, A., Tsutsui, N., Matsudomi, N., Kobayashi, K. and Nakai, S., 1981. Effects of partial denaturation on surface properties of ovalbumin and lysozyme. Agricultural and Biological Chemistry 45(12), 2755-2760.

Kentish, S.E. and Stevens, G.W., 2001. Innovations in separations technology for the recycling and re-use of liquid waste streams. Chemical Engineering Journal 84(2), 149-159.

Kocherginsky, N.M., Yang, Q. and Seelam, L., 2007. Recent advances in supported liquid membrane technology. Separation and Purification Technology 53(2), 171-177.

Kwan, J.J. and Borden, M.A., 2012. Lipid monolayer collapse and microbubble stability. Advances in Colloid and Interface Science 183-184, 82-99.

Largman, T. and Sifniades, S., 1978. Recovery of copper from aqueous solutions by means of supported liquid membranes. Hydrometallurgy 3(2), 153-162.

Li, C.-W., Chen, Y.-M. and Hsiao, S.-T., 2008. Compressed air-assisted solvent extraction (CASX) for metal removal. Chemosphere 71(1), 51-58.

Mandal, S., Das, G., Singh, R., Shukla, R. and Bharadwaj, P.K., 1997. Synthesis and studies of Cu(II)-thiolato complexes: bioinorganic perspectives. Coordination Chemistry Reviews 160, 191-235.

Mandal, S., Gole, A., Lala, N., Gonnade, R., Ganvir, V. and Sastry, M., 2001. Studies on the reversible aggregation of cysteine-capped colloidal silver particles interconnected *via* hydrogen bonds. Langmuir 17(20), 6262-6268.

Masood, F. and Malik, A., 2011. Biosorption of metal ions from aqueous solution and tannery effluent by Bacillus sp. FM1. Journal of Environmental Science and Health. Part A, Toxic/Hazardous Substances & Environmental Engineering 46(14), 1667-1674.

Mine, Y., 1996. Effect of pH during the dry heating on the gelling properties of egg white proteins. Food Research International 29(2), 155-161.

Pagnanelli, F., Petrangeli Papini, M., Toro, L., Trifoni, M. and Veglio, F., 2000. Biosorption of metal ions on arthtobacter sp.: biomass characterization and biosorption modeling. Environmental Science and Technology 34(13), 2773-2778.

Panigrahi, S., Kundu, S., Basu, S., Praharaj, S., Jana, S., Pande, S., Ghosh, S.K., Pal, A. and Pal, T., 2006. Cysteine functionalized copper organosol: synthesis, characterization and catalytic application. Nanotechnology 17(21), 5461-5468.

Parthasarathy, N. and Buffle, J., 1994. Capabilities of supported liquid membranes for metal speciation in natural waters: application to copper speciation. Analytica Chimica Acta 284(3), 649-659.

Preston, J.S. and Luklinska, Z.B., 1980. Solvent extraction of copper(II) with ortho-hydroxyoximes—I kinetics and mechanism of extraction. Journal of Inorganic and Nuclear Chemistry 42(3), 431-439.

Reddad, Z., Gerente, C., Andres, Y. and Le Cloirec, P., 2002. Adsorption of several metal ions onto a low-cost biosorbent: kinetic and equilibrium studies. Environmental Science and Technology 36(9), 2067-2073.

Rigo, A., Corazza, A., di Paolo, M.L., Rossetto, M., Ugolini, R. and Scarpa, M., 2004. Interaction of copper with cysteine: stability of cuprous complexes and catalytic role of cupric ions in anaerobic thiol oxidation. Journal of Inorganic Biochemistry 98(9), 1495-1501.

Ritcey, G.M. and Ashbrook, A.W. 1979. Solvent extraction: principles and application to process metallurgy, Elsevier, Amsterdam (NL).

Rubino, J.T. and Franz, K.J., 2012. Coordination chemistry of copper proteins: How nature handles a toxic cargo for essential function. Journal of Inorganic Biochemistry 107(1), 129-143.

Rupp, H. and Weser, U., 1976. Copper(I) and copper(II) in complexes of biochemical significance studied by X-Ray photoelectron spectroscopy. Bichimica et Biophysica Acta 446(1), 151-165.

Sahu, S.K., Agrawal, A., Pandey, B.D. and Kumar, V., 2004. Recovery of copper, nickel and cobalt from the leach liquor of a sulphide concentrate by solvent extraction. Minerals Engineering 17(7), 949-951.

Sengupta, B., Sengupta, R. and Subrahmanyam, N., 2006. Copper extraction into emulsion liquid membranes using LIX 984N-C®. Hydrometallurgy 81(1), 67-73.

Shchukina, E.M. and Shchukin, D.G., 2011. LbL coated microcapsules for delivering lipid-based drugs. Advanced Drug Delivery Reviews 63(9), 837-846.

Sheng, P.X., Ting, Y.P., Chen, J.P. and Hong, L., 2004. Sorption of lead, copper, cadmium, zinc, and nickel by marine algal biomass: characterization of biosorptive capacity and investigation of mechanisms. Journal of Colloid and Interface Science 275(1), 131-141.

Shindo, H. and Brown, T.L., 1965. Infrared spectra of complexes of L-Cysteine and related compounds with zinc, cadmium, mercury and lead. Journal of the American Chemical Society 87(9), 1904-1908.

Sun, F., Sun, W.-L., Sun, H.-M. and Ni, J.-R., 2011. Biosorption behavior and mechanism of beryllium from aqueous solution by aerobic granule. Chemical Engineering Journal 172(2), 783-791.

Suslick, K.S. and Grinstaff, M.W., 1990. Protein microencapsulation of nonaqeous liquids. Journal of the American Chemical Society 112(1), 7807-7809.

Tarkan, H.M. and Finch, J.A., 2005. Air-assisted solvent extraction: towards a novel extraction process. Minerals Engineering 18(1), 83-88.

Tchuenbou-Magaia, F.L., Norton, I.T. and Cox, P.W., 2011. Suspensions of air cells with cysteine-rich protein coats : Air-filled emulsions. Journal of Cellular Plastics 47(3), 217-232.

Uvdal, K., Bodo, P. and Liedberg, B., 1992. L-cysteine adsorbed on gold and copper : An X-Ray photoelectron spectroscopy study. Journal of Colloid and Interface Science 149(1), 162-173.

Valenzuela, F., Fonseca, C., Basualto, C., Correa, O., Tapia, C. and Sapag, J., 2005. Removal of copper ions from a waste mine water by a liquid emulsion membrane method. Minerals Engineering 18(1), 33-40.

Van der Plancken, I., Van Loey, A. and Hendrickx, M.E., 2006. Effect of heat-treatment on the physico-chemical properties of egg white proteins: A kinetic study. Journal of Food Engineering 75(3), 316-326.

Vassileva, E.D. and Koseva, N.S. 2010. Sonochemically born proteinaceous micro- and nanocapsules, Advances in Protein Chemistry and Structural Biology 80, 205-248.

Villaescusa, I., Fiol, N., Martinez, M., Miralles, N., Poch, J. and Serarols, J., 2004. Removal of copper and nickel ions from aqueous solutions by grape stalks wastes. Water Research 38(4), 992-1002.

Volesky, B., 2007. Biosorption and me. Water Research 41(18), 4017-4029.

Wang, X.-H., Song, R.-H., Teng, S.-X., Gao, M.-M., Ni, J.-Y., Liu, F.-F., Wang, S.-G. and Gao, B.-Y., 2010. Characteristics and mechanisms of Cu (II) biosorption by disintegrated aerobic granules. Journal of Hazardous Materials 179(1), 431-437.

Wang, X.S., Li, Z.Z. and Sun, C., 2009. A comparative study of removal of Cu(II) from aqueous solutions by locally low-cost materials: marine macroalgae and agricultural by-products. Desalination 235(1), 146-159.

Wasilewska, M., Goessler, W., Zischka, M., Maichin, B. and Knapp, G., 2002. Efficiency of oxidation in wet digestion procedures and influence from the residual organic carbon content on selected techniques for determination of trace elements. Journal of Analytical Atomic Spectrometry 17(9), 1121-1125.

White, J.M., Manning, R.A. and Li, N.C., 1956. Metal interaction with sulfur-containing amino acids. Nickel and copper complexes. Journal of the American Chemical Society 78(11), 2367-2370.

Xu, H. and Liu, Y., 2008. Mechanisms of Cd^{2+}, Cu^{2+} and Ni^{2+} biosorption by aerobic granules. Separation and Purification Technology 58(3), 400-411.

Zheng, J.-C., Feng, H.-M., Lam, M.H.-W., Lam, P.K.-S., Ding, Y.-W. and Yu, H.-Q., 2009. Removal of Cu(II) in aqueous media by biosorption using water hyacinth roots as a biosorbent material. Journal of Hazardous Materials 171(1), 780-785.

Zhou, M., Cavalieri, F. and Ashokkumar, M., 2011. Tailoring the properties of ultrasonically synthesised microbubbles. Soft Matter 7(2), 623-630.

Chapter 4. Biosorption of copper, nickel and cobalt ions from dilute solutions using BSA-coated air bubbles

4.1. Introduction

Immense quantities of heavy metal waste are discharged into the aquatic environment by means of both intentional release (industrial waste) and accidental release (chemical or oil spill). Acid mine drainage (AMD), a major source of heavy metal bearing effluents, has been increasing over the years as a result of mining and the mineral processing operations (Feng *et al.*, 2000), and is produced by the natural oxidation of sulfur bearing minerals (Demopoulos, 1998; Kuyucak, 2002). AMD has become a worldwide environmental concern due to its significant impact on the environment, both flora and fauna (Johnson and Hallberg, 2005; Akcil and Koldas, 2006). The cost of both control and treatment of AMD is extremely high, estimated to be greater than $3 billion in Canada (Tremblay and Hogan, 2001). AMD treatment methods are divided into active and passive mechanisms. An active mechanism involves a series of physico-chemical techniques such as pH modification, extraction using membranes, ion exchange and electrochemical treatments (Gélinas *et al.*, 2000; Utgikar *et al.*, 2000). Each process has drawbacks, including high energy requirements and capital cost. Biosorption is a promising technique which has recently been received growing attention for heavy metal ion removal by means of a biomass of microorganisms consisting of algae, bacteria, fungi and yeasts and products derived from these organisms (Sadowski, 2001; Deng *et al.*, 2003; Volesky, 2007; Wang *et al.*, 2009; Masood and Malik, 2011). Adsorption mechanisms of biomasses are attributed to the different functional groups (such as carboxylate, hydroxyl, sulfate, thiol, phosphate, ether, alcoholic, amide and amino) found on the biomass surface (Deng and Ting, 2005; Chen and Yang, 2006; Volesky, 2007; Arief *et al.*, 2008; Sud *et al.*, 2008; Zheng *et al.*, 2009). Finch and co-workers developed a novel technique known as air-assisted solvent extraction (AASX) based on the increasing specific surface area of organic by means of solvent-coated bubbles (Chen *et al.*, 2003; Tarkan and Finch, 2005). However, some parameters such as time required to form solvent-coated bubbles currently make this technique impractical to treat

large volumes of AMD. Properties of various treatment methods based on increasing interfacial surface area between metal ions and extractant are illustrated in Table 4.1.

Table 4.1: Comparison of different treatment methods for metal-containing aqueous systems

Technique	Mechanism	Advantages	Disadvantages	Reference
Membranes	Diffusion of the selected species to a permeable barrier to make concentrated stream	Selectivity, effective from 0.1 to 10,000 ppm,	Membrane instability, fouling	(Largman and Sifniades, 1978; Parthasarathy and Buffle, 1994; Valenzuela *et al.*, 2005; Sengupta *et al.*, 2006; Kocherginsky *et al.*, 2007)
Colloidal gas aphrons	Adsorption of the metal ions (electrostatic force or chemical bond) at the surface of surfactant-coated bubbles to make concentrated stream	Selectivity, high specific surface area of surfactant, formation of highly dispersed colloidal system to treat very dilute solution <100 ppm	High chemical dosage	(Ciriello *et al.*, 1982; Cabezon *et al.*, 1994)
Air-assisted solvent extraction	Metal ion adsorption at the surface of the solvent-coated bubbles to make concentrated stream	High specific surface area of organic phase, high aqueous/organic ratio, excellent phase separation, effective for < 100 ppm	low contact time of solvent-coated bubbles and metal ions, rapid disengagement of the bubbles, air flow rate limitation	(Chen *et al.*, 2003; Tarkan and Finch, 2005)

Tchuenbo-Magaia *et al.* (2011) sonicated cysteine-rich protein solutions to generate egg white protein (EWP) and bovine serum albumin (BSA)-stabilised air bubbles (<10 μm) which were dispersed through an aqueous medium. The aim of their research was to reduce the calorie content of food (Tchuenbou-Magaia *et al.*, 2011). This colloidal system, known as air-filled emulsion (AFE), is similar to the AASX technique in terms of both extent of specific surface area of organic phase and phase separation resulted from presence of fine coated bubbles; although they are distinguishable in light of bubble size, mechanism of bubble formation as well as the nature of coating material. In addition, waste obtained from the food and dairy industries are a good candidate to prepare cysteine-rich protein, rendering AFE a potentially cost-efficient and ecofriendly material (Myrnes and Johansen, 1994; Batista, 1999; Ostojić *et al.*, 2005).

Due to the presence of multiple heavy metal ions in AMD, in order to assess the feasibility of using AFE as a method of removing metal ions from aqueous systems, the uptake of copper, nickel and cobalt in a ternary mixture, along with the adsorption capacity of BSAEM were explored under different experimental conditions including pH, sorbent concentration, metal concentration and temperature.

4.2. Materials and methods

4.2.1. Materials

Dried bovine serum albumin (BSA) (fraction V) was purchased from Bishop Canada Inc. to generate AFE. Anhydrous copper (II) sulfate ($CuSO_4$) (Fisher Scientific, Canada), nickel (II) sulfate ($NiSO_4 \cdot 6H_2O$) (Anachemia, Canada), cobalt (II) sulfate heptahydrate ($CoSO_4 \cdot 7H_2O$) (Acros Organics, U.S.A.) were used to produce the aqueous copper, nickel and cobalt solutions respectively. All solutions were prepared using reverse osmosis purified water (pH of 5.8 at 25 ^oC). Hydrochloric acid (36%), nitric acid (67%) and hydrogen peroxide (50%) (Fisher Scientific, Canada) were used for BSA acid digestion. The solution pH was adjusted using 1 M sulfuric acid (98%).

4.2.2. Emulsion preparation

5 g of BSA was dissolved in 100 g of water stirred for 2 hours. Natural pH of BSA solution (7) was used to generate BSA emulsion. The solution was irradiated using a high intensity sonicator (UP 400 S, 24 kHz, Hielscher Inc, US). The emulsions are termed BSAEM. For more detailed description of the experimental protocol, please see Section 3.2.2.

4.2.3. Sorption experiments

0.01-0.1 g/L of copper (II), nickel (II) and cobalt (II) solution was made by dissolving copper (II) sulfate, nickel (II) sulfate and cobalt (II) sulfate in water. Details of batch experiments can be found in Section 3.2.3. Table 4.2 indicates the experimental condition parameters that were altered during sorption experiments to investigate qualitatively and

quantitatively their effect on metal removal. C_{EM} and $C_{Cu,Ni,Co}$ represent the concentration of BSAEM and metal ion respectively.

Table 4.2: Experimental conditions were examined during the batch experiments.

Parameter	pH	Temperature	$C_{Cu, Ni, Co}$	C_{EM}
pH	1.5-5	20 °C	0.1 g/L	10 g/L
Temperature	5	20 °C-65 °C	0.1 g/L	10 g/L
$C_{Cu, Ni, Co}$	5	20 °C	0.01-0.1 g/L	10 g/L
C_{EM}	5	20 °C	0.1 g/L	1.5-25 g/L

4.2.4. Contact time experiments

Figure 4.1 illustrates the extraction column used to investigate the time-dependent sorption behavior of BSAEM in 0.1 g/L of copper, nickel and cobalt. In the adsorption experiment, 250 mL of BSAEM was placed in 1 L of metal-ion solution. The column dimensions were: height 40 cm; diameter 9 cm; with an inlet near the bottom for biosorbent entry into the metal solution. The solution was mixed using a Cole Parmer lab stirrer for 7 hours at a speed of 400 rpm.

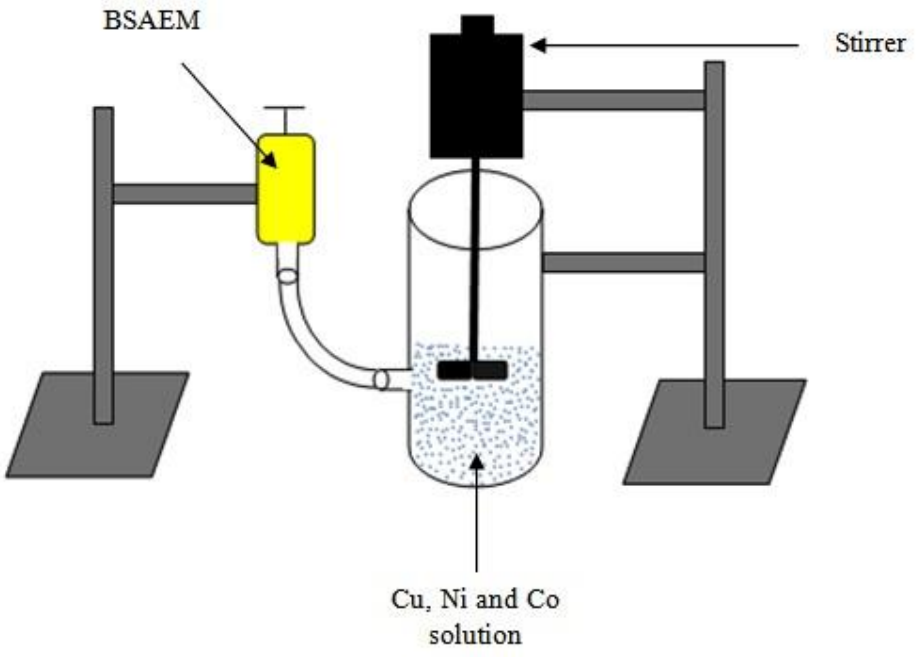

Figure 4.1: Schematic view of test setup to examine contact time effect on metal ion removal

4.2.5. Inductively Coupled Plasma Emission Spectroscopy (ICP)

Details of protein acid digestion are available in Section 3.2.4. The residual copper, nickel and cobalt concentrations were measured by inductively coupled plasma emission spectroscopy (ICP-ES) (Thermo Scientific 6000 series). The amount of copper adsorbed by BSA-coated microbubbles was quantified using the copper removal percentage (R, %), calculated from the following equation:

$$R\%=\frac{C_i-C_e}{C_i}\times 100 \qquad 4.1$$

Where C_i is the initial copper concentration (g/L), C_e is the equilibrium metal concentration (g/L). The equilibrium condition is considered when no more change in the metal concentration is detected. The volume of protein added to the metal ions solution is taken into account in determining the initial concentration of copper ions.

4.2.6. X-ray photoelectron spectroscopy

Interaction between metal ions and functional groups of BSAEM was elucidated using a monochromatic X-ray photoelectron spectrometer (Thermo Fisher scientific). The XPS was equipped with an Al Kα X-ray source (1486.6 eV, 0.834 nm), a microfocused monochromator, and ultrahigh vacuum chamber (10^{-9} Torr). Prior to XPS measurements, BSA powder and also precipitates of BSAEM obtained after metal ion adsorption were dried at 60 °C for 72 h in a vacuum oven (VWR shellabs 1430). Afterwards the samples were finely ground using a mortar and pestle to homogenise the powder. An electron flood gun was employed during XPS analysis to prevent surface charge effects. Elemental surveys from 0 to 1400 eV and high resolution were conducted with the pass energy adjusted to 1 and 0.1 eV respectively. Measurements were carried out on the three points for each sample with a spot size of 400 µm. The spectral deconvolution was performed using the software Thermo Avantage (version 4.60).

4.2.7. Fourier transform infrared

Infrared spectra of BSAEM before and after adsorbing copper, nickel and cobalt ions were recorded using a Bruker Tensor 27 IR spectrometer within the wavenumber range of 500-

4000 cm^{-1} in order to investigate which functionalities are capable of metal adsorption. 1024 scans and 4 cm^{-1} resolutions were applied in collecting spectra. The background obtained from the scan of KBr was automatically subtracted from the sample spectra.

4.2.8. Light microscopy

The microstructure of AFE before and after metal ion adsorption was examined using light microscopy (Olympus BX-51, Japan). One droplet of solution was placed on a microscopic slide and observed with a 20X objective lens.

4.3. Results and Discussion

4.3.1. FTIR results

The absorbance spectra of BSA before and after metal ion adsorption in the range of 500-4000 cm^{-1} were recorded to determine which functionalities on BSA-coated bubbles are responsible for sorbing metal ions. The resulting infrared peak assignments are given in Table 4.3. As illustrated in Figure 4.2, the intense and broad absorbance peak before sorbing metal at 3342 cm^{-1} is representative of amino groups (NH), consistent with the peak at 1174 to C–N stretching vibration. The bands at 2967 and 2875 cm^{-1} are due to the presence of asymmetric and symmetric vibration of CH_2. Strong band at 1692 BSA cm^{-1} is attributed to the C=O and C–N (amide I) stretching vibration, although amide (II) band at 1555 points to C–N stretching and N–H bending. The absorbance bands at 1404, 1174 and 1126 cm^{-1} are the result of C–O stretching, C–N bending and C=O deformation respectively. Therefore, functional groups such as carboxyl and amino groups are present on BSA. No vibrational band centered around 2550 cm^{-1} (Mandal *et al.*, 2001; Panigrahi *et al.*, 2006) was detected for S–H for BSA.

Metal-loaded BSAEM spectra illustrates that the absorbance band assigned to C=O and C–N stretching moves to higher band (1700 cm^{-1}); while $–NH_2$ stretching, C–H asymmetric stretching of $–CH_2$, C–N stretching and N–H bending wave numbers are shifted to lower bands; IR bands assigned to C–O stretching as well as C–N and C=O bending disappear. This indicates a major role of carboxylic group, imidazole, amino and peptide nitrogens of BSAEM in copper,

nickel and cobalt sorption which is in agreement with previous findings stated by Sadler *et al.* (1994) and Zhang *et al.* (2002) (Sadler *et al.*, 1994; Zhang and Wilcox, 2002).

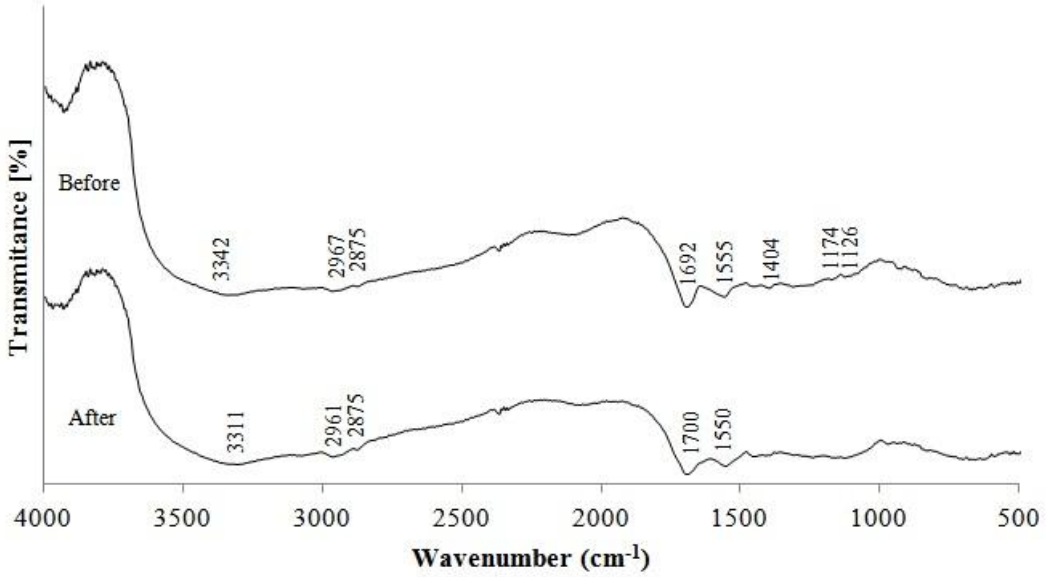

Figure 4.2: FTIR spectra of BSA before and after copper, nickel and cobalt adsorption

Table 4.3: Wave numbers for main band in FTIR

Functional group	Wave number (cm^{-1})		
	BSA	Cu, Ni and Co -loaded BSAEM	Ref.
$–NH_2$ stretching	3342	3311	(Pagnanelli *et al.*, 2000)
C–H asymmetric stretching of $–CH_2$	2967	2961	(Wang *et al.*, 2010)
C–H symmetric stretching of $–CH_2$	2875	2875	(Wang *et al.*, 2010)
C=O and C–N (amide I) stretching	1692	1700	(Deng and Ting, 2005; Dokken *et al.*, 2009)
C–N stretching and N–H (amide II) bending	1555	1550	(Sun *et al.*, 2011)
C–O stretching	1404	-----	(Ihs *et al.*, 1991)
C–N bending	1174	-----	(Deng and Ting, 2005)
C=O bending	1126	-----	(Deng *et al.*, 2003)

4.3.2. XPS results

XPS is a powerful technique for studying the nature of chemical bonds between adsorbates and adsorbents (Deng and Ting, 2005; Chen and Yang, 2006; Zheng *et al.*, 2009). In this work, XPS analysis was employed to probe the chemical interaction between functional groups present on the surface of BSA-coated bubbles and adsorbed copper, nickel and cobalt ions.

The S2p spectral region of neat BSA (Figure 4.3A) and metal-loaded BSAEM (Figure 4.3B) shows a doublet peak at a binding energy (BE) of 163.5-164.7 eV and 163.6-164.8 eV respectively, attributed to S–S bonds. No detectable intensity is present for the thiol group which is consistent with the results obtained from FTIR. Figure 4.3B reveals the presence of a doublet peak at BE of 161.8 and 162.9, indicating that the sulfur atoms are bound to the metal atoms as a thiolate species (Castner *et al.*, 1996; Lukkari *et al.*, 1999; Sung *et al.*, 2000). Due to the existence of sulfate ions (SO_4^{2-}) in the solution, an additional doublet peak at BE of 167.8-168.9 eV, attributed to oxidized sulfur, is observed (Rupp and Weser, 1976).

Table 4.4: Binding energy in BSAEM before and after metal ion adsorption

Valence state	Sample	Component	Binding energy (eV)	Reference
S2p3/2	BSA	S–S	163.5	(Castner et al., 1996)
	Cu, Ni and Co-loaded BSAEM	Metal–S	161.8	(Lukkari et al., 1999; Sung et al., 2000)
		S–S	163.6	(Castner et al., 1996)
		S–O	167.8	(Rupp and Weser, 1976)
S2p1/2	BSA	S–S	164.7	(Castner et al., 1996)
	Cu, Ni and Co-loaded BSAEM	Metal–S	162.9	(Lukkari et al., 1999; Sung et al., 2000)
		S–S	164.8	(Castner et al., 1996)
		S–O	168.9	(Rupp and Weser, 1976)

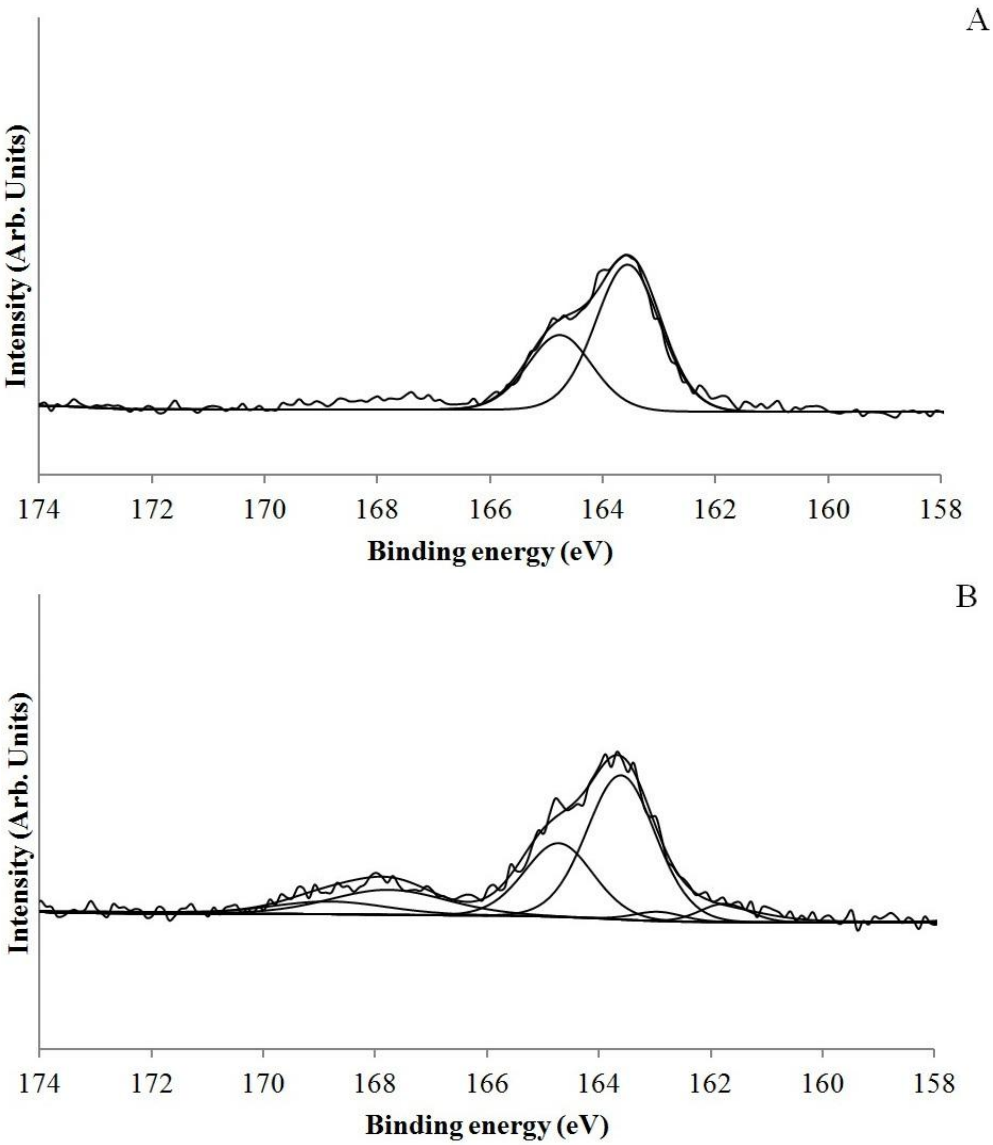

Figure 4.3: S2p spectra of BSAEM A) before and B) after metal adsorption

4.3.3. Effect of contact time

The adsorption kinetics of copper, nickel and cobalt on BSA-protein coated bubbles is shown in Figure 4.4. BSAEM exhibited approximately the same sorption behavior for copper, nickel and cobalt, and equilibrium was reached within 90 min. Adsorption kinetics of BSAEM demonstrated two steps during metal removal: (i) Extremely quick metal uptake stage (steep slope), as functional groups being responsible for copper, nickel and cobalt-ions are readily available on the surface of protein-coated bubbles and metal ions could diffuse rapidly through the protein layer surrounding the air core and eventually bind to the groups; (ii) Slow metal removal stage (low gradient) indicated by a slow rate of increase in metal uptake before equilibrium is reached and there is no further change in copper removal. This is due to the increasing coverage resulting in decreasing the availability of the active binding sites, rendering metal ions to compete with each other for the adsorption sites. The residual copper, nickel and cobalt concentrations were measured after one day, and they were similar to the one for 90 min.

As observed in Figure 4.5A, fine BSA-coated microcells are evenly distributed through the structure before injection into the metal ion solution. After metal adsorption, microbubbles are linked together by means of metal precipitate on their surfaces (Figure 4.5B). As illustrated in Figure 4.6, BSA-coated bubbles containing copper, nickel and cobalt precipitate accumulate in a top layer resulting from the buoyancy of bubbles, and full phase separation is achieved demonstrating an interesting property of AFE which could be utilised in a separation process.

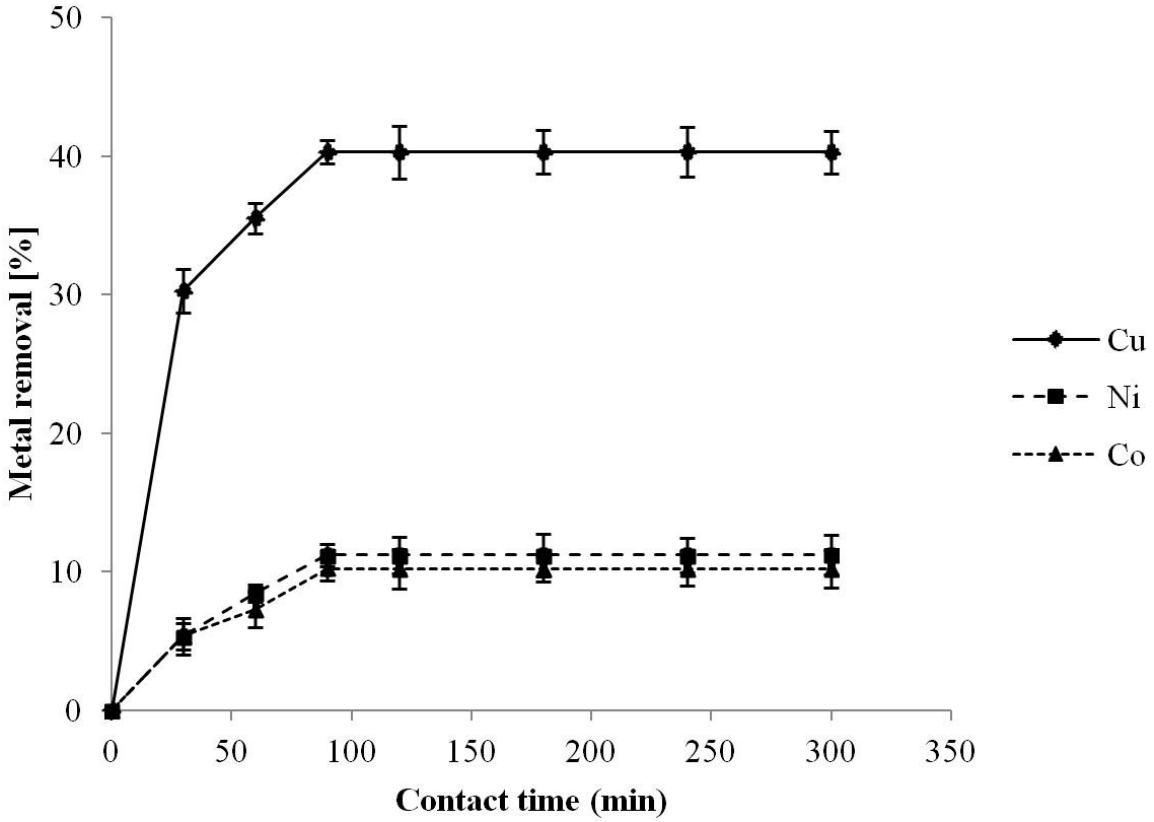

Figure 4.4: Effect of contact time on metal removal (copper, nickel and cobalt concentration: 0.1 g/L, biosorbent concentration: 10 g/L, temperature: 20 °C, solution pH: 5). Each error bar illustrates the standard deviation of five measurements.

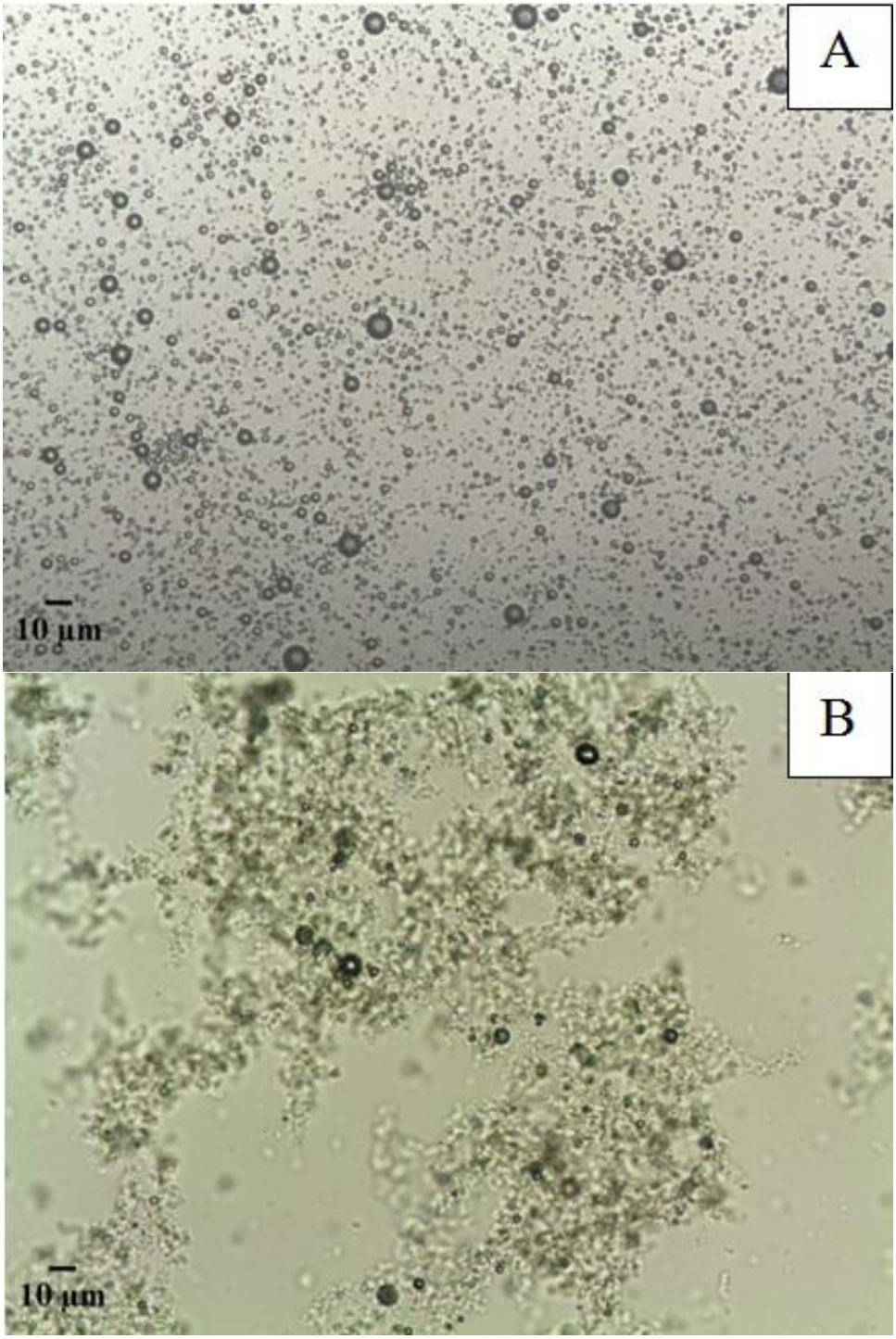

Figure 4.5: Optical micrograph of A) BSA-coated bubbles and B) copper, nickel and cobalt-loaded BSAEM

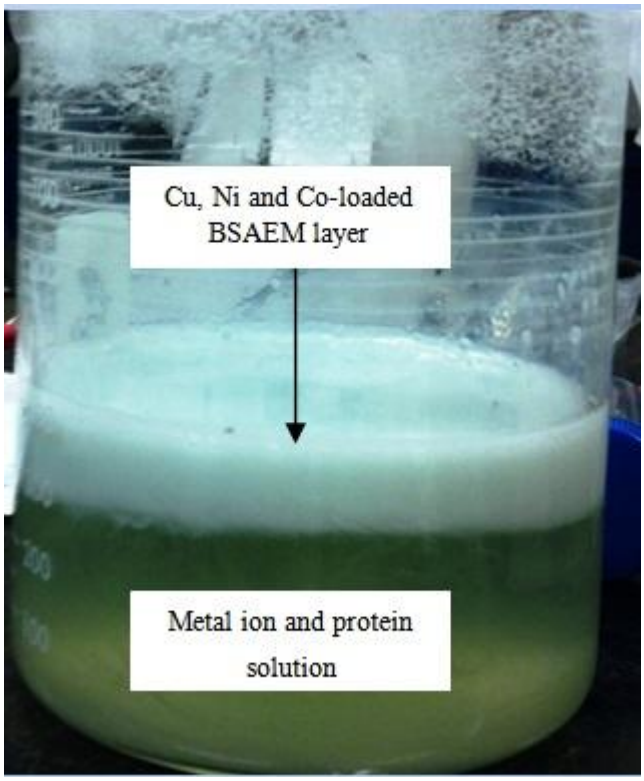

Figure 4.6: Metal-loaded BSAEM layer separated from the aqueous solution after one hour.

4.3.4. Effect of pH

The pH dependence of metal removal is described in terms of both surface functional group of BSA-coated bubbles and solution chemistry of copper, nickel and cobalt (Deng and Ting, 2005). In order to investigate pH impact on metal uptake metal solution pH was adjusted between 1.5-5, as copper exists entirely in its free ionic form (Cu^{2+}) at pH below 5 (Doyle and Liu, 2003); however nickel and cobalt ions present as Ni^{2+} and Co^{2+} until pH 8 (Krishnan and Anirudhan, 2008; Bhatnagar *et al.*, 2012). Figure 4.7 indicates that copper, nickel and cobalt adsorption as a function of metal solution pH follow a similar trend. At lower pH (1.5 and 2) no copper, nickel and cobalt removal was noticed in the light of the high concentration of hydrogen ions bound to the active binding sites of BSAEM rather than metal ions, and a strong repulsive electrostatic force hindering the transport of metal ions from the bulk solution to the bubble surface. At low pH, the protein surface exhibits an overall positive charge due to the protonation of the functional groups, consequently it is unable to adsorb positively charged heavy metal ions

(ζ potential diagrams of BSAEM can be found in Section 3.3.3). Copper uptake capacity of BSAEM increased sharply over the pH range from 2 to 4; however adsorption slightly increased in the case of nickel and cobalt. This is due to the fact that not only the hydrogen ion concentration diminishes, but also repulsive electrostatic force between metal ions and functional groups of BSA-coated microcells weakens, causing metal ions to be able to interact extensively with more ligands carrying negative charges. Once pH 4 was reached, a plateau was observed with additional pH increase, illustrating that electrostatic interaction was no longer dominant for copper, nickel and cobalt removal.

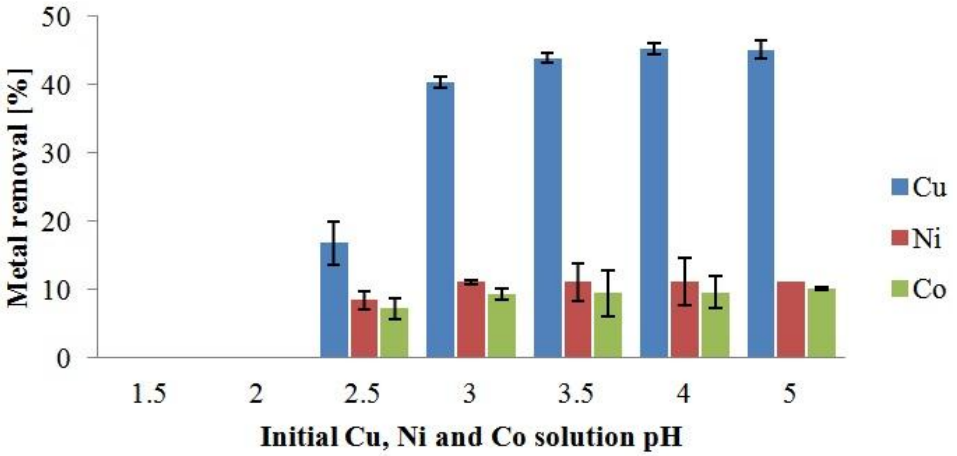

Figure 4.7: Effect of copper, nickel and cobalt solution pH on metal removal (copper, nickel and cobalt concentration: 0.1 g/L, biosorbent concentration: 10 g/L, Contact time: one day, temperature: 20 °C). Each error bar illustrates the standard deviation of five measurements.

Figure 4.7 demonstrates that copper ions are favorably adsorbed on BSA-coated bubbles over nickel and cobalt ions (Cu > Ni > Co); however Cu^{2+}, Ni^{2+} and Co^{2+} are all divalent cations. Heavy metal ions affinity are dependent upon different parameters such as ionic and hydrated ionic radius of metal ions, their hydration energy, charge and surface complexation (Deng and Ting, 2005; Lv *et al.*, 2005). Of the three, copper ions are the most readily adsorbed due to both their smaller radius and lower affinity to sorbent (low solubility), coupled with the lower hydrolysis constant, as shown in Table 4.5. The small ionic radius of copper ions results in higher charge densities on their surface, and consequently greater coulombic interactions between copper ions and active sites. Furthermore, the copper ions can diffuse through the

sorption sites easier than the nickel and cobalt ions and are bound to the functional groups. Irving-Williams order for the bivalent metal ions indicates that copper ions create the most stable ligand-metal complexes (Cu > Ni > Co) (Irving and Williams, 1952). Results obtained from Section 3.3.3 indicate that the extent of copper removal in a unary system is greater than that for ternary system, since nickel and cobalt ions suppress the reaction of copper ions with functional groups by means of blocking the sites on the BSA-coated bubbles.

Table 4.4: Ionic radius, hydrolysis constant (pK_h) and solubility product (K_{sp}) of metal ions (Yavuz *et al.*, 2003).

Metal ion	Copper (II)	Nickel (II)	Cobalt (II)
Ionic radius (Å)	0.7	0.72	0.74
pK_h	7.53	9.4	9.6
K_{sp} of $M(OH)_2$	1.6×10^{-19}	1.6×10^{-16}	2.5×10^{-16}

4.3.5. Effect of temperature

As shown in Figure 4.8, increasing temperature increased copper removal from 44% to 98%, although nickel and cobalt sorption increased only slightly to 16% and 13% respectively. The growth of metal uptake with temperature is owed not only to the revealing of more functional groups that are initially hidden in the interior of the BSA structure (Kato *et al.*, 1981; Dickinson, 1986; Mine, 1996; Van der Plancken *et al.*, 2006), but also increasing the diffusion rate of metal ions into the BSA layer; this subsequently increases the adsorption kinetics of copper, nickel and cobalt. Slower rates of increase in nickel and cobalt uptake illustrates both extremely high affinity of copper ions for binding sites, and decease in preventing effect of nickel and cobalt ions on copper removal.

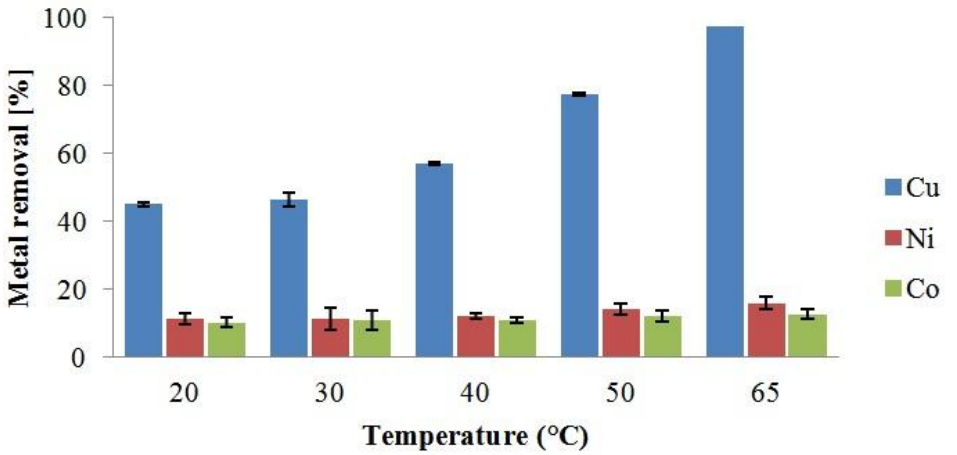

Figure 4.8: Effect of temperature on metal removal (copper, nickel and cobalt concentration: 0.1 g/L, biosorbent concentration: 10 g/L, Contact time at respective temperature: two hours, solution pH: 5). Each error bar illustrates the standard deviation of five measurements.

4.3.6. Effect of biosorbent concentration

The impact of BSAEM loading (1.5 - 25 g/L) on copper, nickel and cobalt removal in a ternary system was investigated. Figure 4.9 illustrates that increasing the BSAEM dosage led to a greater copper removal, until the maximum copper uptake was achieved at a concentration of approximately 10 g/L, due to an increase in the adsorption surface area and the availability of free active sites. Further biomass addition reduced the copper removal and approximately 2% copper adsorption was observed at concentrations above 17.5 g/L. Nickel and cobalt exhibited a similar trend to that of copper; maximum nickel and cobalt sorption (11%) was reached at 10 g/L. This might be attributable to the formation of aggregates occurred at higher concentration of BSAEM resulting in lower number of functional groups available for metal ions (Esposito *et al.*, 2001; Miretzky *et al.*, 2008).

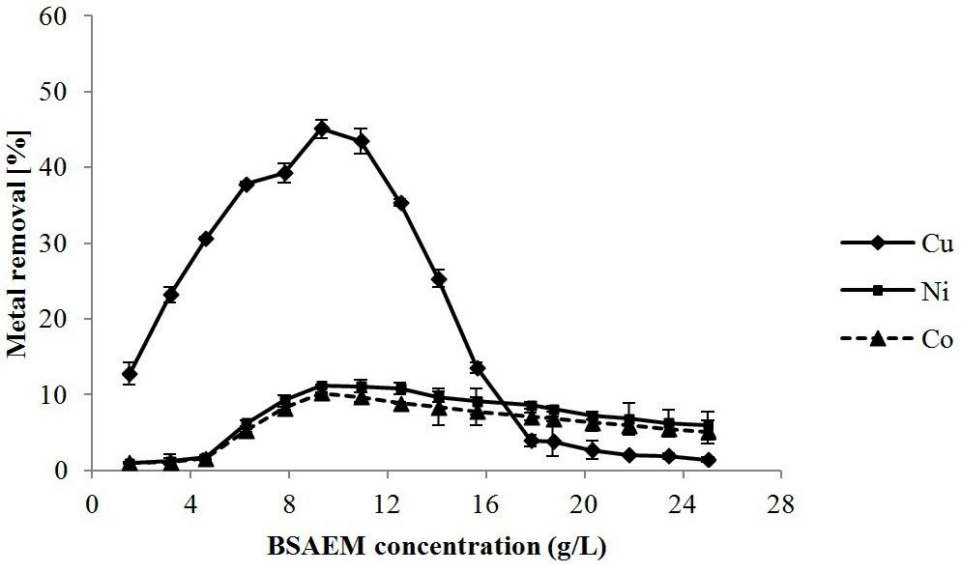

Figure 4.9: Effect of BSAEM concentration on metal removal (copper, nickel and cobalt concentration: 0.1 g/L, biosorbent concentration: 10 g/L, metal solution pH: 5, Contact time: one day, temperature: 20 °C). Each error bar illustrates the standard deviation of five measurements.

4.3.7. Effect of metal concentration

The metal ion concentration plays an important role in the removal through BSAEM. Batch experiments were carried out at various metal ion concentrations (0.01-0.1 g/L) to examine extent of copper, nickel and cobalt removal for 1.2, 5 and 10 g/L of BSAEM. Figure 4.10 shows that the BSAEM displayed interesting behavior at higher dosage compared to that of the other biosorbents reported (Blazquez *et al.*, 2012). In the case of 5 and 10 g/L of BSAEM, maximum copper removal was attained at 0.1 g/L, and a further decrease in metal ion concentration diminished copper removal. It is evident from Figure 4.10A and 4.10B that nickel and cobalt show the opposite behavior, and metal ion removal increases with decreasing concentration of nickel and cobalt. This trend could be explained as a consequence of aggregation of microcells that were formed in the solution resulting in a lower number of active sites, as BSAEM dosage increases. At 0.1 g/L of metal concentration, the probability of interaction between metal species and functional groups of BSA-coated bubbles is higher than that at lower metal ion concentration which results in higher copper ion removal (Blazquez *et al.*, 2012). In contrast, reducing biosorbent addition to 1.2 g/L, (subsequently decreasing the amount

of aggregates) led to an increase in copper, nickel and cobalt removal as the metal ion concentration decreases (Figure 4.10C).

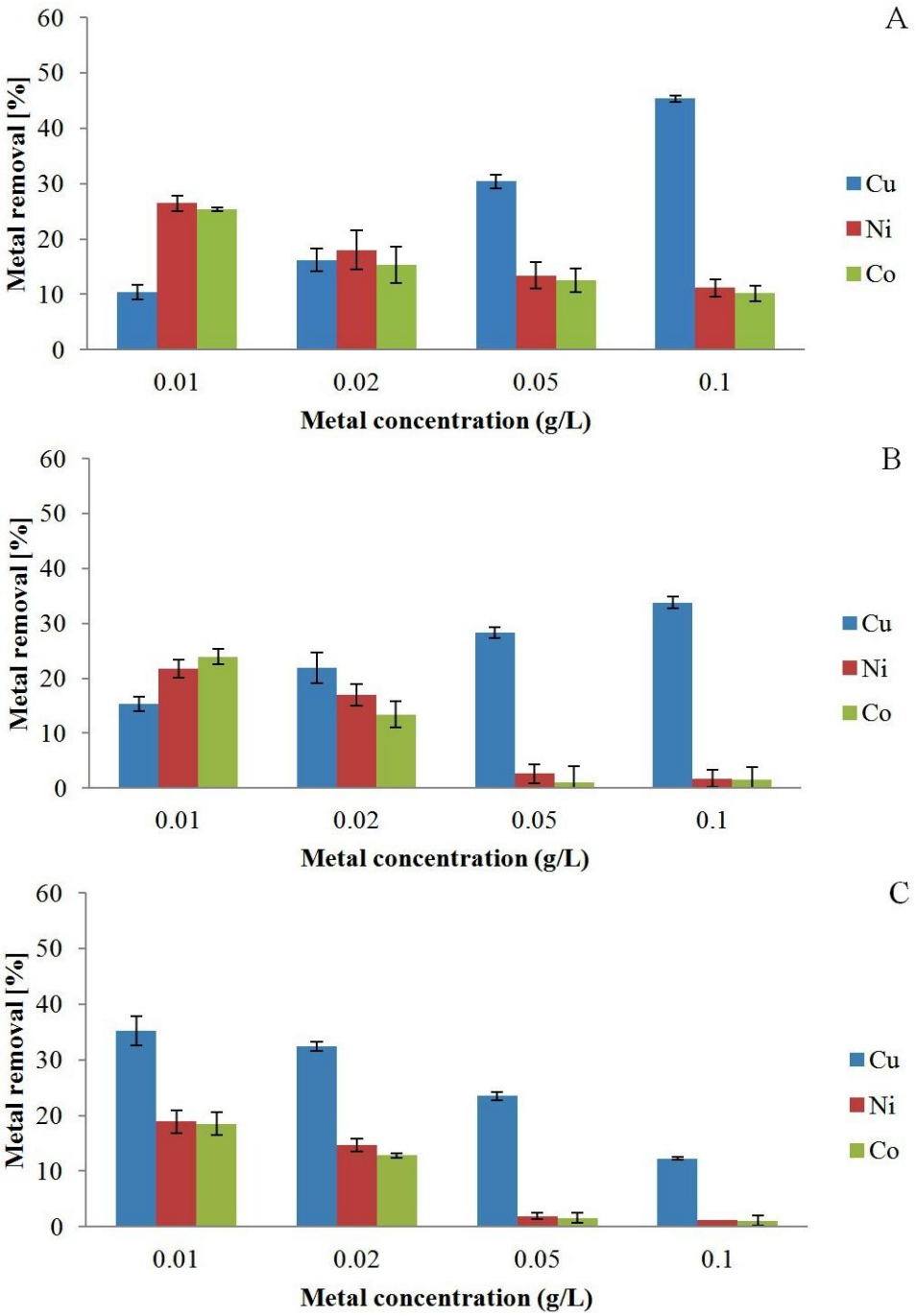

Figure 4.10: Effect of copper, nickel and cobalt concentration on metal removal (BSAEM concentration: A) 10, B) 5 and C) 1.2 g/L, Contact time: 1 day, metal solution pH: 5). Each error bar illustrates the standard deviation of five measurements.

4.4. Conclusions

Adsorption capacity of BSA-coated bubbles for a ternary system including copper, nickel and cobalt ions were examined. It is concluded that manipulation of experimental conditions has noticeable effect on metal ion removal. Increasing solution pH increases copper removal due to the exposure of more ligands containing negative charges and an increase in the attractive electrostatic interaction between positively charged metal ions and functional groups. Temperature was determined to be a significant factor in increasing metal ion sorption by revealing more ligands that are responsible for metal ion adsorption; and also increasing the probability of metal ion-ligand interaction. FTIR and XPS results indicated carboxylic, amino and thiol groups of BSAEM are capable of sorbing metal ions. The probable mechanism for metal ion adsorption is initial metal ion diffusion through the surface of the biomass coated microbubbles, thereafter ions are physically adsorbed by negative functional groups of BSA *via* electrostatic interaction, and finally metal ions are chemically bound to the functional groups.

It was evident that AFE is an effective material to selectively uptake metal ions using very low biomass dosage at very dilute metal ion solution (<0.05). Likewise, BSA-coated bubbles while linked together by heavy metal precipitate are placed in a top layer of the solution, and consequently could be easily removed from the solution. This phase disengagement as well as selectively heavy metal ion removal coupled with food and dairy industry waste as an abundant source of cysteine protein rendering this method potentially cost-effective and ecofriendly.

References

Akcil, A. and Koldas, S., 2006. Acid mine drainage (AMD): causes, treatment and case studies. Journal of Cleaner Production 14(12), 1139-1145.

Arief, V.O., Trilestari, K., Sunarso, J., Indraswati, N. and Ismadji, S., 2008. Recent progress on biosorption of heavy metals from liquids using low cost biosorbents: characterization, biosorption parameters and mechanism studies. Clean - Soil, Air, Water 36(12), 937-962.

Batista, I., 1999. Recovery of proteins from fish waste products by alkaline extraction. European Food Research and Technology 210(2), 84-89.

Bhatnagar, A., Vilar, V.J.P., Santos, J.C., Botelho, C.M.S. and Boaventura, R.A.R., 2012. Valorisation of marine Pelvetia canaliculata Ochrophyta for separation and recovery of nickel from water: Equilibrium and kinetics modeling on Na-loaded algae. Chemical Engineering Journal 200-202, 365-372.

Blazquez, G., Martin-Lara, M.A., Dionisio-Ruiz, E., Tenorio, G. and Calero, M., 2012. Copper biosorption by pine cone shell and thermal decomposition study of the exhausted biosorbent. Journal of Industrial and Engineering Chemistry 18(5), 1741-1750.

Cabezon, L.M., Caballero, M. and Perez-Bustamante, J.A., 1994. Coflotation separation for the determination of heavy metals in water using colloidal gas aphrons systems. Separation Science and Technology 29(11), 1491-1500.

Castner, D.G., Hinds, K. and Grainger, D.W., 1996. X-ray photoelectron spectroscopy sulfur 2p study of organic thiol and disulfide binding interactions with gold surfaces. Langmuir 12(21), 5083-5086.

Chen, F., Finch, J.A., Distin, P.A. and Gomez, C.O., 2003. Air assisted solvent extraction. Canadian Metallurgical Quarterly 42(3), 277-280.

Chen, J.P. and Yang, L., 2006. Study of a heavy metal biosorption onto raw and chemically modified Sargassum sp. *via* spectroscopic and modeling analysis. Langmuir 22(21), 8906-8914.

Ciriello, S., Barnett, S.M. and Deluise, F.J., 1982. Separation science and technology removal of heavy metals from aqueous solutions using microgas dispersions. Separation Science and Technology 17(4), 521-534.

Demopoulos, G.P., 1998. Review aqueous processing and its role in the production of inorganic materials and environmental protection. Canadian Metallurgical Quarterly 37(1), 1-18.

Deng, S., Bai, R. and Chen, J.P., 2003. Aminated polyacrylonitrile fibers for lead and copper removal. Langmuir 19(12), 5058-5064.

Deng, S., Bai, R. and Chen, J.P., 2003. Behaviors and mechanisms of copper adsorption on hydrolyzed polyacrylonitrile fibers. Journal of Colloid and Interface Science 260(2), 265-272.

Deng, S. and Ting, Y.-P., 2005. Characterization of PEI-modified biomass and biosorption of Cu, Pb and Ni. Water Research 39(10), 2167-2177.

Dickinson, E., 1986. Mixed proteinaceous emulsifiers: review of competitive protein adsorption and the relationship to food colloid stabilization. Food Hydrocolloids 1(1), 3-23.

Dokken, K.M., Parsons, J.G., McClure, J. and Gardea-Torresdey, J.L., 2009. Synthesis and structural analysis of copper cysteine complexes. Inorganica Chimica Acta 362(2), 395-401.

Doyle, F.M. and Liu, Z., 2003. The effect of triethylenetetraamine (Trien) on the ion flotation of Cu^{2+} and Ni^{2+}. Journal of Colloid and Interface Science 258(2), 396-403.

Esposito, A., Pagnanelli, F., Lodi, A., Solisio, C. and Veglio, F., 2001. Biosorption of heavy metals by Sphaerotitus natans: an equilibrium study at different pH a biomass concentrations. Hydrometallurgy 60(2), 129-141.

Feng, D., Aldrich, C. and Tan, H., 2000. Treatment of acid mine water by use of heavy metal precipitation and ion exchange. Minerals Engineering 13(6), 623-642.

Gélinas, S., Finch, J.A. and Vreugdenhil, A.J., 2000. Complexation of copper ions by DETA-terminated magnetic carriers. International Journal of Mineral Processing 59(1), 1-7.

Ihs, A., Liedberg, B., 1991. Chemisorption of L-cysteine and 3-mercaptopropionic acid on gold and copper surfaces : An infrared reflection-absorption study. Journal of Colloid and Interface Science 144(1), 282-292.

Irving, H. and Williams, R.J.P., 1952. The Stability of transition-metal complexes. Journal of Chemical Society (Resumed), 3192-3210.

Johnson, D.B. and Hallberg, K.B., 2005. Acid mine drainage remediation options: a review. Science of the Total Environment 338(1), 3-14.

Kato, A., Tsutsui, N., Matsudomi, N., Kobayashi, K. and Nakai, S., 1981. Effects of partial denaturation on surface properties of ovalbumin and lysozyme. Agricultural and Biological Chemistry 45(12), 2755-2760.

Kocherginsky, N.M., Yang, Q. and Seelam, L., 2007. Recent advances in supported liquid membrane technology. Separation and Purification Technology 53(2), 171-177.

Krishnan, K.A. and Anirudhan, T.S., 2008. Kinetic and equilibrium modelling of cobalt(II) adsorptiononto bagasse pith based sulphurised activated carbon. Chemical Engineering Journal 137(2), 257-264.

Kuyucak, N., 2002. Acid mine drainage prevention and control options. CIM Bulletin 95, 96-102.

Largman, T. and Sifniades, S., 1978. Recovery of copper from aqueous solutions by means of supported liquid membranes. Hydrometallurgy 3(2), 153-162.

Lukkari, J., Meretoja, M., Kartio, I., Laajalehto, K., Rajama, M., Lindstrom, M. and Kankare, J., 1999. Organic thiosulfates (bunte salts): novel surface-active sulfur compounds for the preparation of self-assembled monolayers on gold. Langmuir 15(10), 3529-3537.

Lv, L., Hor, M.P., Su, F. and Zhao, X.S., 2005. Competitive adsorption of Pb^{2+}, Cu^{2+}, and Cd^{2+} ions on microporous titanosilicate ETS-10. Journal of Colloid and Interface Science 287(1), 178-184.

Mandal, S., Gole, A., Lala, N., Gonnade, R., Ganvir, V. and Sastry, M., 2001. Studies on the reversible aggregation of cysteine-capped colloidal silver particles interconnected *via* hydrogen bonds. Langmuir 17(20), 6262-6268.

Masood, F. and Malik, A., 2011. Biosorption of metal ions from aqueous solution and tannery effluent by Bacillus sp. FM1. Journal of Environmental Science and Health. Part A, Toxic/Hazardous Substances & Environmental Engineering 46(14), 1667-1674.

Mine, Y., 1996. Effect of pH during the dry heating on the gelling properties of egg white proteins. Food Research International 29(2), 155-161.

Miretzky, P., Muñoz, C. and Carrillo-Chávez, A., 2008. Experimental binding of lead to a low cost on biosorbent: Nopal (Opuntia streptacantha). Bioresource Technology 99(5), 1211-1217.

Myrnes, B. and Johansen, A., 1994. Recovery of lysozyme from scallop waste. Preparative Biochemistry & Biotechnology 24(1), 69-80.

Ostojić, S., Pavlović, M., Živić, M., Filipović, Z., Gorjanović, S., Hranisavljević, S. and Dojčinović, M., 2005. Processing of whey from dairy industry waste. Environmental Chemistry Letters 3(1), 29-32.

Pagnanelli, F., Petrangeli Papini, M., Toro, L., Trifoni, M. and Veglio, F., 2000. Biosorption of metal ions on arthtobacter sp.: biomass characterization and biosorption modeling. Environmental Science and Technology 34(13), 2773-2778.

Panigrahi, S., Kundu, S., Basu, S., Praharaj, S., Jana, S., Pande, S., Ghosh, S.K., Pal, A. and Pal, T., 2006. Cysteine functionalized copper organosol: synthesis, characterization and catalytic application. Nanotechnology 17(21), 5461-5468.

Parthasarathy, N. and Buffle, J., 1994. Capabilities of supported liquid membranes for metal speciation in natural waters: application to copper speciation. Analytica Chimica Acta 284(3), 649-659.

Rupp, H. and Weser, U., 1976. Copper(I) and copper(II) in complexes of biochemical significance studied by X-Ray photoelectron spectroscopy. Bichimica et Biophysica Acta 446(1), 151-165.

Sadler, P.J., Tucker, A. and Viles, H.J., 1994. Involvement of a lysine residue in the N-terminal Ni^{2+} and Cu^{2+} binding site of serum albumins. European Journal of Biochemistry 220(1), 193-200.

Sadowski, Z., 2001. Effect of bisorption of Pb, Cu and Cd on the zeta potential and flocculation of Nacardia SP. Minerals Engineering 14(5), 547-552.

Sengupta, B., Sengupta, R. and Subrahmanyam, N., 2006. Copper extraction into emulsion liquid membranes using LIX 984N-C®. Hydrometallurgy 81(1), 67-73.

Sud, D., Mahajan, G. and Kaur, M.P., 2008. Agricultural waste material as potential adsorbent for sequestering heavy metal ions from aqueous solutions - a review. Bioresource Technology 99(14), 6017-6027.

Sun, F., Sun, W.-L., Sun, H.-M. and Ni, J.-R., 2011. Biosorption behavior and mechanism of beryllium from aqueous solution by aerobic granule. Chemical Engineering Journal 172(2), 783-791.

Sung, M.M., Sung, K., Kim, C.G., Lee, S.S. and Kim, Y., 2000. Self-assembled monolayers of alkanethiols on oxidized copper surfaces. The Journal of Physical Chemistry B 104(10), 2273-2277.

Tarkan, H.M. and Finch, J.A., 2005. Air-assisted solvent extraction: towards a novel extraction process. Minerals Engineering 18(1), 83-88.

Tchuenbou-Magaia, F.L., Norton, I.T. and Cox, P.W., 2011. Suspensions of air cells with cysteine-rich protein coats : Air-filled emulsions. Journal of Cellular Plastics 47(3), 217-232.

Tremblay, G.A. and Hogan, C.M., 2001. CANMET Mend Manual Volume 1.

Utgikar, V., Chen, B.-Y., Tabak, H.H., Bishop, D.F. and Govind, R., 2000. Treatment of acid mine drainage: I. Equilibrium biosorption of zinc and copper on non-viable activated sludge. International Biodeterioration & Biodegradation 46(1), 19-28.

Valenzuela, F., Fonseca, C., Basualto, C., Correa, O., Tapia, C. and Sapag, J., 2005. Removal of copper ions from a waste mine water by a liquid emulsion membrane method. Minerals Engineering 18(1), 33-40.

Van der Plancken, I., Van Loey, A. and Hendrickx, M.E., 2006. Effect of heat-treatment on the physico-chemical properties of egg white proteins: A kinetic study. Journal of Food Engineering 75(3), 316-326.

Volesky, B., 2007. Biosorption and me. Water Research 41(18), 4017-4029.

Wang, X.-H., Song, R.-H., Teng, S.-X., Gao, M.-M., Ni, J.-Y., Liu, F.-F., Wang, S.-G. and Gao, B.-Y., 2010. Characteristics and mechanisms of Cu (II) biosorption by disintegrated aerobic granules. Journal of Hazardous Materials 179(1), 431-437.

Wang, X.S., Li, Z.Z. and Sun, C., 2009. A comparative study of removal of Cu(II) from aqueous solutions by locally low-cost materials: marine macroalgae and agricultural by-products. Desalination 235(1), 146-159.

Yavuz, O., Altunkaynak, Y. and Guzel, F., 2003. Removal of Copper, Nickel, Cobalt and Manganese from Aqueous Solution by Kaolinite. Water Research 37, 948-952.

Zhang, Y. and Wilcox, D.E., 2002. Thermodynamic and spectroscopic study of Cu(II) and Ni(II) binding to bovine serum albumin. Journal of Biological Inorganic Chemistry 7(3), 327-337.

Zheng, J.-C., Feng, H.-M., Lam, M.H.-W., Lam, P.K.-S., Ding, Y.-W. and Yu, H.-Q., 2009. Removal of Cu(II) in aqueous media by biosorption using water hyacinth roots as a biosorbent material. Journal of Hazardous Materials 171(1), 780-785.

Chapter 5. Biosorptive flotation of copper ions from dilute solutions using BSA-coated bubbles

5.1. Introduction

Toxic heavy metal-bearing effluents generated in mining, metallurgical operations, petroleum, chemical manufacturing are considered to be a serious threat to human health and living organisms. The danger is not only the heavy metal concentration in the wastes being several times above permissible level, but also that they disperse into the environment by means of flowing ground water (Chen *et al.*, 2002; Deng *et al.*, 2003; Sheng *et al.*, 2004). Therefore, efforts have been directed to develop low-cost and eco-friendly methods and materials to recover metal ions from industrial streams over the past few decades. Biosorbents, including a biomass of microorganisms such as algae, bacteria, fungi and yeasts, have become promising materials to removing heavy metal ions from metal-bearing effluents due to the diversity of active sites for metal uptake, as well as its low-cost (Sadowski, 2001; Deng *et al.*, 2003; Volesky, 2007; Wang *et al.*, 2009; Masood and Malik, 2011). The by-products, sludge and wastes obtained from food, beverage, dairy and agricultural industries are an abundant source of biosorbent (Reddad *et al.*, 2002; Deng and Ting, 2005; Xu and Liu, 2008).

In addition to the capacity of biosorbents for metal sorption, the removal of heavy metal-loaded biomass from waste streams is a key factor to determine the efficiency of the technique. Centrifugation and sedimentation, the conventional separation techniques, are not suitable in the case of metal-bearing biosorbent due to the small size of solid particles present. In sedimentation large settling tanks are needed due to long retention times. Moreover, centrifugation is an expensive technique for fine particle separation owing to the power demand per unit mass of biosorbents recovered (Matis *et al.*, 1994; Peleka and Matis, 2009). Flotation has received much attention in the field of wastewater treatment due to its ability to float fine and ultrafine particles from a suspension. Several researchers have used flotation to separate metal-loaded biosorbent from the waste streams (Aldrich and Feng, 2000; Zouboulis *et al.*, 2001; Zouboulis and Matis, 2009; Zamboulis *et al.*, 2011).

A novel material known as air-filled emulsion (AFE), introducing high surface area between metal ions and biosorbent, was used for copper removal. AFE is a highly stable colloidal system containing fine cysteine protein-coated bubbles as a dispersed phase distributed through the aqueous phase. Flocculation is a process in which the particles of a colloidal suspension form large aggregates. Flocculants carry active groups which interact with charged particles, leading to destabilization of the suspension by means of either bridging or charge neutralization (Subrahmanyam and Forssberg, 1990; Guibal and Roussy, 2007). Aggregates either float or settle (sedimentation) which is dependent upon the density of the dispersed phases in the colloidal system. The cationic flocculant was added to the solution to form large clusters of copper-loaded bubbles in order to achieve two goals: (i) Destabilization of the AFE; (ii) Formation of the large bubble aggregates resulting in an increase in the buoyancy of the bubbles, as well as higher interaction between flotation bubbles and bubble flocs. Thereafter, copper-loaded microbubbles were separated from the solution using flotation. Recovery of copper ions was examined under different experimental conditions including solution pH and collector concentration.

5.2. Materials and methods

5.2.1. Materials

BSA (fraction V) was purchased from Bishop Canada Inc. to synthesize BSA-coated microcells. All solutions were prepared using reverse osmosis purified water (pH of 5.8 at 25 ^{o}C), unless otherwise stated. Hexadecyltrimethyl ammonium bromide (HTAB) from Fluka, dodecylamine (DA) and hexadecylamine (HA) from Aldrich were used as cationic collectors. They were dissolved in ethanol (Acros) with final concentration was 0.6% v/v. Polyacrylamide FLOPAM FO 4125 SH (cationic flocculant) was provided by SNF, USA. Flocculant stock solution (5 g/L) was made by dissolving flocculant powder in purified water, and stirred for 5 hours. Anhydrous cupric sulfate ($CuSO_4$) (Fisher Scientific, Canada) was used for preparation of metal solution. Solution pH was adjusted using 10^{-1} M sodium hydroxide and 10^{-1} M sulfuric acid (Fisher Scientific, Canada). Hydrochloric acid (36%), nitric acid (67%) and hydrogen peroxide (50%) (Fisher Scientific, Canada) were used for acid digestion of the proteins.

5.2.2. Emulsion preparation

Fifty g/L BSA solution was prepared by dissolving BSA in purified water, stirred for 2 hours in room temperature. The temperature of BSA solution was increased to 50 °C (well below the thermal denaturation temperature) using water bath, to increase the hydrophobic interaction between proteins by revealing more hydrophobic groups. Afterwards, 80 mL of BSA solution was transferred into the jacketed beaker (Figure 5.1) in order to both maintain the temperature at 50 °C and prevent local heat effect (to minimize flocculation) producing during sonication. An ultrasonic probe (22 mm in diameter) was positioned at the protein-air interface. The solution was irradiated with a high intensity sonicator (UP 400 S, 24 kHz, Hielscher Inc., U.S.A.) while compressed air was bubbled through the solution at 60 mL/min using a frit. Sonication time and power were 3 min and 90 W respectively.

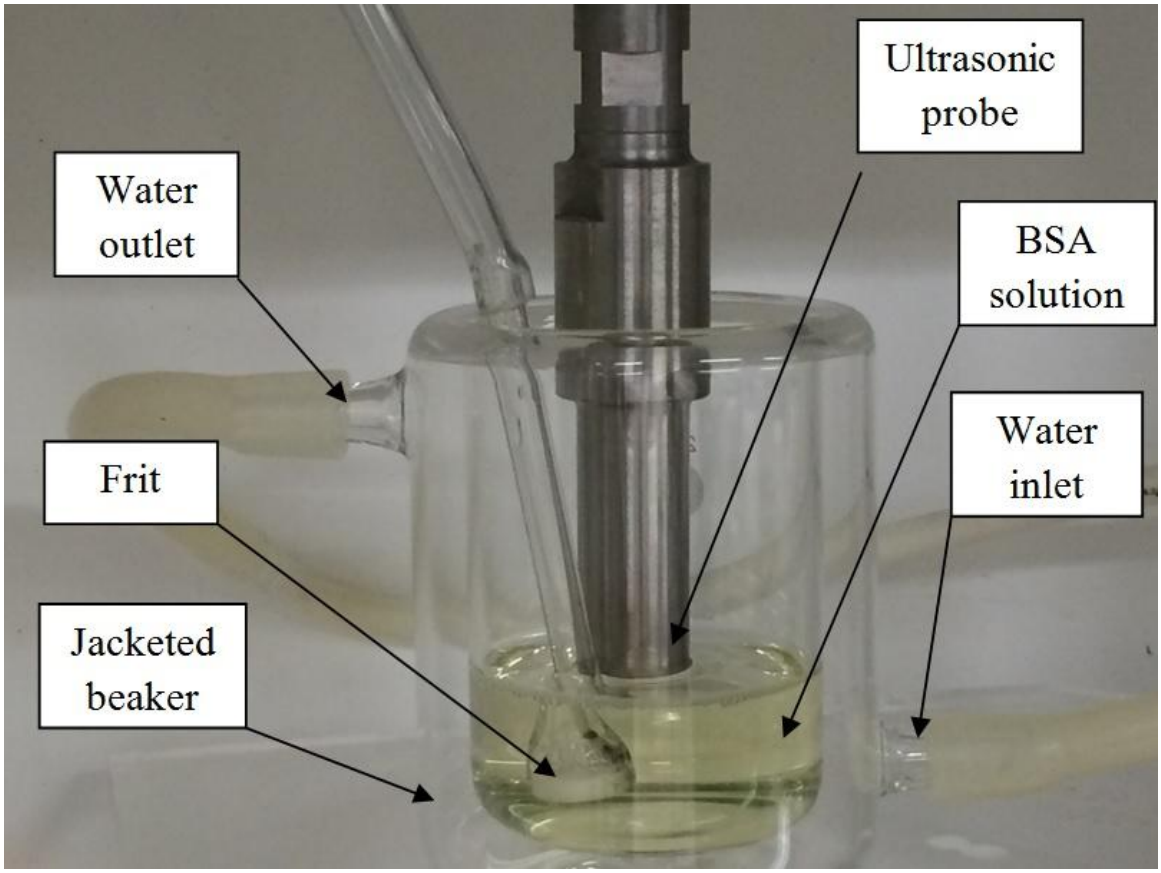

Figure 5.1: Schematic view of test setup for emulsion preparation

5.2.3. Sorption experiments

Copper (II) sulfate was dissolved in water for two hours to prepare 0.02 g/L copper solution. To determine optimum amount of biosorbent concentration for metal uptake, different amounts of BSAEM (0.5-5 g/L) were added to the copper solution using an electronic pipette, and afterwards the solution was hand shaken for 2 min. All experiments were carried out in 50 mL centrifuge tubes. Samples were thereafter centrifuged (IEC Centra CL2 centrifuge, Thermo Electron Co.) (15 min, 4000 rpm) and subsequently filtered (Filter Paper No. P8, Fisher Scientific, Canada) to separate copper loaded-BSAEM from the solution. According to the finding in Section 3.3.3, pH 5 was selected as a copper solution pH at which maximum copper removal was reached.

5.2.4. Contact time experiments

In order to investigate the kinetics of copper adsorption by BSA-coated bubbles and determine the required time for copper removal, a series of contact time experiments were performed. 50 mL of BSAEM was added into the 950 ml of copper solution, while the solution was being stirred using a Cole-Parmer lab stirrer (IKA RW 20 digital) for 5 hours at a speed of 300 rpm. The final concentration of copper solution and BSAEM were 0.02 and 2.5 g/L respectively. The samples were taken out from the solution at various time intervals followed by centrifugation and filtration.

5.2.5. Biosorptive flotation experiment

Each biosorptive flotation test comprised two consecutive steps: (i) copper biosorption experiments at the optimum experimental conditions (copper solution pH: 5, Temperature: 20 °C, BSAEM dosage: 2.5 g/L) which were conducted similar to that of contact time experiments, and (ii) batch dispersed-air micro flotation experiments which were performed in order to separate copper-loaded BSAEM from the solution. Figure 5.2 displays a modified Smith-Partridge micro flotation cell (Partridge and Smith, 1971) consisting of a ceramic frit located at a distance of 10 mm above the flat bottom of the column, 60 mL volume, and 18 cm height. Air was supplied by a compressor to the column through a digital flow meter used to adjust required

air flow rate. The air flow rate and flotation time were kept constant at 20 mL/min and 2 min respectively. The conditioning time after surfactant addition was 30 min. The amount of copper ions removed from the solution was considered to be the flotation recovery. Therefore, 5 mL of solution was withdrawn from the tailing after flotation experiment to quantify residual, and therefore recovered copper.

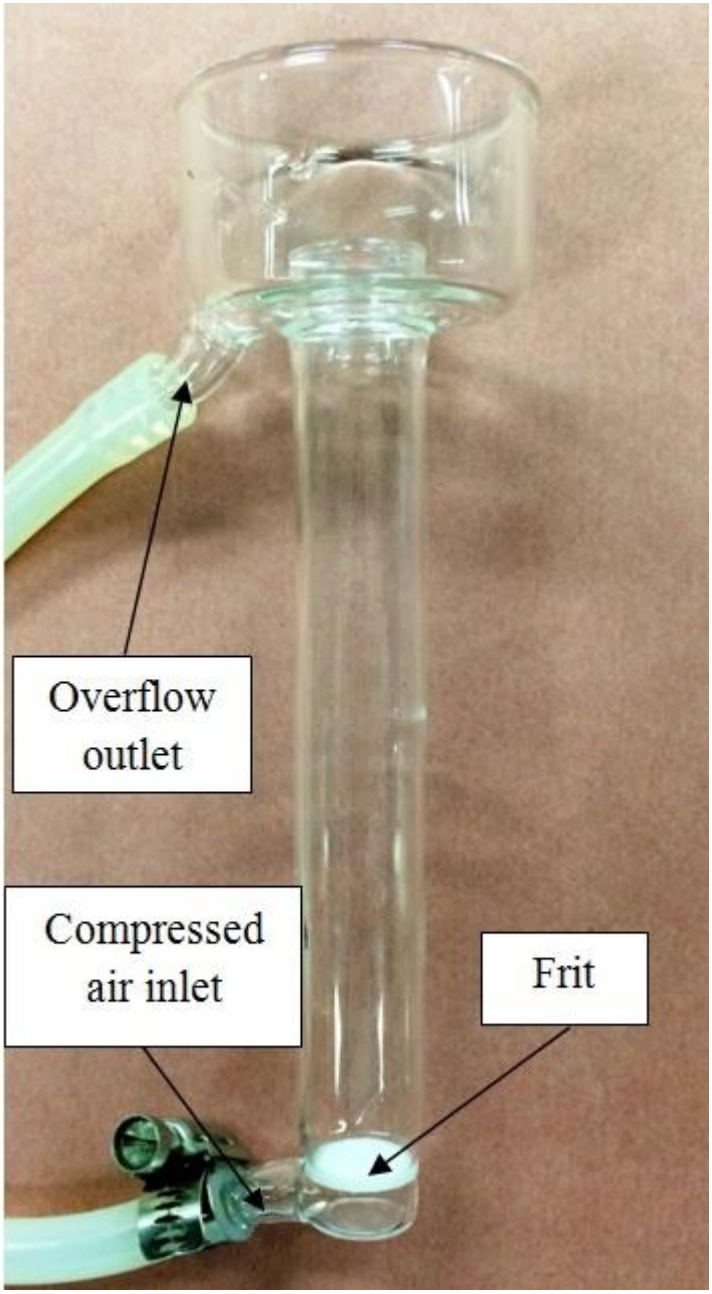

Figure 5.2: Schematic view of the cell used for flotation

5.2.6. Inductively Coupled Plasma Emission Spectroscopy (ICP)

Five mL of supernatant was acid digested to remove carbon from the solution matrix, as presence of carbon causes interference in inductively coupled plasma emission spectroscopy (ICP-ES). Details of acid digestion procedures were explained in Section 3.2.4. The residual copper concentration percentage (R,%) was measured using ICP-ES (Thermo Scientific 6000 series) from the following equation:

$$R\% = \frac{C_i - C_e}{C_i} \times 100 \qquad 5.1$$

Where C_i is the initial copper concentration (g/L), C_e is the equilibrium metal concentration (g/L) in biosorption experiments. The equilibrium condition is considered since no more change in the metal concentration is detected. In the flotation experiments, C_e is the copper concentration of the tailings.

5.2.7. Zeta potential measurements

ζ-potential measurements were performed on copper-loaded BSAEM using the microelectrophoretic apparatus ZetaPlus (Brookhaven Instruments Corporation, U.S.A.). This instrument determines the electrophoretic mobility and converts to ζ-potential using Smoluchowski approximation. Reported values are an average of 10 measurements.

5.2.8. Light microscopy

The microstructure of AFE before and after metal ion adsorption at different flocculant concentrations was examined using light microscopy (Olympus BX-51, Japan). One droplet of solution was placed on a microscopic slide and observed with a 20X objective lens. 5.3.

Results and Discussion

5.3.1. Effect of contact time

In this part, time dependant adsorption behavior of BSA-coated microbubbles in removing copper ions is examined. Variations of copper concentration over 5 hours are illustrated in Figure 5.3. The rate of copper uptake was fast in the first few minutes (48 % copper removal in 10 min) and afterwards slowly approached to the equilibrium condition. Eventually 54 % copper ions were removed from the solution after 40 min. Generally, adsorption rate of a biomass is directly dependent upon the number of functional groups present on the surface of biosorbent. Adsorption kinetics of BSAEM illustrated two stages for copper removal: (i) Steep slope or rapid copper uptake, due to availability of high number of functional groups on the surface of BSA-coated microcells; (ii) Low slope or slow copper removal and finally equilibrium is reached, owing to increasing coverage and subsequently presence of fewer active binding sites on bubbles, and also copper ions compete with each other for functionalities. The residual copper concentration was measured after one day, and it was similar to that for 40 min. Therefore the contact time for all experiments was fixed for 1 day.

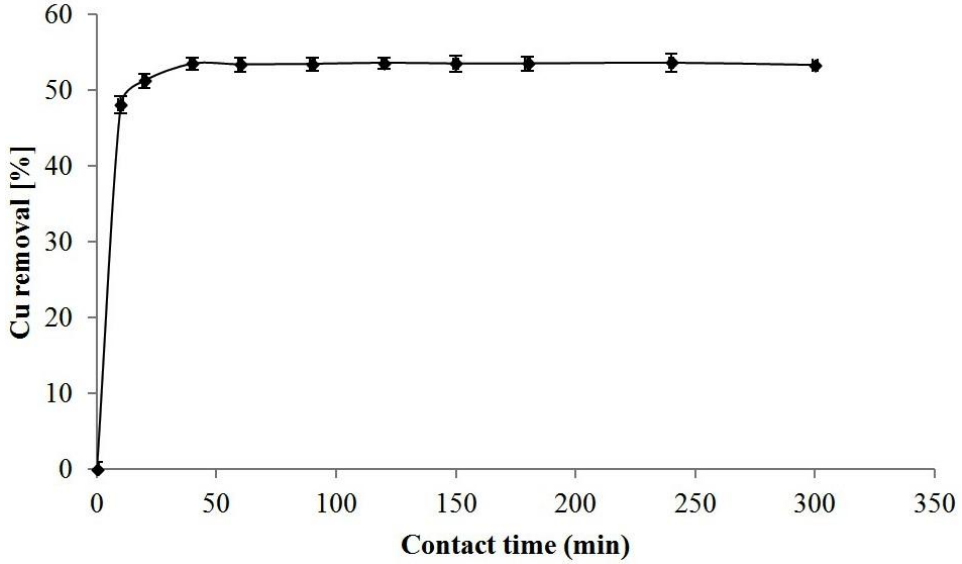

Figure 5.3: Effect of contact time on metal removal (copper concentration: 0.02 g/L, biosorbent concentration: 2.5 g/L, temperature: 20 °C, solution pH: 5). Each error bar illustrates the standard deviation of five measurements.

5.3.2. Effect of biosorbent concentration

Figure 5.4 shows that an increase in BSAEM concentration improved copper adsorption, until the highest metal removal (53%) was reached at 2.5 g/L due to the availability of greater active sites. Additional increases in BSAEM diminished copper removal, and 33% metal uptake was obtained at a BSAEM concentration of 5 g/L. The decrease in copper removal resulting from the formation of microbubble aggregates at higher biosorbent dosage (pH 5 is close to the isoelectric point of BSAEM), which block the functional groups from contacting with metal ions. In all biosorptive flotation experiments, BSAEM dosage was fixed at 2.5 g/L.

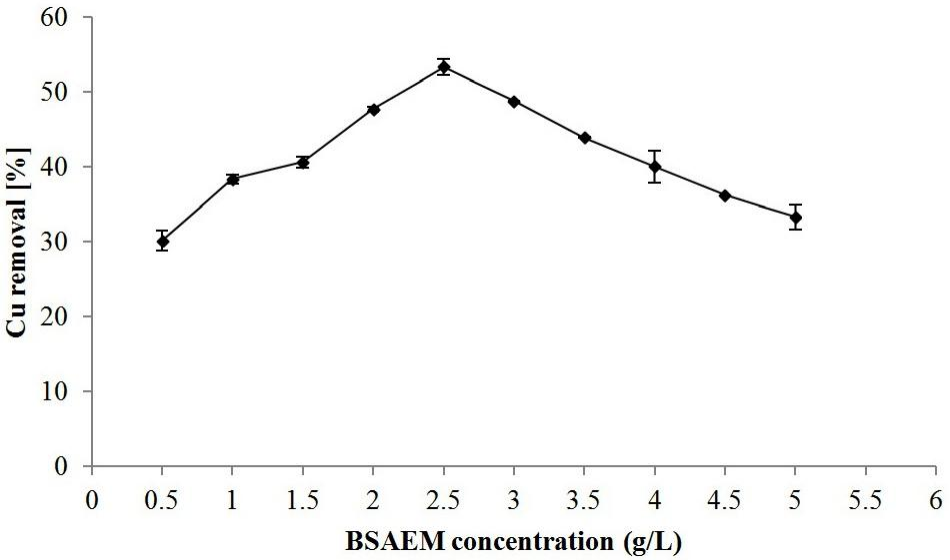

Figure 5.4: Effect of BSAEM concentration on metal removal (copper concentration: 0.02 g/L, biosorbent concentration: 2.5 g/L, metal solution pH: 5, Contact time: one day, temperature: 20 °C). Each error bar illustrates the standard deviation of five measurements.

5.3.3. Zeta-potential

The ζ-potential provides an indication of the surface charge of copper-loaded BSA microcells. Figure 5.5 shows the ζ-potential of copper-BSAEM as a function of pH. Increasing pH from 5 increases ζ-potential magnitude, and number of negatively charged counter ions at the slipping plane. In basic solution, a cysteine protein is deprotonated and NH_3^+ acts as the acidic site, donating a proton to the solution; moreover, COO^- and S^- groups are negatively charged. In other words, the number of negatively charged active sites is increased with an increase in pH.

Figure 5.5 and data obtained from the previous findings (Section 3.3.3) clearly demonstrate that BSAEM has a higher negative ζ-potential compared to that of copper-loaded BSAEM, as copper ions physically approached to the negative active binding sites due to the attractive electrostatic interaction, and then are chemically bound to the functional groups. This causes a decrease in the number of negative functional groups available on bubbles' surface.

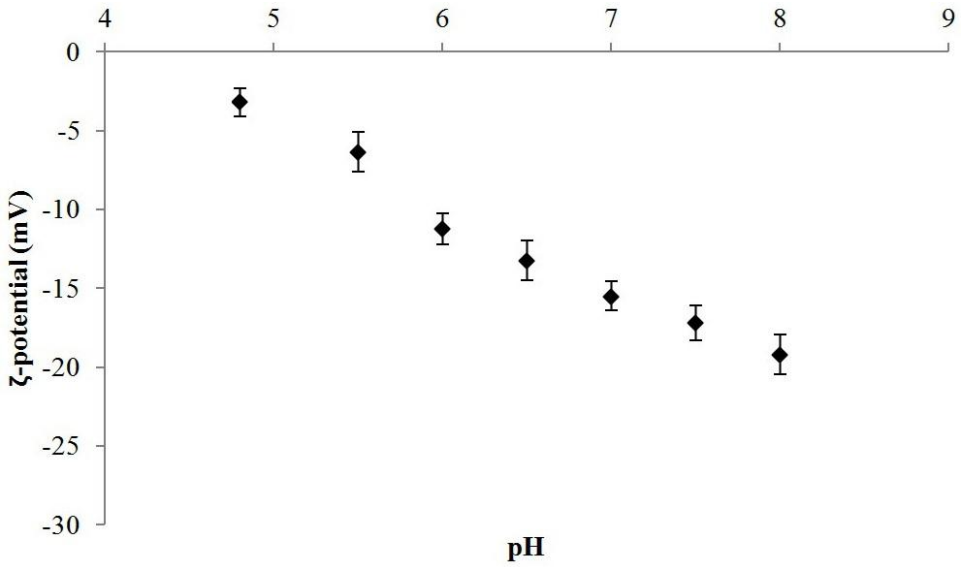

Figure 5.5: pH- Zeta potential diagrams of copper-loaded BSAEM

5.3.4. Effect of cationic flocculant on emulsion and copper-loaded BSA

This part deals with the destabilization of the BSA-coated microcells present in the solution. This work was performed since the flocculation of copper-loaded microbubbles can assist phase separation. Due to the high number of negatively-charged ions on coated-bubbles illustrated by Figure 5.5 and the previous results (Section 3.3.3), a cationic flocculant was used to destabilize the AFE. A series of experiments was systematically carried out to measure the required flocculant dosage. Flocculant at different concentrations was added to the emulsion (Figure 5.6A) with a constant concentration of 2.5 g/L; similar to that used for biosorptive flotation experiments. Figure 5.6B displays BSA-coated bubbles smaller than 10 μm evenly dispersed. As illustrated in Figure 5.6C, the cationic flocculant demonstrated the best flocculating activity at concentration of 0.025 g/L, since a thick layer of BSA-coated bubbles

aggregates were entirely separated in a few seconds and placed in the top of the solution. Either a decrease or an increase in flocculant dosage from 0.025 g/L decreased the flocculating action, and most of the bubbles remained dispersed in the solution. However, only few aggregates could be observed thorough the structure pointed by black arrows in Figure 5.6D. Turbidity of the solution indicates presence of coated-bubbles as shown in Figure 5.6E. Therefore, the concentration of flocculant used in all flotation experiments was set at 0.025 g/L, unless otherwise stated.

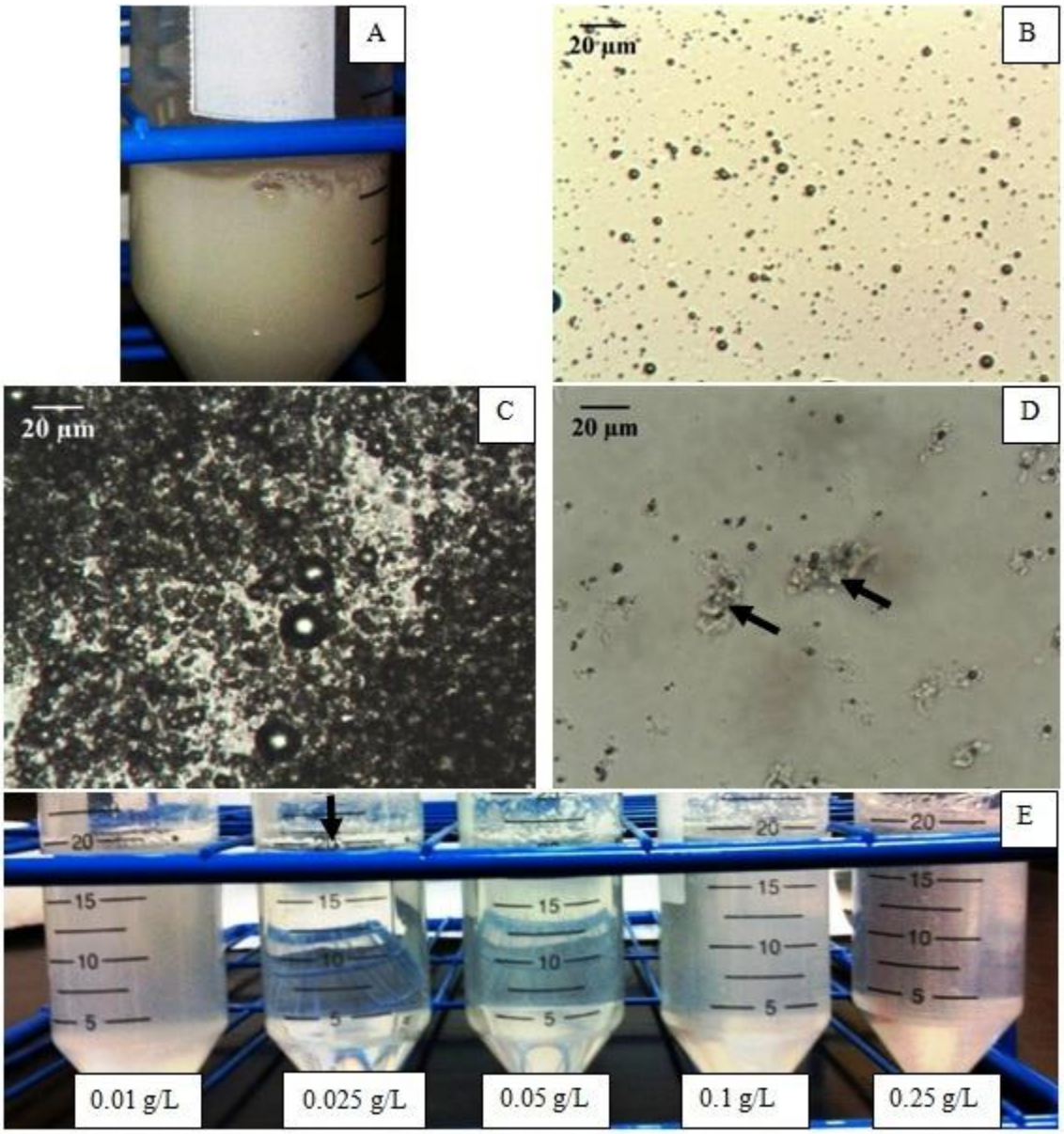

Figure 5.6: A) A tube consisting of BSA-AFE, and light microscopy micrograph of BSA air-filled emulsion containing B) 0 g/L, C) 0.025 g/L (top layer), D) 0.25 g/L of cationic flocculant, and E) effect of cationic flocculant dosage (0.01-0.25 g/L) on phase disengagement of air-filled emulsion at pH 7 after 1 hour.

The effect of copper-BSAEM solution pH on the flocculation activity was examined at various pH values (5 to 8). As presented in Figure 5.7A, at pH 7 and 8, copper-loaded bubbles were linked together by means of bridging flocculation to form the large flocs, which were quickly separated in a few minutes, and were accumulated in the top layer due to buoyancy (Figure 5.7B). The weak performance of flocculant at lower pH results from the low number of

negatively-charged ions surrounding bubbles compared to that of copper-loaded BSAEM at pH 7, where small aggregates were unable to group together and form the larger flocs (Figure 5.7C). The milky color of solution in tubes (Figure 5.7A) at pH 5 and 6 confirm the existence of small aggregates of microbubbles.

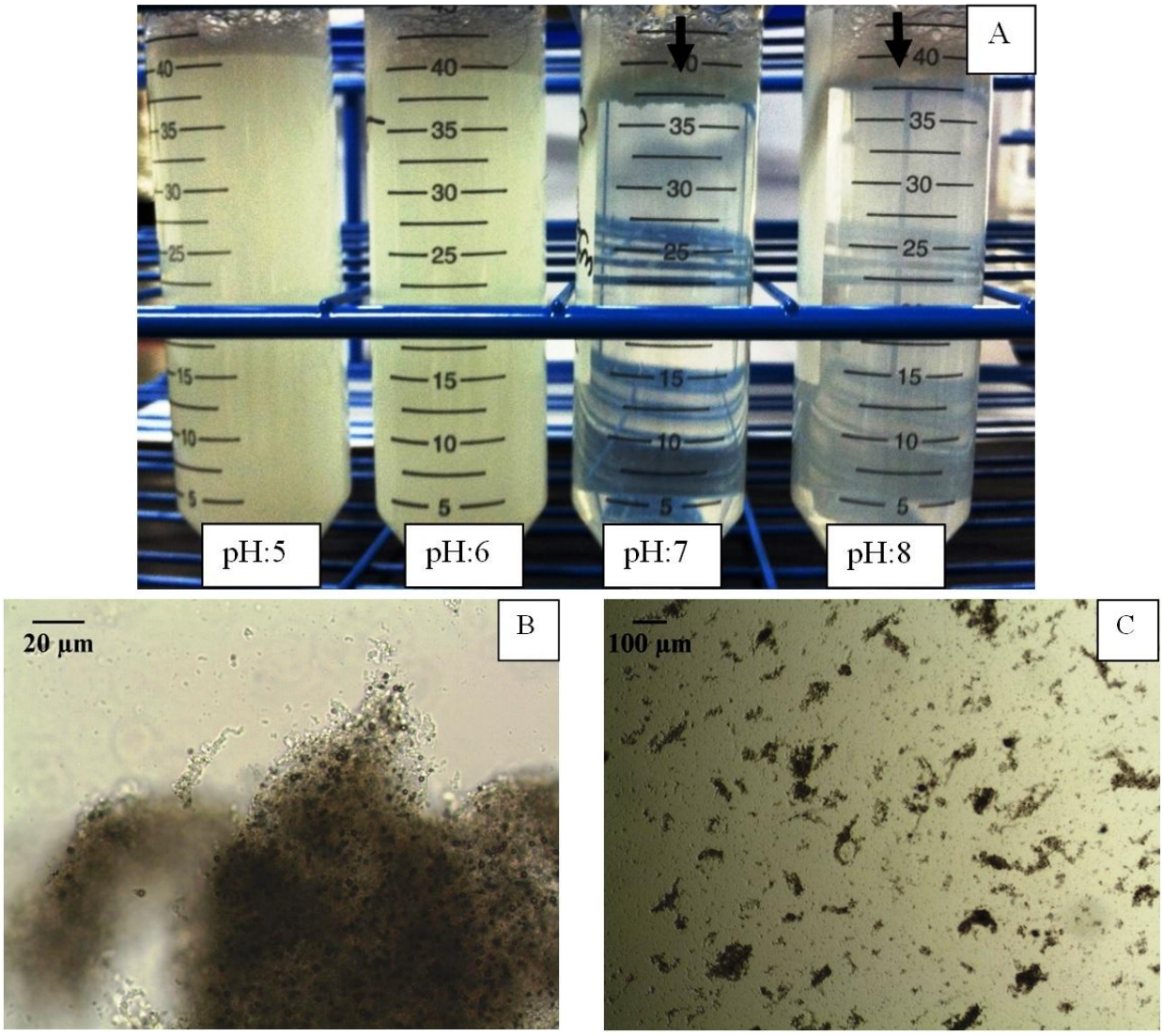

Figure 5.7: A) Effect of pH (5-8) on phase separation of Cu-loaded BSAEM after 1 hour (flocculants concentration in all tubes was 0.25 g/L), and light microscopy image of copper-loaded BSAEM containing 0.025 g/L of cationic flocculant at B) pH 7 and C) pH 5.

5.3.5. Effect of pH on copper recovery

The pulp pH is one of the most important parameters in flotation which determines the floatability of a particle. pH not only influences the ionization of functional groups existing on the surface of particle, but also modifies solution chemistry. In the case of copper solutions, increasing pH above 5 causes both copper speciation and a decrease in Cu^{2+} concentration. Several experiments were carried out to probe the effect of copper-BSAEM solution pH on the copper recovery. The final copper-BSAEM solution pH was 5, once equilibrium condition was achieved (40 min). Afterwards, the final solution pH was increased using 0.1 M NaOH until pH 8. It is worth noting that the final pH was not decreased, since a decrease in pH results in competition between copper and hydrogen ions for binding active site of BSA-coated microcells, consequently reducing copper removal. Furthermore, decreasing pH leads to forming positively charged ions on the surface and giving rise to repulsive electrostatic force between copper ions and functional groups (Section 3.3.3). Figure 5.8 illustrates copper recovery at different pH values ranging from 5 to 8. Copper recovery in absence of collector and flocculant was approximately 0.5% due to the lack of hydrophobic groups present on the microbubbles' surface. BSA-coated bubbles were surrounded and linked together by copper precipitates hindering hydrophobic patches of BSA to be exposed in the solution (Section 4.3.3). The addition of 0.025 g/L of cationic flocculant improved copper recovery to some extent (pH 5-6.5); however metal recovery sharply increased over pH range from 6.5 to 7. As explained in Section 5.3.4, copper-loaded microcells were completely destabilized, forming large aggregates, which were lifted upwards by means of bubbles produced by frit. Further pH increases resulted in lower copper recovery (despite complete separation of copper-BSAEM in top layer) caused by hydrolysis of Cu^{2+} ions and subsequent formation of $Cu(OH)_3^-$ and $Cu(OH)_4^{-2}$ in more alkaline solutions. Copper removal at pH from 5 to 8 are given in Table 5.1. Increase in copper removal up to 68% at pH 6 is due to the formation of copper hydroxide precipitates in solution. Copper uptake began to diminish from pH 6.5 and 10.5% metal uptake was obtained at pH 8. Due to the presence of negatively charged functional groups on the bubbles' surface, three different cationic surfactants (DA, HA and HTAB) were used to improve hydrophobic properties of copper-loaded BSA bubbles. The hydrophilic head of collector containing positively-charged group interacts with negatively-charged ions, and consequently the hydrophobic tail is oriented towards/into the

solution. As shown in Figure 5.9, DA, HA and HTAB exhibited the same trend, and nearly 21% copper recovery was obtained at pH 5. Increasing pH up to 7 led to copper recovery build up to approximately 35% for HA, HTAB and DA due to the availability of higher number of negatively-charged groups around bubbles (discussed in Section 5.3.3). As illustrated in Figure 5.9, additional rises in pH to 8 reduced copper recovery to 11%. Whereas the ζ-potential is significantly negative at pH 8, speciation of copper ions reduced copper removal and consequently copper recovery.

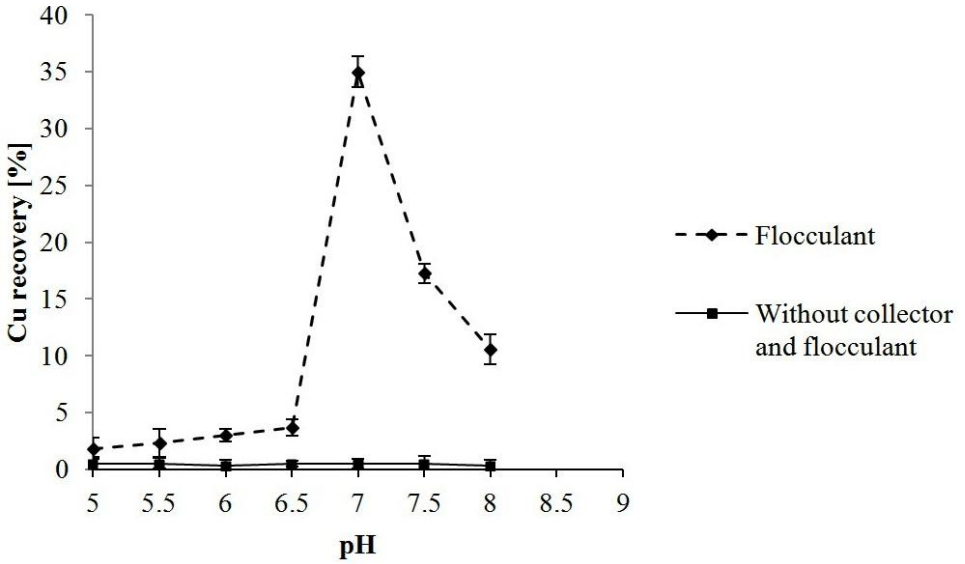

Figure 5.8: Effect of copper-BSAEM pH on metal recovery in presence and absence of cationic flocculant (Air flow rate: 20 mL/min, flotation time: 2 min, flocculant concentration: 0.025 g/L). Each error bar illustrates the standard deviation of five measurements.

Table 5.1: Copper removal percentage at different final solution pH in absence of surfactants

Copper removal percentage (%)	Final solution pH
53.3	5
66.5	5.5
68.2	6
55.6	6.5
34.9	7
17.6	7.5
10.5	8

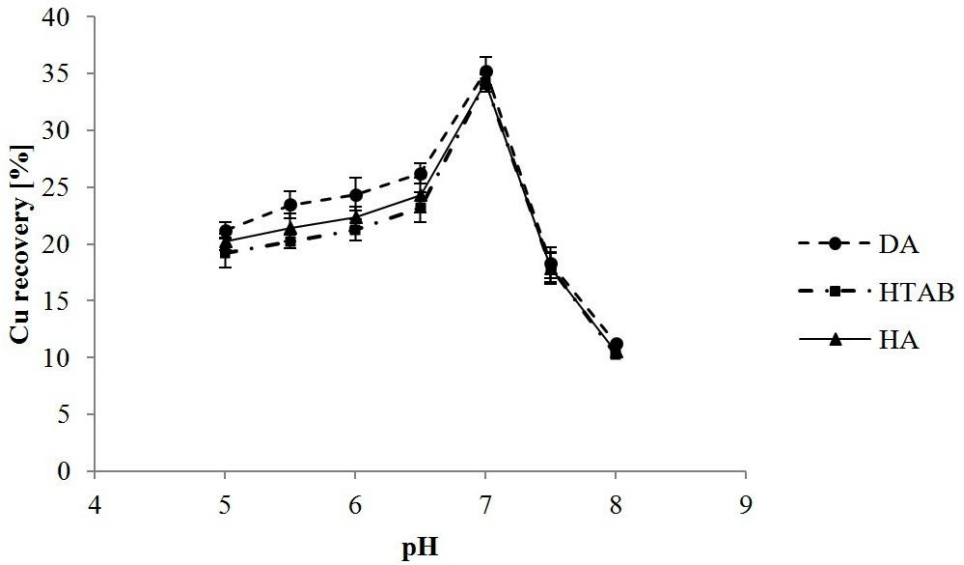

Figure 5.9: Effect of copper-BSAEM pH on metal recovery for different types of surfactant (Air flow rate: 20 mL/min, flotation time: 2 min, surfactant concentration: 3×10^{-4} M, cationic flocculant concentration: 0.025 g/L). Each error bar illustrates the standard deviation of five measurements.

5.3.6. Effect of surfactant dosage

Three types of cationic surfactant were used at different concentrations ($1\text{-}9\times10^{-4}$ M) to determine optimum dosage of surfactant. As shown in Figure 5.10, increasing surfactant concentration at final solution pH 5 increased copper recovery, and maximum recovery was reached at a concentration of 3×10^{-4} M. Further addition of surfactant did not show any noticeable effect on copper recovery.

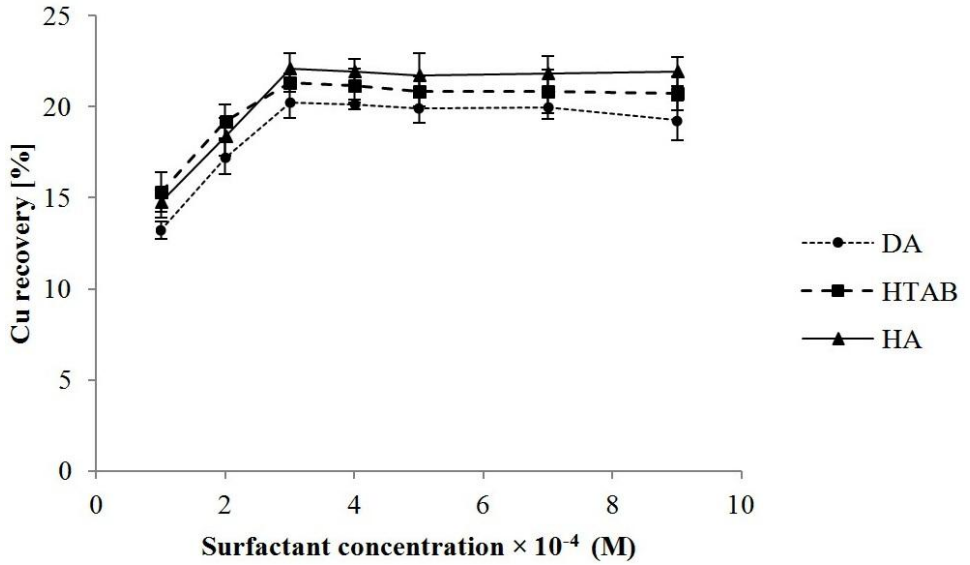

Figure 5.10: Effect of surfactant dosage on metal recovery for different types of surfactant (Final copper-BSA solution pH: 5, air flow rate: 20 mL/min, flotation time: 2 min, cationic flocculant concentration: 0.025 g/L). Each error bar illustrates the standard deviation of five measurements.

5.4. Conclusions

Biosorptive flotation of dilute copper solution (0.02 g/L) was carried out in two steps:

- The first was biosorption of metal ions using BSA-coated bubbles, and suitable operational conditions were determined. 2.5 g/L of the BSAEM emulsion was an optimum dosage to reach the maximum copper removal. Further increases in BSAEM loading led to the formation of bubble aggregates, which reduced the probability of interaction between copper ions and active binding sites, and consequently metal ion removal. Moreover, it was found that 40 min was required to achieve equilibrium condition for copper removal.
- The second stage was both the separation of copper-loaded BSAEM from the solution using flotation, and investigating the effect of collector and flocculant on the metal recovery. In absence of a cationic surfactant and flocculant, copper recovery was approximately 0.5% due to lack of hydrophobic groups around copper-loaded microcells. It was noted that solution pH and flocculant dose noticeably impacts the separation of BSAEM and subsequently copper recovery. 0.025 g/L of flocculant led to complete disengagement of copper-BSAEM from the

solution above pH 7, while copper recovery declined from 35% to 11% owing to copper speciation occurring at high pH. Collector addition increased the floatability of copper-loaded BSA at pH ranging from 5 to 6.5. Cationic collectors had a similar effect to that of flocculant above pH 7. In order to perform efficient biosorptive flotation, pH selection should be based on a trade off between copper recovery and copper removal. It is worth mentioning that BSA-coated microbubbles might exhibit superior performance in biosorptive flotation of those ions such as nickel and cobalt which do not hydrolyze at alkaline pH values.

References

Aldrich, C. and Feng, D., 2000. Removal of heavy metals from wastewater effluents by biosorptive flotation. Minerals Engineering 13(10), 1129-1138.

Chen, J.P., Hong, L., Wu, S. and Wang, L., 2002. Elucidation of interactions between metal ions and Ca alginate-based ion-exchange resin by spectroscopic analysis and modeling simulation. Langmuir 18(24), 9413-9421.

Deng, S., Bai, R. and Chen, J.P., 2003a. Aminated polyacrylonitrile fibers for lead and copper removal. Langmuir 19(12), 5058-5064.

Deng, S., Bai, R. and Chen, J.P., 2003b. Behaviors and mechanisms of copper adsorption on hydrolyzed polyacrylonitrile fibers. Journal of Colloid and Interface Science 260(2), 265-272.

Deng, S. and Ting, Y.-P., 2005. Characterization of PEI-modified biomass and biosorption of Cu, Pb and Ni. Water Research 39(10), 2167-2177.

Guibal, E. and Roussy, J., 2007. Coagulation and flocculation of dye-containing solutions using a biopolymer (Chitosan). Reactive & Functional Polymers 67(1), 33-42.

Masood, F. and Malik, A., 2011. Biosorption of metal ions from aqueous solution and tannery effluent by Bacillus sp. FM1. Journal of Environmental Science and Health. Part A, Toxic/Hazardous Substances & Environmental Engineering 46(14), 1667-1674.

Matis, K.A., Zouboulis, A.I. and Hancock, I.C., 1994. Biosorptive flotation in metal ions recovery. Separation Science and Technology 29(8), 1055-1071.

Partridge, A.C. and Smith, G.W., 1971. Flotation and adsorption characteristics of the hematite-dodecylamine-starch system. Canadian Metallurgical Quarterly 10(3), 229–234.

Peleka, E.N. and Matis, K.A., 2009. Bioremoval of metal ion and water treatment in a hybrid unit. Separation Science and Technology 44(15), 3597-3614.

Reddad, Z., Gerente, C., Andres, Y. and Le Cloirec, P., 2002. Adsorption of several metal ions onto a low-cost biosorbent: kinetic and equilibrium studies. Environment Science & Technology 36(9), 2067-2073.

Sadowski, Z., 2001. Effect of bisorption of Pb, Cu and Cd on the zeta potential and flocculation of Nacardia SP. Minerals Engineering 14(5), 547-552.

Sheng, P.X., Ting, Y.P., Chen, J.P. and Hong, L., 2004. Sorption of lead, copper, cadmium, zinc, and nickel by marine algal biomass: characterization of biosorptive capacity and investigation of mechanisms. Journal of Colloid and Interface Science 275(1), 131-141.

Subrahmanyam, T.V. and Forssberg, K.S.E., 1990. Fine particles processing: shear-flocculation and carrier flotation — a review. International Journal of Mineral Processing 30(3), 265-286.

Volesky, B., 2007. Biosorption and me. Water Research 41(18), 4017-4029.

Wang, X.S., Li, Z.Z. and Sun, C., 2009. A comparative study of removal of Cu(II) from aqueous solutions by locally low-cost materials: marine macroalgae and agricultural by-products. Desalination 235(1), 146-159.

Xu, H. and Liu, Y., 2008. Mechanisms of Cd^{2+}, Cu^{2+} and Ni^{2+} biosorption by aerobic granules. Separation and Purification Technology 58(3), 400-411.

Zamboulis, D., Peleka, E.N., Lazaridis, N.K. and Matis, K.A., 2011. Metal ion separation and recovery from environmental sources using various flotation and sorption techniques. Journal of Chemical Technology and Biotechnology 86(3), 335-344.

Zouboulis, A.I., Matis, K.A. and Lazaridis, N.K., 2001. Removal of metal ions from simulated wastewater by Saccharomyces yeast biomass: combining biosorption and flotation processes. Separation Science and Technology 36(3), 349-365.

Zouboulis, A.I. and Matis, K.A., 2009. Biosorptive flotation for metal ions removal: the influence of surface tension. Desalination 248(1), 740-752.

Chapter 6. Copper and nickel ion removal from synthetic process water using BSA air-filled emulsion

6.1. Introduction

Enormous quantities of industrial contaminants including heavy metals, synthetic compounds and waste nuclear liquids are released into the environment, which result in deterioration of the ecosystems (Volesky, 1990; Volesky, 2007). Mining and metallurgical waste water is a main source of heavy metal pollution. Environment Canada reported that 74.9% of total consumed water (497.2 million cubic meters) by mining industries in 2009 was withdrawn by the metal mines, and 77.2% of intake water was sourced from surface freshwater (rivers, lakes). They also claimed that 72.8%, 10.8% and 9% of wastewaters were discharged to the surface freshwater, tailing ponds and ground water respectively, and 59.9% of effluents were not treated while discharged (Statistics Canada, 2012). Therefore, many studies have been conducted to propose effective and economic metal removal technologies. Some techniques have been recently introduced on the basis of increasing interfacial surface area between sorbent and sorbate to eliminate metal ions from dilute solutions in lab-scale such as air assisted solvent extraction (AASX) (Chen *et al.*, 2003; Tarkan and Finch, 2005), colloidal liquid aphrons (CLAs) and membrane (Parthasarathy and Buffle, 1994; Sengupta *et al.*, 2006). Nevertheless, some drawbacks for example required time for formation of solvent-coated bubbles (AASX) and liquid membrane instability and fouling (membrane) lead them to be impractical to treat large volumes of waste water.

Air-filled emulsion (AFE) is an innovative material which was first generated by Feinstein ad co-workers as contrast agents in echosonography (Keller *et al.*, 1986; Feinstein *et al.*, 1988). AFE was afterwards employed by Tchuenbou-Magaia *et al.* to reduce fat content of the food, since the taste of food remained constant (Tchuenbou-Magaia *et al.*, 2009; Tchuenbou-Magaia *et al.*, 2011). AFE is a high stable colloidal suspension composed of fine bubbles which are encapsulated with a cysteine protein thin film. Previous results demonstrated that AFE is a promising material to uptake copper ions even at low concentration (0.01 g/L) (Section 3.3.5). In

this study, the capability of AFE for metal ion uptake from synthetic process water and effect of various experimental factors such as pH and biosorbent dosage were investigated.

6.2. Materials and methods

6.2.1. Materials

Dried bovine serum albumin (BSA) (fraction V) was provided from Bishop Canada Inc. to construct AFE. Anhydrous copper (II) sulfate ($CuSO_4$) (Fisher Scientific, Canada), nickel (II) sulfate ($NiSO_4 \cdot 6H_2O$) (Anachemia, Canada) and calcium sulfate ($CaSO_4$) (Acros Organics, U.S.A.) were used to produce the aqueous copper, nickel and calcium solution. All solutions were prepared using reverse osmosis purified water (pH of 5.8 at 25 ºC). Acid digestion of BSA were carried out using hydrochloric acid (36%), nitric acid (67%) and hydrogen peroxide (50%) (Fisher Scientific, Canada). Solution pH was adjusted using 10^{-1} M sodium hydroxide and 10^{-1} M sulfuric acid (Fisher Scientific, Canada).

6.2.2. Emulsion preparation

BSA-coated air bubbles were synthesized using sonication technique. A high intensity sonicator (UP 400 S, 24 kHz, Hielscher Inc., U.S.A.) was placed at the interface of air and protein solution, and AFE was formed. Details of microcells formation is found in Section 3.2.2.

6.2.3. Sorption experiments

The stock solution containing 0.01 g/L of copper (II), 0.02 g/L of nickel (II) and 0.25 g/L calcium ions (the recipe of the water was made up to Vale's tailings pond in Sudbury) was prepared. Details of sorption experiments can be found in Section 3.2.3. The experimental parameters that were examined during sorption experiments are given in Table 1. C_{AFE} and C_{Cu}, C_{Ni} and C_{Ca} represent concentration of BSAEM, copper, nickel and calcium in the solution respectively.

Table 6.1: Experimental conditions were examined during the batch experiments.

Parameter	pH	Temperature	C_{Cu}	C_{Ni}	C_{Ca}	C_{AFE}
pH	2-5	20 °C	0.01 g/L	0.02 g/L	0.25 g/L	3 g/L
C_{Ca}	5	20 °C	0.01 g/L	0.02 g/L	0.02-0.5 g/L	3 g/L
C_{AFE}	5	20 °C	0.01 g/L	0.02 g/L	0.25 g/L	1.2-22 g/L

6.2.4. Inductively Coupled Plasma Emission Spectroscopy (ICP)

Details of protein acid digestion are available in Section 3.2.4. Inductively coupled plasma emission spectroscopy (ICP-ES) (Thermo Scientific 6000 series) was used to measure concentration of copper and nickel ions present in the solution, once equilibrium condition was reached. The percentage of copper and nickel removed by AFE was calculated using the following equation:

$$R\% = \frac{C_i - C_e}{C_i} \times 100 \qquad 6.1$$

Where R% is metal removal percentage, C_i the initial copper and nickel concentration (g/L), C_e the equilibrium metal concentration (g/L).

6.2.5. Light microscopy

The microstructure of AFE before and after metal ion adsorption was examined using light microscopy (Olympus BX-51, Japan). One droplet of solution was placed on a microscopic slide and observed with an objective lens.

6.2.6. Biomass Characterization

Potentiometric titration was carried out to assign concentration of functional groups present on the surface of BSA-coated bubbles. 50 mL of BSAEM (50 g/L, natural pH: 7) was first acidified by 1M HCl to decrease the pH to 2. The solution was thereafter titrated using a titremeter (888 titrando, Metrohm, Canada) with an automatic burette, while the suspension was gently stirred. The pH of the suspension was elevated by adding standard solution of NaOH (0.1 M). The pH of the suspension was automatically recorded after each addition of titrant. Duplicate experiments were performed to confirm reproducibility of the titration results.

6.2.7. Particle size analysis

The size distribution of proteinaceous microcapsules was measured using laser scattering particle size analyzer (Horiba, LA-920, USA). Small volumes of sample were placed in the sample presentation chamber in distilled water while stirred. The refractive index of BSAEM was set at 1.45.

6.3. Results and Discussion

6.3.1. Characterization of metal binding sites of BSAEM

Surface titration of biosorbent is one of the most important measurements to assess the approximate characterization of biomass. Biosorbent titration curve depicts distinct behavior which is dependent upon the types and amount of functional groups accessible on the surface of biomass. In addition, potentiometric titration curves enable one to determine qualitatively and quantitatively the nature and number of active binding sites present on the surface of BSA-coated air bubbles. As illustrated in Figure 6.1, the titration curves of BSA-coated bubbles did not reveal the existence of inflection points due to the low number of functional groups on the bubbles' surface. Hence, a proton-binding model proposed by Yun *et al.* was used (Equation 6.2) to calculate both the amount of active sites and respective pK values:

$$[OH^-]_{Added} = \sum_{j=1}^{N} \left[\frac{b_j X}{1 + \left(\frac{[H^+]}{K_j} \right)} \right] + \frac{K_W}{[H^+]} - [H^+] \qquad 6.2$$

Where b_j, X and K_j represent the quantity of active sites per gram of biosorbent (mol/g), BSAEM concentration (g/L) and equilibrium constant respectively (Detailed derivation procedures of the theoretical model are found in Appendix D). N describes the number of functional groups on the surface of microcells. K_w is expressed as the equilibrium constant of water at 25 °C (1.023×10^{-14}). The proton-binding model was fitted to the experimental data, where N value was fixed from 1 to 6. Accordingly, the three-site model was able to follow the trend of titration plot of BSAEM shown in Figure 6.1. The negative logarithm of equilibrium

constants (K_i) was calculated to obtain pK values of the functionalities. Estimated parameters are given in Table 6.2. The first active site is attributed to the carboxyl which is the most abundant group present on the surface of coated bubbles, since the pK value of carboxylic group in cysteine proteins ranges from 1.7 to 1.9 (Mateo Marti *et al.*, 2004; Yao *et al.*, 2007). The second functional group is attributed to thiol group being as a side chain in cysteine-rich protein. The last active site with pK value of 10.6 corresponds to the amino groups (Graff and Bukowska, 2005), as it generally shows pK values between 10.2-10.5.

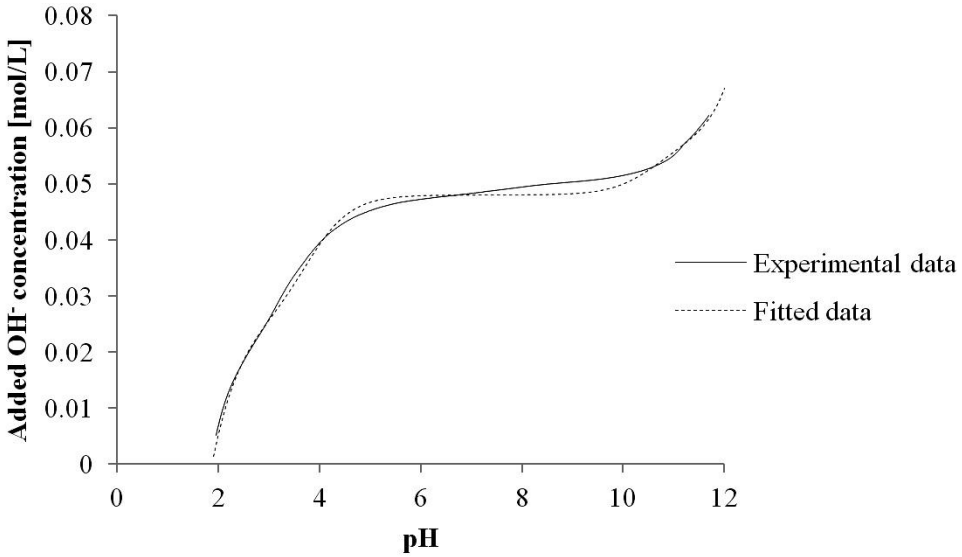

Figure 6.1: Potentiometric titration plot of BSAEM to assess the number of sorption sites and pK values with fitted and experimental data (N=3).

Table 6.2: Characterization of functional groups present on the surface of BSA-coated bubbles.

Type of active binding site	mmol/g	pK
Carboxylic	0.497	1.8
Thiol	0.463	3.7
Amine	0.187	10.6

6.3.2. Effect of pH

pH is a main experimental parameter which influences metal ion removal by controlling both biosorbate solution chemistry, and ionization of functional groups present on the biosorbent surface. This part investigates the effect of pH on copper and nickel removal in presence of calcium ions. The pH range between 2 to 5 was selected, as a typical pH for tailings pond water

is between 2 to 4. Furthermore, copper ions exist in the form of Cu^{2+} at pH below 5. Nickel ions, on the other hand, do not hydrolyze until pH 8. As shown in Figure 6.2, no metal uptake was observed at pH 2, due to the high concentration of hydrogen ions competing with copper and nickel for functionalities of BSAEM. Nickel and copper removal rapidly increased to 4% and 10% respectively, as pH increased from 2 to 3.5. Further increases in pH to 5 enhanced nickel and copper removal to 7% and 13% respectively, as the pH increase led to a decrease in both repulsive Coulomb force between metal ions and active sites present on the surface of bubbles and the concentration of hydrogen ions. pK values obtained in Section 6.3.1 obviously demonstrated the presence of higher number of deprotonated active functionalities compared to that of lower pHs. However calcium ions compete with copper and nickel ions and are bound to the functional groups. Copper ions were favorably adsorbed rather than nickel ions, which confirms the previous findings about biosorption behavior of BSAEM in a ternary system (copper, nickel and cobalt) (Section 4.3.4).

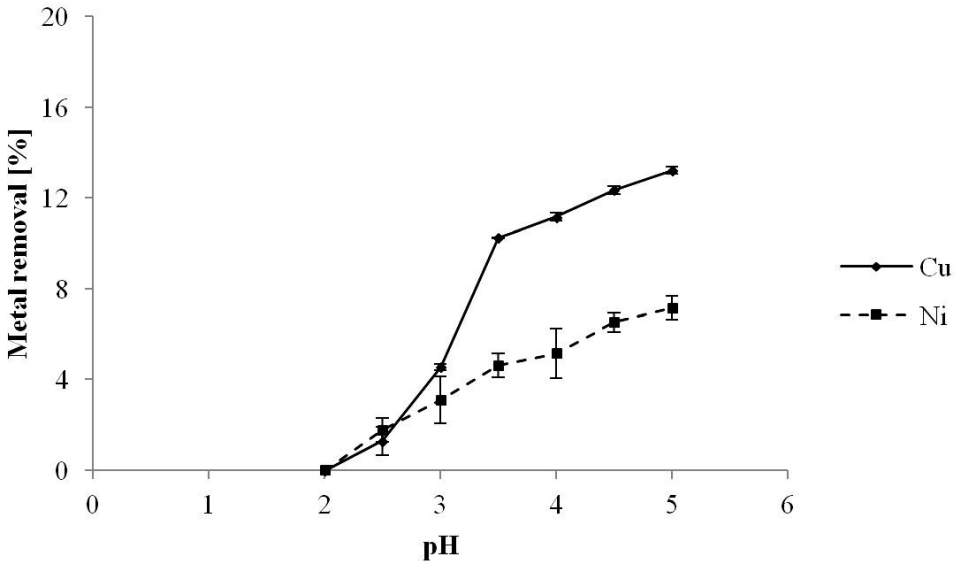

Figure 6.2: Effect of equilibrium copper, nickel solution pH on metal removal (C_{Cu}: 0.01 g/L, C_{Ni}: 0.02 g/L, C_{Ca}: 0.25 g/L, biosorbent concentration: 3 g/L, Contact time: one day, temperature: 20 °C). Each error bar illustrates the standard deviation of five measurements.

6.3.3. Effect of calcium concentration

A series of experiments were performed to monitor effect of calcium ion concentration (0.02-0.5 g/L) on biosorption of nickel and copper ions. Metal ion removal was markedly inhibited by approximately 70 % compared to that in the absence of calcium ions. As illustrated in Figure 6.3, the extent of metal ion removal dropped significantly even at low concentration of calcium ions. Increasing the calcium dosage reduced copper and nickel ion removal, and 8% and 4% uptake were reached at a calcium concentration of 0.5 g/L for copper and nickel respectively. Calcium ions not only compete with nickel and copper ions for active binding sites of BSA-coated air bubbles, but also form large bubble aggregates by means of bridging flocculation. Figure 6.4 illustrates presence of large bubble flocs at various calcium ion concentrations ranging from 0.2 to 0.5 g/L indicating number of functionalities for removing metal ions is diminished.

Figure 6.5A and 6.5B display particle size distributions in the absence and presence of 0.1 g/L of calcium ions respectively. BSAEM illustrates a bimodal particle size distribution, which the minor peak corresponds to both small protein debris and fine BSA-coated microcells; the larger peak is assigned to the coarser microcells. Addition of calcium ions led to change in the size distribution from bimodal to polymodal. The comparison between light microscopy images (Figure 4B) and overall trends of size distribution curve (Figure 5B) implies that the small peak indicates both fine bubbles and protein debris. Furthermore, the larger peak is attributed to the coarser coated-bubbles, and broader peak is assigned to large bubble flocs.

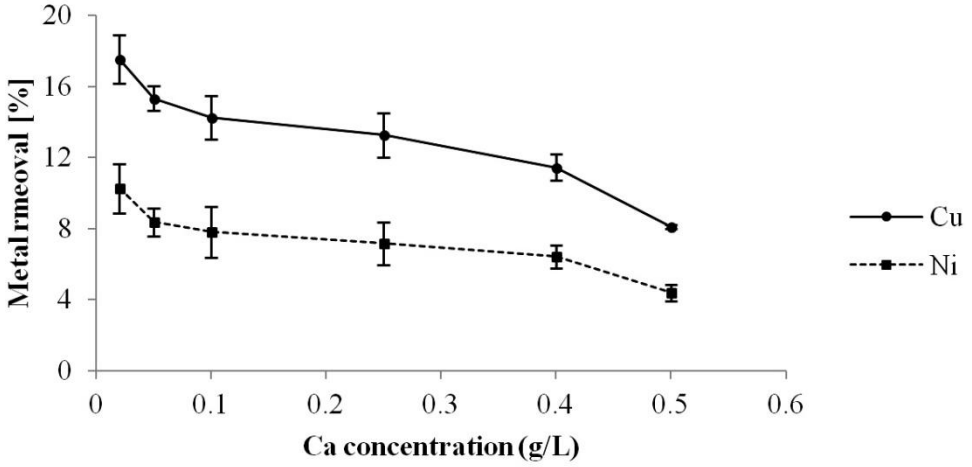

Figure 6.3: Effect of calcium concentration on metal removal (equilibrium solution pH: 5, C_{Cu}: 0.01 g/L, C_{Ni}: 0.02 g/L, biosorbent concentration: 3 g/L, Contact time: one day, temperature: 20 °C). Each error bar illustrates the standard deviation of five measurements.

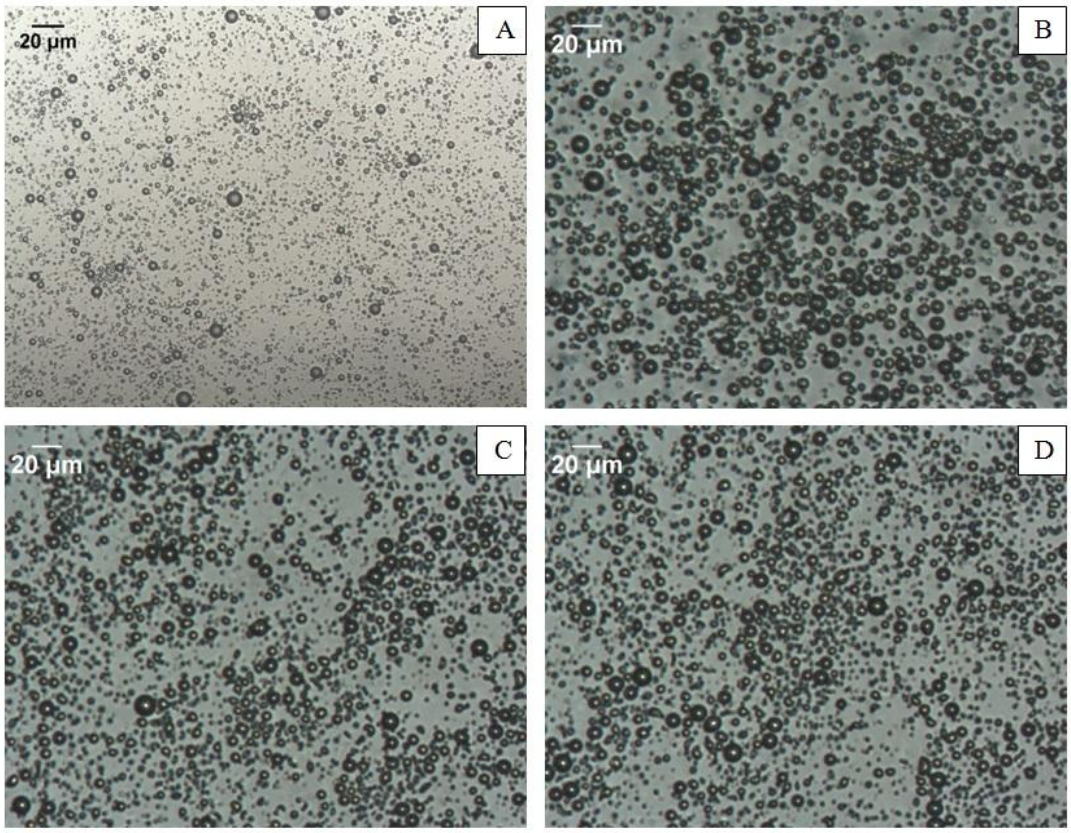

Figure 6.4: Light microscopy image of BSA-coated bubbles at calcium concentration of A) 0, B) 0.02, C) 0.1 and D) 0.5 g/L.

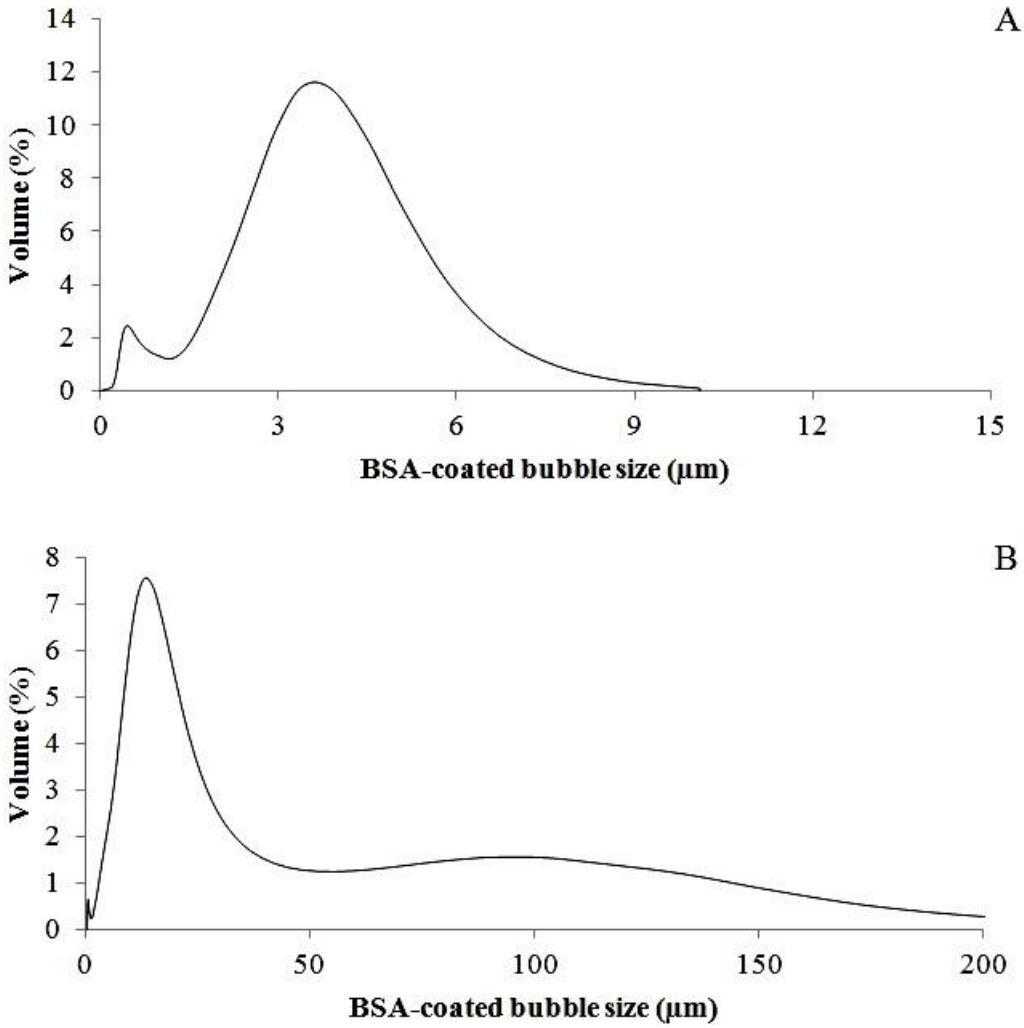

Figure 6.5: Size distribution and of BSA-coated bubbles at A) 0 and B) 0.02 g/L of calcium ion concentration.

6.3.4. Effect of biosorbent concentration

Effect of sorbent loading on metal ion removal was investigated in presence of calcium ions. Different dosages of BSAEM (1.5-22 g/L) were injected into the solution at fixed pH and metal concentration. As shown in Figure 6.6, increasing BSAEM from 1.5 g/L decreased metal ion removal for both copper and nickel. In the case of copper, removal decreased to 5 g/L of BSAEM and afterwards a plateau was reached. Decrease in metal removal is due to aggregation between BSA coated-bubbles leading to decrease probability of interaction between metal ions with binding sites.

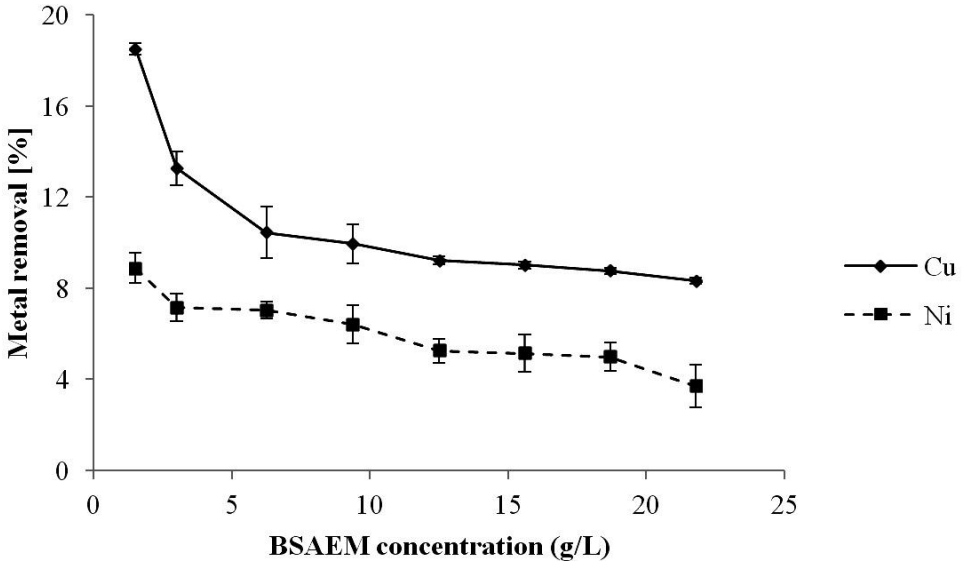

Figure 6.6: Effect of biosorbent dosage on metal removal (equilibrium solution pH: 5, C_{Cu}: 0.01 g/L, C_{Ni}: 0.02 g/L, C_{Ca}: 0.25 g/L, Contact time: one day, temperature: 20 °C). Each error bar illustrates the standard deviation of five measurements.

6.4. Conclusions

Fine air bubbles encapsulated with a thin film of BSA were constructed through sonochemical technique to remove copper and nickel ions from process water containing 0.25 g/L of calcium ions. It was evident that calcium ions, even at low concentration (0.02 g/L), drastically diminish metal ion removal. Calcium ions establish bridging flocculation of BSA-coated microcells, confirmed by both light microscopy and particle size analysis, this led to a decrease in the number of active functional groups exposed in the solution. Concentration of active binding sites and respective pK values were quantified by means of potentiometric titration method, and the data supported the result obtained from FTIR and XPS analysis. It was clearly shown that maximum metal ion removal was achieved at pH 5. An increase in BSAEM concentration resulted in a decrease in metal ion uptake due to formation of bubble aggregates.

References

Chen, F., Finch, J.A., Distin, P.A. and Gomez, C.O., 2003. Air assisted solvent extraction. Canadian Metallurgical Quarterly 42(3), 277-280.

Feinstein, S.B., Lang, R.M., Dick, C., Neumann, A., Al-Sadir, J., Chua, K.G., Carroll, J., Feldman, T. and Borow, K.M., 1988. Contrast echocardiography during coronary arteriography in humans: perfusion and anatomic studies. Journal of the American College of Cardiology 11(1), 59-65.

Graff, M. and Bukowska, J., 2005. Adsorption of enantiomeric and racemic cysteine on a silver electrode-SERS sensitivity to chirality of adsorbed molecules. The Journal of Physical Chemistry B 109(19), 9567-9574.

Keller, M.W., Feinstein, S.B., Briller, R.A. and Powsner, S.M., 1986. Automated production and analysis of echo contrast agents. Journal of Ultrasound in Medicine 5(9), 493-498.

Mateo Marti, E., Methivier, C. and Pradier, C.M., 2004. (S)-cysteine chemisorption on Cu110, from the gas or liquid phase: an FT-RAIRS and XPS study. Langmuir 20, 10223-10230.

Parthasarathy, N. and Buffle, J., 1994. Capabilities of supported liquid membranes for metal speciation in natural waters: application to copper speciation. Analytica Chimica Acta 284(3), 649-659.

Sengupta, B., Sengupta, R. and Subrahmanyam, N., 2006. Copper extraction into emulsion liquid membranes using LIX 984N-C®. Hydrometallurgy 81(1), 67-73.

Statistics Canada (2012) Industrial water use-2009, Ministry of Industry, Ottawa, Canada.

Tarkan, H.M. and Finch, J.A., 2005. Air-assisted solvent extraction: towards a novel extraction process. Minerals Engineering 18(1), 83-88.

Tchuenbou-Magaia, F.L., Norton, I.T. and Cox, P.W., 2009. Hydrophobins stabilised air-filled emulsions for the food industry. Food Hydrocolloids 23(7), 1877-1885.

Tchuenbou-Magaia, F.L., Norton, I.T. and Cox, P.W., 2011. Suspensions of air cells with cysteine-rich protein coats : Air-filled emulsions. Journal of Cellular Plastics 47(3), 217-232.

Volesky, B. (1990) Biosorption of heavy metals, CRC press, Florida (USA).

Volesky, B., 2007. Biosorption and me. Water Research 41(18), 4017-4029.

Yao, H., Fukui, T. and Kimura, K., 2007. Chiroptical responses of D-/L-penicillamine-capped gold clusters under perturbations of temperature change and phase transfer. The Journal of Physical Chemistry C 111(41), 14968-14976.

Yun, Y.S., Park, D., Park, J.M. and Volesky, B., 2001. Biosorption of trivalent chromium on the brown seaweed biomass. Environmental Science & Technology 35(21), 4353-4358.

Chapter 7. Conclusions, contribution to original knowledge and future work

7.1. Conclusions

This thesis addressed copper, nickel and cobalt removal using a novel material known as air-filled emulsion (AFE) under different experimental conditions, as well as the recovery of metal-loaded bubbles from the solution. The following conclusions are drawn from the study:

(i) BSA- and EWP-protein coated bubbles were synthesized through a sonochemical process at appropriate protein concentration (50 g/L); protein solution pH (pH 4 for EWP and 7 for BSA), sonication time (3 min), power (90 W); and air flow rate (60 ml/min). The suspensions of cysteine-coated bubbles showed promising stability which is attributed to the covalent disulfide bond (S-S) leading to a cage-like structure around a gas core.

(ii) The capacity of BSAEM and EWPEM for metal adsorption was investigated in a unary system consisting of copper ions. BSA-coated microcells exhibited good copper sorption (55% at pH 5) compared to that of EWP-coated bubbles (15% at pH 5), due to the greater number of functional groups present on the surface of BSA-coated bubbles. The other advantage of BSAEM over EWPEM is that natural pH of BSA solution is suitable for AFE construction, whereas the pH of EWP solutions should be decreased to approximately 4 to produce EWP-coated bubbles.

(iii) Competitive biosorption behavior of a ternary system containing copper, nickel and cobalt ions by BSAEM was investigated. It was observed that the copper ions (45% at pH 5) were favorably adsorbed by active sites of BSA-coated microcells rather than nickel and cobalt ions (10% at pH 5). The quantity of copper removal in a unary system is higher compared to that in the ternary system as nickel and cobalt ions inhibit uptake of copper ions by functional groups by blocking the sites on the BSA-coated bubbles.

(iv) It was shown that experimental conditions have a noticeable impact on metal-sorbing performance of AFE.

- pH 5 was selected as the optimum pH for both BSA- and EWP-coated bubbles, as not only it is well below the region where the copper hydrolysis occurs, but also it leads to a decrease in both the repulsive electrostatic force between metal species and active binding sites, and hydrogen ion concentration (isoelectric point of both BSAEM and EWPEM is between pH 4 and 5).
- Increasing dosage of BSA-coated bubbles improved metal ion adsorption until a specific concentration; however additional increase in BSAEM loading led to a decrease in metal ion removal due to the formation of aggregates, which resulted in loss of sorption sites for metal ion uptake. Contrary to the BSAEM behavior, an increase in EWPEM concentration led to an increase in metal ion removal due to the presence of a greater number of functional groups at higher dosages of EWP-coated bubbles.
- Increased temperature led to an increase in copper ion removal, up to approximately 100% for BSAEM at 65 °C. This was due to the exposure of more functional groups initially hidden in the structure coupled with the increase in diffusion rate of ions resulting in greater interaction between metal species and active sites. In the case of the ternary system, no significant change was observed for nickel and cobalt removal indicating dominance of copper removal at high temperature.
- It was shown that the greatest rate of uptake was accomplished by BSAEM in the first 90 min (0.1 g/L of cobalt, nickel and copper ions), and afterwards equilibrium conditions were reached. For lower concentration of copper, 0.02 g/L, the equilibrium region was reached in the first 10 min.
- BSAEM displayed an unexpected behavior at various metal ion concentrations, which was not reported by other research to the best of the author's knowledge. At 5 and 10 g/L of BSAEM, maximum copper removal was achieved at 0.1 g/L of copper ion. Nickel and cobalt showed different behavior compared to that of copper. In contrast, addition of the lower BSAEM dose (1.2 g/L) led to an increase in copper, nickel and cobalt uptake at lower metal ion concentration and maximum removal was reached at 0.01 g/L of metal ions.

(v) XPS and FTIR results showed that amino, thiol and carboxylic groups of BSA- and EWP-coated bubbles are capable of metal ion adsorption. Furthermore, metal ion adsorption by BSAEM and EWPEM is through the combination of two steps: Physical adsorption and complexation, where metal ions are initially attracted *via* electrostatic interaction; and thereafter chemical bonds created between metal ions and active binding sites.

(vi) Using flotation to break the emulsion, copper recovery was close to 0.5% (pH range from 5 to 8) in absence of cationic surfactant and flocculant due to the lack of hydrophobic groups around the copper-loaded microcells. It was shown that both solution pH and flocculant concentration had a significant influence on copper recovery. Cationic flocculant at concentration of 0.025 g/L resulted in excellent separation of copper-BSAEM from the solution above pH 7; however copper recovery decreased from 35% to 11% as copper species hydrolyze at high pH. Collector addition increased the floatability of copper-loaded BSA at pH ranging from 5 to 6. To carry out efficient biosorptive flotation, pH selection should be based on a trade-off between copper recovery and copper removal.

(vii) It was demonstrated that the presence of calcium ions in solution decreased metal removal by 70% as the calcium ions not only competed with other metal ions for functional groups of BSA-coated microcells, but also caused bridging flocculation of air bubbles, which subsequently reduced number of active sites.

7.2. Contributions to original knowledge

As noted in Chapter 2, current waste water treatment methods have several disadvantages for removing metal ions from dilute solution, including low selectivity and high energy consumption. AFE has been proposed as a novel material containing a large number of coated microcells introducing a high specific surface area in contact with metal ions. In addition, metal-loaded AFE completely disengages from the solution and accumulates at a top layer due to the buoyancy of coated bubbles. This phase separation as well as selectively heavy metal ion removal coupled with food and dairy industry waste as an abundant source of cysteine protein rendering this method potentially cost-effective and ecofriendly.

7.3. Future work

- Alternative cysteine-rich proteins such as hydrophobin should be employed to generate fine air bubbles to remove metal ions. However, since hydrophobin is now quite expensive current work has been directed toward the synthesis of hydrophobin from mushrooms to decrease the production cost.

- Biosorptive flotation of copper ions should be conducted in a bank of cells to investigate the metal ion recovery.

- Biosorptive flotation of a binary system encompassing nickel and cobalt ions by BSAEM should be investigated at pH above 5, as nickel and cobalt are in the form of divalent ions until pH 8.

- Biosorption of rare earth elements (REEs) could be examined using BSAEM at different operational conditions to determine capacity of BSA-coated bubbles for rare earth ion removal. This would be good due to the current critical nature of the REEs.

- The process of metal ion removal from pregnant solution containing metal-loaded AFE (stripping) should be investigated.

Appendix A: Emulsion stability

The main purpose of this part was to control the size distribution of the microspheres of the emulsion. The formation of air-filled emulsion and the size distribution of coated bubbles is influenced by both emulsification and cavitation. These two processes dependent upon energy input, including sonication power, time and volume of sonicated material. Several experiments were systematically performed to explore the impact of three experimental parameters: power amplitude; length of sonication; and air flow rate. The emulsion stability was investigated by comparing the data obtained from both light microscopy images of EWP microcells and the respective size distributions. Figure A.1 and A.2 illustrate the effect of sonication power on the mean size and size distribution of EWP microspheres. It was observed that the number of air cells and the mean size increased with increasing sonication power due to the extra energy. However, no obvious change was observed between size distribution curves except for 160 W. This statement is contrary to the findings of Zhou *et al.* (2011) . They suggested that with an increase in the ultrasonic power, the size distribution widens and the size distribution changes from mono-dispersion to a bi/polymodal dispersion. Microbubbles formed at sonication powers of 70 W, 90W and 130W exhibit a bimodal dispersion with two distinct peaks. The comparison between light microscopy images and overall trends of size distribution curves implies that the minor peak is attributed to the distribution of both protein debris and very fine bubbles, while the larger one is assigned to the dispersion of coarser bubbles. At 30% amplitude (70 W), energy level required for formation of superoxide radical and crosslinking of thiol groups were not sufficient, generating less stable bubbles. However sonication at 90 W leads to coarser and well-dispersed microspheres due to the presence of a greater amount of crosslinked protein at the A/W interface. As it is shown in Figure A.1C, further increases in the ultrasonic power result in the initiation of flocculation. Zhou *et al.* (2011) proposed that bubble coalescence is responsible for the generation of larger bubbles and an increase in the size distribution; nevertheless, no coalescence effect was found in optical microscope pictures (Zhou *et al.*, 2011). The increase in the mean size and size dispersion of bubbles as well as the formation of polymodal size distribution are attributed to flocculation in that two or more microbubbles form aggregates due

to the net attractive microbubbles form aggregates due to the net attractive interaction between them such as electrostatic and hydrophobic forces.

As illustrated in Figure A.1D, large bubbles are covered by a few small bubbles and protein aggregates (bridging and depletion flocculation). It is speculated that a high amount of energy produced at high ultrasonic power (160 W) increases the temperature of protein solution leading to thermal denaturation of protein, exposure of nonpolar amino acid groups and consequently increase of protein hydrophobicity.

Replicate experiments were carried out at various bubbling rates in order to probe the role of air (*i.e.* oxygen) content in size and size distribution of the microbubbles in the air-filled emulsion. Analysis of data derived from both an optical microscope and particle size analyzer points out that increasing the air flow rate up to 80 mL/min a) increases the number of stable bubbles b) narrows the size distribution and c) the size dispersion changes from poly-dispersion to bimodal dispersion. This is due to the elevation of both the oxygen and superoxide radical amount present in the protein solution and consequent enhancement of oxidative crosslinking of thiol groups, in agreement with Sulick and Grinstaff (1990) for mechanisms of proteinaceous microbubble formation. As illustrated in Figure A.3A, no stable bubble could be seen in the absence of an aeration system (Suslick and Grinstaff, 1990). Furthermore, the size distribution consists of two peaks attributed to the dispersion of protein debris (small peak) and protein aggregates (larger peak). Although the increase of bubbling rate up to 50 mL/min improves the formation of bubbles, the number of microbubbles is still low in the structure. The data shown in Figure A.3B and C indicate the size distribution plots consist of three different peaks ascribed to the dispersion of protein debris and very fine air cells (small peak), large EWP-coated bubbles (intermediate peak) and protein aggregates (large peak).

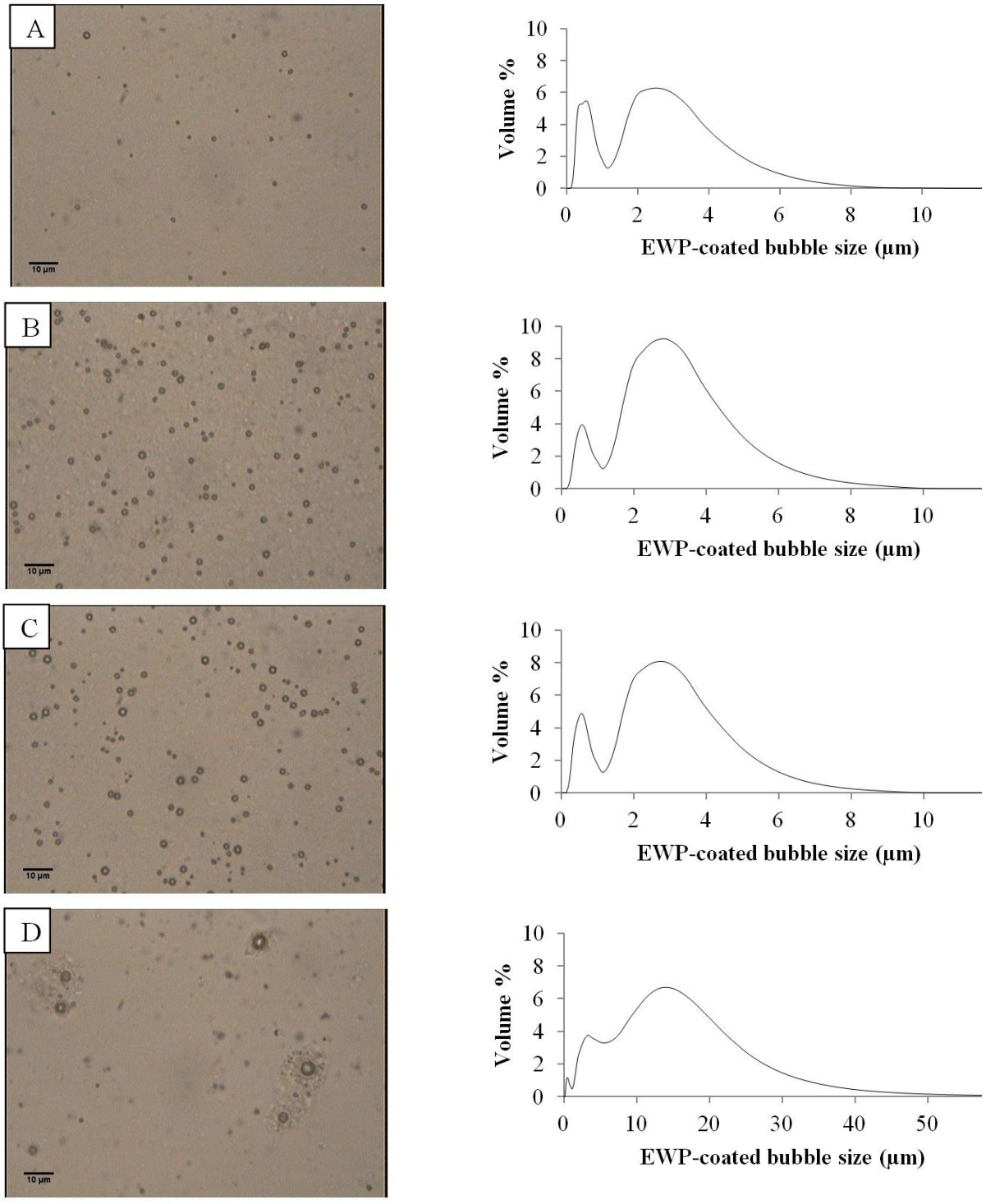

Figure A.1: Size distribution and of EWP-coated bubbles at different acoustic power A)70W(30%), B)90W (50%), C)130W (70%), D)160W (90%), generated at a protein concentration of 50 g/L and sonication time and bubbling rate of 3 min and 70 mL/min

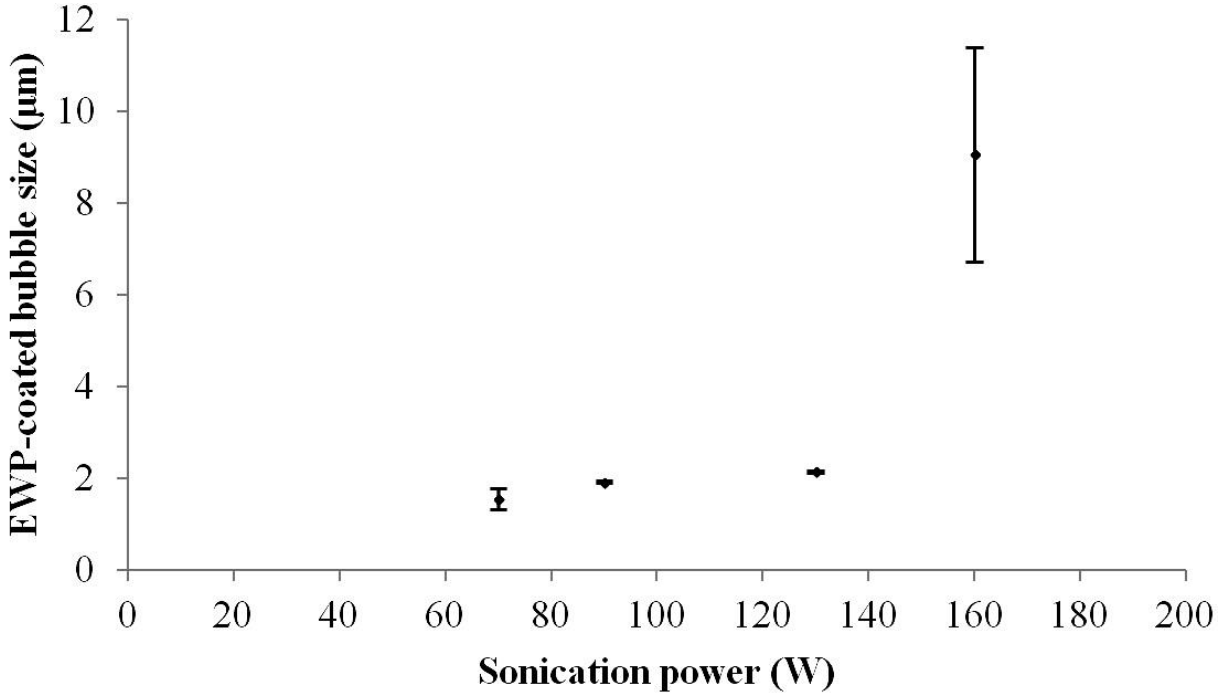

Figure A.2: Mean size of EWP-coated microcells with sonication time, air flow rate and concentration of 3 min, 70 mL/min and 50 g/L respectively at various ultrasonic powers. Each error bar illustrates the standard deviation of five measurements.

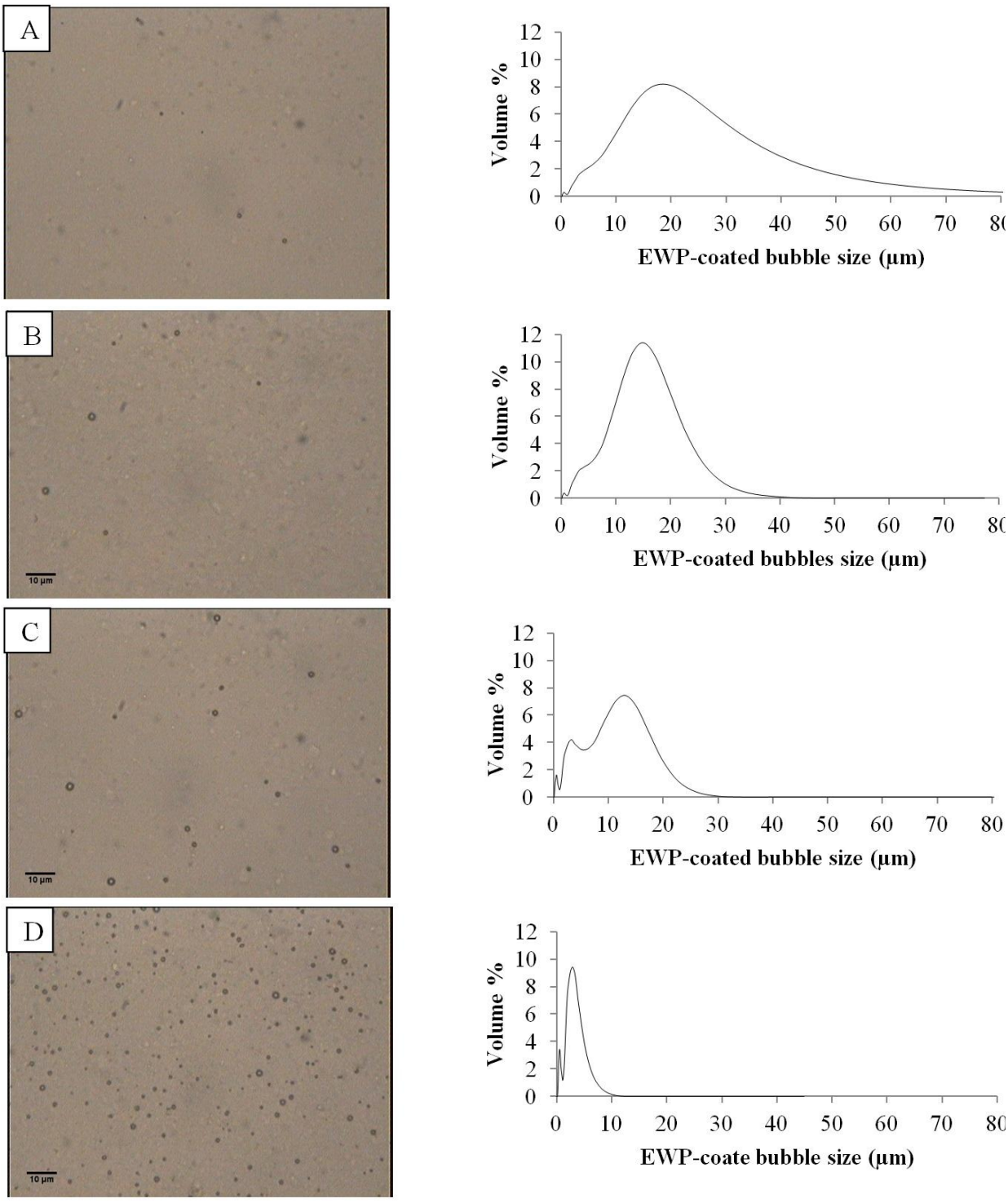

Figure A.3: Particle size distribution of EWP-coated bubbles at bubbling rate of A)0 mL/min, B)20 mL/min, C)50 mL/min, D)80 mL/min generated at a protein concentration of 50 g/L and sonication power and time of 90 W and 3 min respectively.

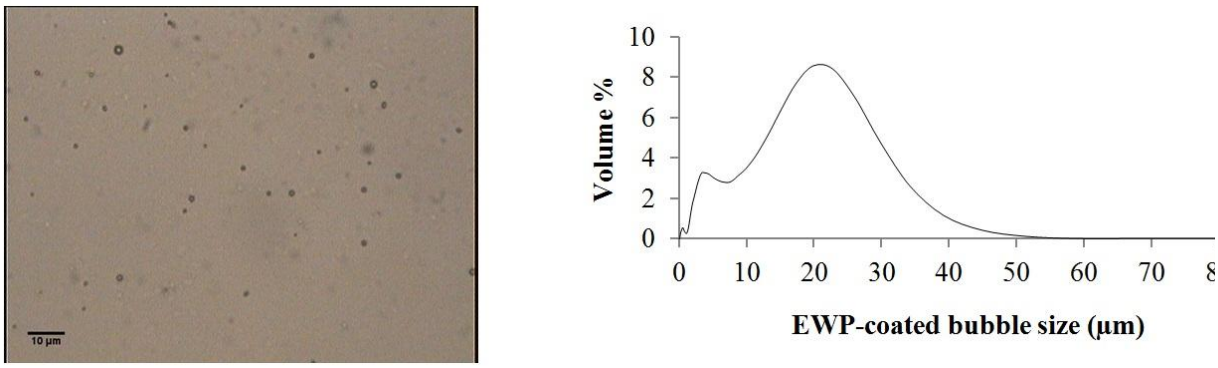

Figure A.4: Particle size distribution of EWP-coated bubbles at bubbling rate of 100 mL/min generated at a protein concentration of 50 g/L and sonication power and time of 90 W and 3 min respectively.

Additional increases in the air flow rate to 80 mL/min causes a drastic effect on the number and size distribution of proteinaceous microspheres (Figure A.3D), the size distribution of microbubbles changes to bimodal dispersion. In other words, the third peak attributed to the protein aggregate distribution is eliminated at high air flow rate. The higher bubbling rate (100 mL/min) results in the destruction of stable microspheres due to high agitation formed, and polymodal size distribution of microbubbles as shown in Figure A.4.

References

Suslick, K.S. and Grinstaff, M.W., 1990. Protein microencapsulation of nonaqeous liquids. Journal of the American Chemical Society 112(1), 7807-7809.

Zhou, M., Cavalieri, F. and Ashokkumar, M., 2011. Tailoring the properties of ultrasonically synthesised microbubbles. Soft Matter 7(2), 623-630.

Appendix B: Physico-chemical properties of some hydrophobins and other cysteine-rich proteins

Table B.1: Physico-chemical properties of some cysteine-rich proteins.

Protein	Source	MW*(kDa)	S-S bonds	SH-groups	iep*	T_d* °C	ST* (mN/m)
Class I Hydrophobin (HFB)							
ABH3	Agaricus (common white button mushroom)	9.2	8	0	4.5	-	37
POH1	Pleurotus ostreatus (oyster mushroom)	11	8	0	4.68	-	40
POH2	Pleurotus ostreatus (oyster mushroom)	8.3	8	0	4.81	-	40
SC3	Schizophyllum commune	13.6	8	0	-	-	24,29
H*Protein A	Recombinant protein	47	-	-	4.9	-	40-45
H*Protein B	Recombinant protein	19	-	-	4.9	-	40-45
Class II Hydrophobin							
HFBI	Trichoderma reesei	7.5	8	0	5.7	>90; >80	37
HFBII	Trichoderma reesei	7.2	8	0	6.5; 4.8	>80	28-30
Other proteins							
BSA	Bovine	67	1	17	4.9	65	50
Ovalbumin	Egg white	45	4	1	4.5-4.7	71.5	45
Ovotransferrin	Egg white	787.7	0	15	6.5	57.3	46
Lysozime	Egg white	14.4	0	4	10.7	70	43

MW: Molecular weight; iep: Isoelectric point; T_d: Denaturation temperature; ST: Surface tension.

References

Tchuenbou-Magaia, F.L., 2012. Hydrophobins and air filled emulsions. Ph.D thesis, University of Birmingham (UK).

Appendix C: Speciation diagrams of copper, nickel and cobalt

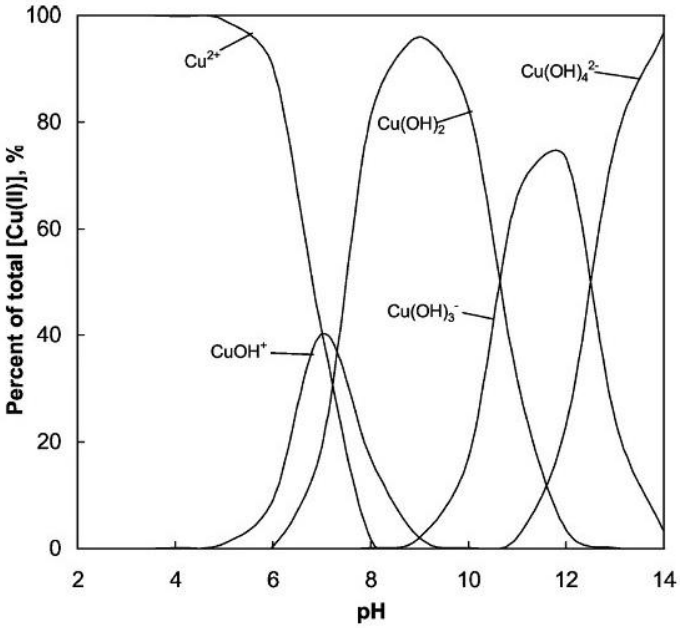

Figure C.1: Species distribution diagram for copper (II)-H_2O system (Doyle and Liu, 2003).

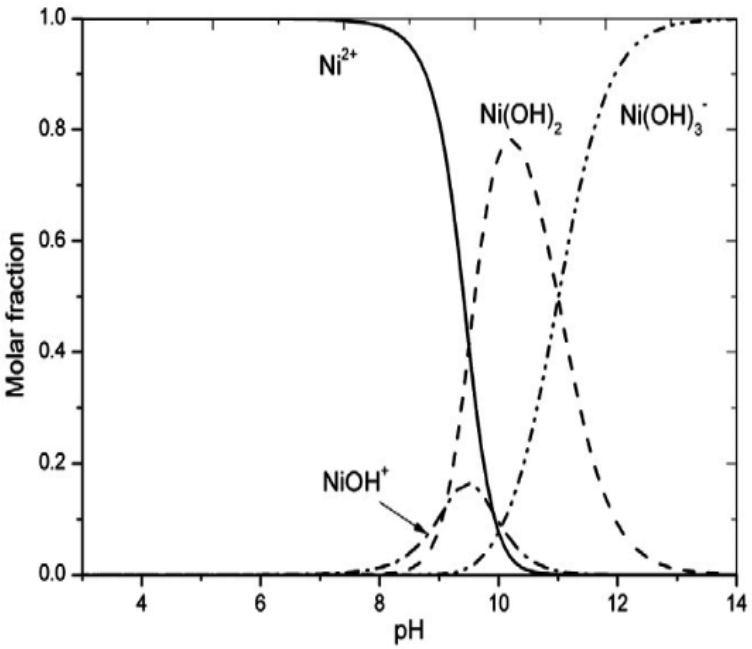

Figure C.2: Speciation diagram of nickel (II) (Bhatnagar *et al.*, 2012).

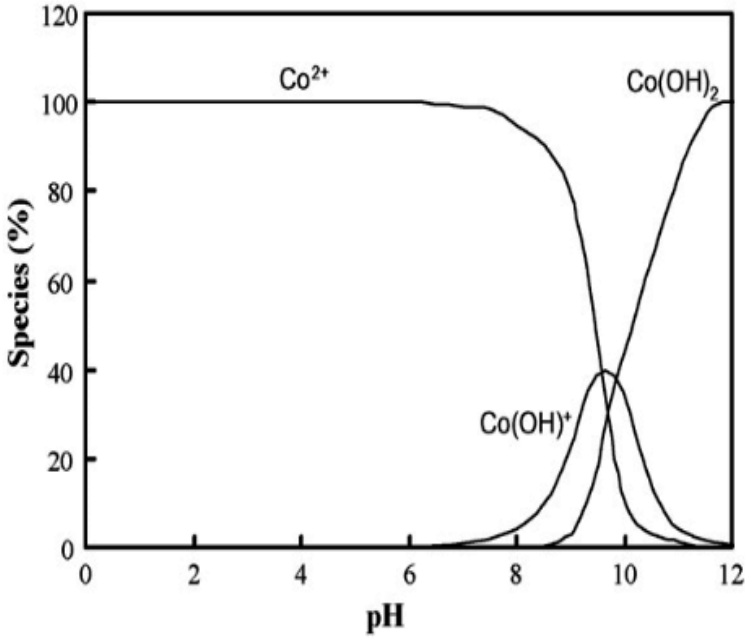

Figure C.3: Species distribution diagram for cobalt (II) in aqueous solution (Krishnan and Anirudhan, 2008).

References

Bhatnagar, A., Vilar, V.J.P., Santos, J.C., Botelho, C.M.S. and Boaventura, R.A.R., 2012. Valorisation of marine Pelvetia canaliculata Ochrophyta for separation and recovery of nickel from water: Equilibrium and kinetics modeling on Na-loaded algae. Chemical Engineering Journal 200-202, 365-372.

Doyle, F.M. and Liu, Z., 2003. The effect of triethylenetetraamine (Trien) on the ion flotation of Cu^{2+} and Ni^{2+}. Journal of Colloid and Interface Science 258(2), 396-403.

Krishnan, K.A. and Anirudhan, T.S., 2008. Kinetic and equilibrium modelling of cobalt(II) adsorptiononto bagasse pith based sulphurised activated carbon. Chemical Engineering Journal 137(2), 257-264.

Appendix D: Derivation procedures of the proton-binding model

Consider BjH as a certain functional group on the biomass. Its deprotonation reaction and respective equilibrium constant (Kj) are given by Equation D.1.

$$B_jH \leftrightarrow B_j^- + H^+ \qquad K_j = \frac{[B_j^-][H^+]}{[B_jH]} \tag{D.1}$$

The concentration of the protonated group ($[B_jH]$) can be represented by Equation D.2 using Equation D.1.

$$[B_jH] = \frac{[B_j^-][H^+]}{K_j} \tag{D.2}$$

The total concentration ($[B_j]_T$) of the functional group (B_jH) is identical to the sum of the protonated and ionized groups shown in Equation D.3.

$$[B_j]_T = [B_jH] + [B_j^-] \tag{D.3}$$

Also Equation D.3 could be written in the form of Equation D.4 using Equation D.2.

$$[B_j]_T = [B_j^-]\left(1 + \frac{[H^+]}{K_j}\right) \tag{D.4}$$

The concentration of the ionized functional group (B^-) can be expressed as:

$$[B^-] = \frac{[B_j]_T}{1 + \frac{[H^+]}{K_j}} \tag{D.5}$$

In titration experiments, the electroneutrality condition must be satisfied. Therefore:

$$[Na]_{added} + [H^+] = \sum_{j=1}^{N} [B_j^-] + [OH^-] \tag{D.6}$$

Where $[Na]_{added}$ is equal to the concentration of the added hydroxide ions, and $\sum_{j=1}^{N} [B_j^-]$ denotes a sum of the concentration of all types of ionized groups.

Combination of both Equation D.5 and D.6 results:

$$[OH^-]_{Added} = \sum_{j=1}^{N} \left[\frac{b_j X}{1 + \left(\frac{[H^+]}{K_j} \right)} \right] + \frac{K_W}{[H^+]} - [H^+] \qquad \text{D.7}$$

b_j, X and K_j represent the quantity of active sites per gram of biosorbent (mol/g), Biomass concentration (g/L) and equilibrium constant respectively. N describes the number of functional groups on the surface of microcells. K_w is expressed as the equilibrium constant of water at 25 °C (1.023×10^{-14}).

References

Yun, Y.S., Park, D., Park, J.M. and Volesky, B., 2001. Biosorption of trivalent chromium on the brown seaweed biomass. Environmental Science and Technology 35(21), 4353-4358.